GENETIC AND CHEMICAL APPROACHES REVEAL FUNCTION AND DRUGGABILITY OF CHAPERONES IN THE HUMAN MALARIA PARASITE *PLASMODIUM FALCIPARUM*

by

DAVID WAYNE COBB

(Under the Direction of Vasant Muralidharan)

ABSTRACT

Malaria is a deadly disease caused by Eukaryotic, single-cell parasites from the genus *Plasmodium*, with *P. falciparum* associated with the most deadly instances of the disease. With 228 million cases and over 400,000 deaths in 2018, the continuous rise of anti-malarial resistant *P. falciparum* parasites is a threat to global health. Research into the parasite's cellular biology uncovers potential weakness that may be exploited to kill the parasite, but this research has been historically difficult due to the haploid nature of the parasite and its recalcitrance to genetic manipulation. Conditional knockdown systems, in which parasite protein expression is controlled by small molecules, and the adaptation of CRISPR/Cas9 genome editing for use in *P. falciparum* has recently made research into the parasite's cellular biology more feasible. This dissertation combines these advances, presenting a detailed protocol for using CRISPR/Cas9 genome editing to introduce conditional knockdown systems into the parasite and demonstrating how those systems were used to investigate a

protein exported by the parasite into its host red blood cell. Then, these same methods are used and built upon to provide a detailed investigation of *Pf*J2, an essential chaperone and thioredoxin-domain protein located in the parasite's endoplasmic reticulum (ER). The *P. falciparum* ER is an organelle neglected in research, despite its numerous essential functions. I uncover interactions between *Pf*J2 and other essential proteins that reside in or pass through the ER, and I leverage the protein's thioredoxin domain to provide new insights into the process of disulfide bond formation in the oxidative environment of the parasite's ER. This process likely involved *Pf*J2 and members of the Protein Disulfide Isomerase (PDI) family, one of which—*Pf*PDI8—I demonstrate is also essential for parasite survival. Finally, I use a chemical biology approach to show that a small molecule can disrupt the redox interactions between *Pf*J2, *Pf*PDI8, and their substrates. These results suggest that these essential proteins, and the process of disulfide bond formation in the ER, are a new aspect of the parasite's biology that could be exploited for anti-malarial drug development.

INDEX WORDS: *Plasmodium falciparum*, malaria, CRISPR/Cas9, endoplasmic reticulum, chaperone, Protein Disulfide Isomerase, oxidative folding

GENETIC AND CHEMICAL APPROACHES REVEAL FUNCTION AND DRUGGABILITY OF CHAPERONES IN THE HUMAN MALARIA PARASITE *PLASMODIUM FALCIPARUM*

by

DAVID WAYNE COBB

B.S., Mercer University, 2015

A Dissertation Submitted to the Graduate Faculty of The University of Georgia in Partial Fulfillment of the Requirements for the Degree

DOCTOR OF PHILOSOPHY

ATHENS, GEORGIA

2020

GENETIC AND CHEMICAL APPROACHES REVEAL FUNCTION AND DRUGGABILITY OF CHAPERONES IN THE HUMAN MALARIA PARASITE *PLASMODIUM FALCIPARUM*

by

DAVID WAYNE COBB

Major Professor: Vasant Muralidharan
Committee: Belen Cassera
Roberto Docampo
Vincent J. Starai

Electronic Version Approved:

Ron Walcott
Dean of the Graduate School
The University of Georgia
December 2020

DEDICATION

This dissertation is dedicated to the family given to me by genetics—who nurtured my curiosity from day one and trusted my decision to follow this path; and to the family that has formed around me by choice—who have celebrated the highs and whose support has never failed to arrive during the lows.

ACKNOWLEDGEMENTS

I would like to acknowledge all of the teachers and professors I've had throughout my education, who saw my potential for successful far before I did. I would not be here without their support and guidance, and for that I am endlessly grateful.

TABLE OF CONTENTS

Page

LIST OF TABLES

Page

LIST OF FIGURES

Page

CHAPTER 1

INTRODUCTION AND LITERATURE REVIEW

1.1 Malaria and *Plasmodium falciparum*

Plasmodium is a genus of single-cell, Eukaryotic parasites whose infection of humans causes malaria, a disease characterized by cyclic fever, chills, and fatigue[1]. Nearly half the world's population lives at risk of contracting malaria, and in 2018 there were an estimated 228,000,000 cases of the disease, resulting in over 400,000 deaths, overwhelmingly in children under 5 years old[2]. Ninety-three percent of those malaria cases occurred in Africa, primarily in the sub-Saharan region, and were caused almost entirely by infection with *P. falciparum*[2]. Compared to other *Plasmodium* species that infect humans, *P. falciparum* is unique in its membership of the *Laverania* subgenus that infects African great apes and is associated with the most severe forms of malaria, which include cerebral malaria, placental malaria, organ failure, and death[3,4].

P. falciparum is spread by female *Anopheles* mosquitoes[1]. When an infected mosquito prepares to feed on a human, *P. falciparum* sporozoites are injected into the person's skin, from which they travel into the blood stream and arrive at the liver. Within hepatocytes, sporozoites undergo massive replication to form thousands of merozoites, which burst from the hepatocyte and enter the blood. Thus begins the intraerythrocytic asexual replication cycle of the parasite, initiated by a merozoite invading a red blood cell (RBC), after which it will spend

the next 48 hours transitioning from the initial “Ring” stage, to the metabolically active trophozoite stage that consumes the hemoglobin content of the RBC, to the replicative schizont stage that produces new merozoites which egress and perpetuate the cycle (**Figure 1.1**). A subset of parasites exit the asexual cycle to form male and female gametocytes, which are taken up by feeding *Anopheles* mosquitoes to begin the sexual replication of the parasite and further development within the mosquito, producing sporozoites that will be injected into the next host.

The intraerythrocytic, asexual expansion of parasites within the blood stream is of particular research interest. This stage of the *P. falciparum* lifecycle is responsible for all of the symptoms associated with malaria[5]. In particular, the severity of *P. falciparum* malaria is often associated with the ability of RBCs infected with the parasite to adhere to microvasculature, sequestering in tissues to complete its intraerythrocytic development and avoid clearance by the spleen[6,7]. Among human-infected *Plasmodium* parasites, this sequestration phenotype is unique to *P. falciparum*, due to expression of parasite-derived adhesins at the surface of infected RBCs. The adhesin *Pf*EMP1 is a major driver of infected RBC cytoadherence: the transmembrane protein is produced within the parasite and trafficked out to the RBC surface, where it recognizes endothelial cell receptors[7,8].

In the past decades, efforts toward global elimination of malaria have driven down the number of cases and deaths, but the 228,000,000 cases in 2018 demonstrate a plateau in progress that has been observed in recent years[2].

Factors driving this plateau include insecticide resistance and the emergence of *Plasmodium* parasites resistant to anti-malarial drugs[2]. The latter is devastating, as anti-malarial drugs are the primary tool at clinicians' disposal for helping malaria-presenting patients. Historically however, *Plasmodium* parasites have rapidly evolved resistance to drugs soon after their introduction into the field[9]. The continuous presence of rising drug resistance drives the need for research programs focused on the unique cellular biology of *P. falciparum* parasites. The cellular processes occurring within *P. falciparum* are fine-tuned to ensuring parasite survival, replication, and propagation; therefore, understanding these processes uncovers points of weakness within *P. falciparum* biology that might be exploited to kill the parasite.

1.2 The *P. falciparum* endoplasmic reticulum

One of the best examples of *P. falciparum* cellular biology that is potentially filled with drug targets is the parasite's endoplasmic reticulum (ER) and the numerous functions it supports throughout the asexual replication cycle. Like other Eukaryotes, the *P. falciparum* ER is a site of abundant protein translation, with proteins containing an N-terminal signal peptide and/or transmembrane domains co-translationally imported into the ER or inserted into its membrane. Many other Eukaryotes have evolved efficient mechanisms for coping with the stress that arises from such extensive protein production, including signaling mechanisms to upregulate chaperones and globally downregulate transcription/translation, and ER-Associated Degradation (ERAD) machinery to remove proteins from the

ER[10,11]. In contrast, *P. falciparum* has maintained modest means for overcoming ER stress; namely a reduced set of putative ERAD proteins, and the PERK-eIF2α signaling axis to downregulate global translation[12–14]. This apparent dearth of ER stress response capability, which in itself suggests that ER stress could be a therapeutic target, belies the importance of the organelle for the parasite's survival within its host RBC.

A major function for the ER is to serve as the root of the parasite's complex secretory pathway. This pathway begins with proteins entering the ER, from which they are transported to the parasite plasma membrane; the parasitophorous vacuole in which the parasite resides; the host RBC and numerous locations within it; and organelles within the parasite itself, including the metabolically-important apicoplast and apical organelles that allow new parasites to egress and invade host cells. Mechanisms underlying this process, including how the majority of proteins are recognized for downstream trafficking in the ER, remain unknown. The major exception is the discovery of the *Plasmodium* Export Element (PEXEL) motif, which is encoded downstream of the signal peptide of some proteins that will leave the ER and travel to the host RBC[15,16]. This motif is cleaved by the ER-resident protease Plasmepsin V (*Pf*PMV) to mark these proteins for export, and recognition for export appears to occur as proteins are translated into the ER, with incorporation of *Pf*PMV into translocation complexes in the ER membrane[17–20]. However, only a subset of exported proteins contain a PEXEL motif. The mechanisms used to recognize

and facilitate the exit of PEXEL-negative proteins, as well as proteins that leave the ER for numerous other cellular locations, remain elusive.

The proteins that are exported from the ER to the host RBC are required to remodel the host cell into a hospitable niche for parasite replication, and they are required to transport *Pf*EMP1 and other surface proteins to the RBC surface[21]. As such, many *P. falciparum* researchers have sought to identify essential components of the export process. *Pf*PMV is one of the first ER proteins thought to interact with many exported proteins, licensing them for export. Conditional knockdown of *Pf*PMV results in death of asexual parasites, and compounds designed to impair *Pf*PMV function have anti-*P. falciparum* activity[22–24]. Outside of the ER, exported proteins are unfolded and exit the parasitophorous vacuole through the Plasmodium Translocon of Exported proteins (PTEX)[25–28]. Conditional knockdown of PTEX components blocks export and kills asexual parasites, demonstrating that successful export is required for parasite survival[29,30]. Once parasite proteins enter the RBC, the mechanisms used to ensure their correct re-folding and trafficking are largely unknown. *P. falciparum* exports numerous Hsp40 co-chaperones which may support these processes in the RBC, but the parasite exports only a single Hsp70 chaperone[31–34]. Many researchers hypothesized essential roles for this one exported Hsp70, but we and others demonstrated that is in fact dispensable for asexual development and is not likely to be one of the essential factors required for exported protein trafficking (See Chapter 3)[35,36]. Notably, all of these proteins

which were found critical for protein export either reside in or pass through the ER.

The *P. falciparum* secretory pathway has numerous other termination points aside from the parasitophorous vacuole and RBC. Another route of major importance is the trafficking of proteins from the ER to the plastid organelle known as the apicoplast, which produces many metabolites, including the essential compound isopentenyl pyrophosphate[37]. Arising from a secondary endosymbiotic event, the majority of the organelle's genes transferred to the parasite nucleus over time, and proteins that reside in the apicoplast first enter the ER before onward trafficking[38–40]. Other parasite-specific organelles also rely on the ER to receive their proteins. These include the digestive vacuole (DV), whose proteins are trafficked from the ER to the parasitophorous before making their way back inside to the DV, as well as the various organelles that are formed at the end of the asexual life cycle to allow daughter parasite egress and invasion[41–43]. Together, these observations demonstrate the importance of the ER as a protein trafficking hub needed for *P. falciparum* survival.

Aside from its role as the secretory pathway root, the ER has other essential functions for ensuring parasite survival, one of which is likely calcium storage. Ca^{2+} is an important second messenger in biology, used for intracellular signaling that allows cells to perform countless functions required for life. Therefore, the intracellular concentration of Ca^{2+} must be tightly regulated, with low basal levels that can be quickly raised in response to signals. A major, essential use of calcium signaling within the asexual *P. falciparum* lifecycle is the

timed exocytosis of organelles required for parasite escape from the RBC and invasion of new host cells[44]. A spike in cytoplasmic Ca^{2+} concentration precedes exocytosis; tight regulation of Ca^{2+} concentrations within the parasite must therefore occur. The ER often serves as a major store of calcium ions, with the Sarco/Endoplasmic Reticulum Ca^{2+}-ATPase (SERCA) pump filling the organelle with Ca^{2+} to keep cytosolic concentrations low and provide a source of Ca^{2+} that can be released when needed[45]. The role of the *P. falciparum* ER in Ca^{2+} storage has received little direct study, but *P. falciparum* does encode a SERCA pump (PF3D7_0106300) that is predicted to be essential for the asexual lifecycle; the parasite ER is likely an important hub for Ca^{2+} storage and signaling[46,47].

Finally, another essential role for the ER during the asexual lifecycle is lipid biosynthesis, particularly the synthesis of neutral lipids such as tri- and diacylglycerol (TAG, DAG). Canonically, a series of enzymes within the ER membrane synthesizes TAG, beginning with the acylation of glycerol-3-phosphate, to form lysophosphatidic acid, which is converted to phosphatidic acid, then DAG, and finally TAG[48]. TAG is packaged into lipid bodies that bud from the ER, and serve as TAG reserves that can be hydrolyzed to form DAG and release fatty acids for phospholipid synthesis[49]. *P. falciparum* parasites synthesize TAG and produce lipid bodies, with TAG production peaking during the trophozoite and schizont stages and TAG consumption occurring from the schizont stage to the end of the asexual lifecycle[50,51]. The end of the asexual lifecycle is a period in which new secretory organelles are formed and membrane is needed to segment the new daughter merozoites. These membrane demands

perhaps explain the peak of TAG production going into schizogony and consumption of stores as the lifecycle is completing. Indeed, treatment of parasites with Orlistat, an inhibitor of TAG hydrolysis, prevents parasites from utilizing TAG and stalls development in the schizont stage[52].

The process of TAG production in *P. falciparum* has not received much research, but Glycerol-3-phosphate Acyl Transferase (GPAT)—the enzyme which produces lysophosphatidic acid—has been localized to the ER in asexual parasites[53]. The next enzyme in the series, 1-Acylglycerol-3-phosphate-O-acyltransferase (AGPAT) has been localized to the ER of the rodent malaria parasite *P. yoelii*[54]. Both enzymes are predicted to be essential by a genome-wide mutagenesis screen[47]. Clearly, TAG production and hydrolysis are important components of asexual replication, and the *P. falciparum* ER likely houses at least two essential components of the process.

While the downstream cellular processes stemming from the ER—such as protein trafficking, calcium signaling, and lipid production—have received varying levels of attention, the biology of the ER itself that underlies these processes has been neglected. What are the ER proteins that support these functions, how do they work, and are they therapeutic targets themselves? The last question is salient because crippling overall ER function could have disastrous consequences for the parasite's development, given the numerous and diverse roles the ER plays during the asexual lifecycle. As a Eukaryotic organism, certain inferences can be made about the biology of the *P. falciparum* ER, and conserved chaperones likely play a major role in most ER functions. Therefore,

the focus of my research has been the function of parasite chaperones within the asexual lifecycle, with particular attention to conserved chaperones in the ER.

The *P. falciparum* ER is stripped of some conserved proteins that play important roles in stress signaling and trafficking[12,43]. However, the parasite genome does encode a homolog for the crucial ER Hsp70 "Binding immunoglobulin Protein" BiP (PF3D7_0917900), as well as a few putatively ER-localized Hsp40 co-chaperones that are expected to regulate BiP function[31]. One of those Hsp40s, termed *Pf*J2 (PF3D7_1108700) also encodes a predicted thioredoxin (Trx) domain that gives it membership into the Protein Disulfide Isomerase (PDI) family of enzymes. PDI family members are ER-localized proteins with Trx domains, with PDI being the eponymous and most well-studied member[55]. The ER is a highly oxidizing environment, and PDI family members use the "CXXC" active site of the Trx domain to help form and break disulfide bonds within this environment[56]. Disulfide bonds are essential components of some proteins' native states, and they serve regulatory functions in many others[57]. Therefore, the ability to correctly form or reduce disulfide bonds is critical within the processes that the ER controls. In addition to *Pf*J2, the *P. falciparum* PDI family is predicted to include four other members, with *Pf*PDI8 most closely resembling a canonical PDI (i.e., an N-terminal Trx domain, a C-terminal Trx domain, and an ER retention signal)[58,59].

Trx domains are powerful mediators of disulfide bond formation/reduction. The nucleophilic cysteines of the "CXXC" motif help form disulfides in reduced client proteins or reduce disulfides in oxidized client proteins. The propensity for

a Trx domain to participate in either reduction or oxidation depends largely on the redox environment and its own redox potential (i.e., a reduced Trx domain may serve as a reductase, and an oxidized Trx domain may serve to oxidize other cysteines)[56]. In model organisms, PDIs serve well to both oxidize and reduce disulfides, and in vitro data suggests *Pf*PDI8 can similarly form or break disulfides based on its starting redox status[58,59]. In contrast, ERdj5—a mammalian ER Hsp40 with thioredoxin domains, and the protein to which *Pf*J2 bears homology—primarily serves as a reductase, providing key reductive power in the oxidizing ER environment[60–63].

*Pf*J2 likely has central and essential functions in the parasite ER. As an Hsp40 that is predicted to be essential, it likely works with and regulates the activity of PfBiP, an Hsp70 that is also predicted to be essential and is a master regulator of ER function in most Eukaryotes[47,64]. The presence of a Trx domain also suggests that *Pf*J2 may play some undefined role in ER redox biology. Accordingly, the role that *Pf*J2 plays in the *P. falciparum* ER has been one of the major focuses of my research, and those results are presented in Chapters 4 and 5. That work led to the identification of other important ER Trx-domain proteins, namely *Pf*PDI8 and *Pf*PDI11. Our data suggest that *Pf*J2, the *Pf*PDIs, and *Pf*BiP work together in the ER, perhaps cooperating to ensure client proteins that reside in or pass through the ER are properly folded and functional. These essential ER proteins are therefore upstream of the diverse functions that the ER plays, and may serve as points of intervention to disrupt parasite development. As

conserved proteins, however, the question remains whether they would be truly ideal candidates for drug development.

1.3 Conserved proteins are valuable for study and drug development in *P. falciparum*

As Eukaryotic organisms, certain features of *P. falciparum* biology will be shared with other Eukaryotes, including the model organisms that have driven much of biological research. But *P. falciparum* is not a model organism, and several millennia and clades separate the last common ancestor that the parasite shares with most well-studied organisms. For example—like other eukaryotes—*P. falciparum* houses its genome in a nucleus and it replicates that genome for daughter cells, utilizes molecular motors like myosin, and maintains a secretory pathway that traffics out from the ER. But context is critical: nuclear division is part of a process called schizogony, in which a single parasite produces up to 32 daughter cells around which the plasma membrane invaginates to form new merozoites[65]; actin and myosin are used to actively force an entire parasite into a host RBC[66]; and as detailed above, the *P. falciparum* secretory pathway is far more branched and specialized than that of organisms traditionally studied[43]. *P. falciparum* uses many of the same evolutionarily shared "blocks" as other eukaryotes, but time and development into a deadly human parasite has dictated unique ways that those blocks are used to build the organism.

Chaperones are a particularly pointed example of how basic function shared across lifeforms has a particular, parasitic function in *P. falciparum*.

Embedded within the parasitophorous vacuole membrane is the Plasmodium Translocon of Exported Proteins (PTEX). The core components of PTEX are the membrane-spanning/pore-forming *Pf*EXP2, the AAA+ ATPase *Pf*Hsp101, and *Pf*PTEX150 which connects the two[28]. As a AAA+ ATPase, PfHsp101 couples ATP hydrolysis to protein unfolding—a function not unique to *Plasmodium*—but this unfolding is required for exported proteins to exit the parasitophorous vacuole and enter the host cell, supporting the parasitic lifecycle[29,30]. Another example is *Pf*Hsp110c in the cytoplasm of the parasite. *Pf*Hsp110c is uniquely suited to stabilizing the asparagine-rich proteome of *P. falciparum* during heat stress, such as the stress of febrile episodes characteristic of malaria[67]. The roles for these chaperones were uncovered by making hypotheses, informed by potentially conserved function, within the context of *P. falciparum*'s parasite biology. The need for testing hypotheses that are informed by conserved biology is highlighted by the fact that *Pf*Hsp70x, the sole parasite-exported Hsp70, was found to be dispensable for parasite survival in culture (see Chapter 3)[35,36]. Based on the classical roles that Hsp70 chaperones have in protein trafficking, and because *Pf*Hsp70x is unique in its status as the only Hsp70 exported into an environment that requires extensive protein trafficking, many assumed an importance for the chaperone that data suggest may not align with reality.

Research into the parasite-specific functions of conserved proteins advances our knowledge about *P. falciparum* cellular biology. But conserved proteins have also given the field some of its validated and proposed drug targets. For example, the widely-used anti-malarial drug atovaquone targets

Complex III of the mitochondrial electron transport chain[68]. Some other conserved proteins/complexes that have been proposed as anti-malarial drug targets include Cytochrome B[69], the TCP-1 Ring Complex chaperone[70], the ribosome and protein translation[71–73], and the proteasome[74,75].

The precedence for targeting proteins that participate in conserved biology exists; therefore, a proposal to target essential proteins such as the *P. falciparum* PDI family is reasonable. And much like interest in targeting the *P. falciparum* proteasome began with observations that mammalian proteasome inhibitors have anti-malarial activity—which subsequently spurred development of *Plasmodium*-specific inhibitors—drugs designed to target human PDIs could have enough anti-*Plasmodium* activity to warrant the development of specific inhibitors[74,76,77]. Such drug-like inhibitors for human PDI have been identified as potential treatments for certain cancers and neurodegenerative diseases[78–81]. Our data, and the data published by others, show that at least one of these inhibitors has anti-*Plasmodium* activity (See Chapter 4)[12].

1.4 Advances in methods for studying essential *P. falciparum* proteins

The ability to identify and study essential proteins in *P. falciparum* has often been challenging. The parasite spends much of its lifecycle, including the asexual stages, in a haploid state and modification of the genome was a time-intensive process, involving transfection of plasmids targeted to specific points in the genome followed by rounds of drug cycling and months of waiting for crossover events to occur stochastically[82–84]. To study essential proteins in the haploid

parasite, conditional knockdown/knockout systems have been developed for *P. falciparum*. These systems allow researchers, upon the addition or removal of small molecules, to excise segments of DNA from the parasite genome[85], knockdown mRNA translation[86,87], or disrupt protein function[88,89]. With these methods, essential proteins are expressed and function as normal until knockdown is initiated, after which phenotypic results of their perturbation can be observed.

The second difficulty in studying *P. falciparum* cellular biology—the genetic intractability of the organism—has largely been overcome with the introduction of Clustered Regularly Interspaced Palindromic Repeat/Cas9 (CRISPR/Cas9) genome editing into the field[90,91]. This genome editing system uses a "guide" RNA sequence with homology to a specific site in the genome to direct Cas9 endonuclease to create a double-stranded break at that site, after which the parasite repairs its genome using a repair template. All of these required components—the guide RNA, Cas9, and repair templates containing sequences for epitope tags and conditional knockdown systems—are encoded on plasmids and introduced into the parasite by transfection[92].

The growing use of conditional methods for disrupting protein function in the parasite, combined with easier genetic manipulation are two major factors currently pushing *P. falciparum* research forward. The work presented in this dissertation first provides a detailed method for using CRISPR/Cas9 technology to create *P. falciparum* conditional knockdown parasite lines and how those parasite lines were used to investigate the function of the exported chaperone

*Pf*Hsp70x (Chapters 2 and 3). Then, these same methods are used and further built upon to provide the first detailed investigation of the PDI family members *Pf*J2, *Pf*PDI8, and *Pf*PDI11 and the roles that these ER proteins play in supporting the parasitic cellular biology of *P. falciparum* (Chapters 4 and 5).

1.5 References

1. Cowman, A. F., Healer, J., Marapana, D. & Marsh, K. Malaria: Biology and Disease. *Cell* **167**, 610–624 (2016).
2. World Heath Organization, C. World Malaria Report 2019. 232 (2019).
3. Loy, D. E. *et al.* Out of Africa: origins and evolution of the human malaria parasites Plasmodium falciparum and Plasmodium vivax. *Int. J. Parasitol.* **47**, 87–97 (2017).
4. Otto, T. D. *et al.* Genomes of all known members of a Plasmodium subgenus reveal paths to virulent human malaria. *Nat. Microbiol.* **3**, 687–697 (2018).
5. Venugopal, K., Hentzschel, F., Valkiūnas, G. & Marti, M. Plasmodium asexual growth and sexual development in the haematopoietic niche of the host. *Nat. Rev. Microbiol.* **18**, 177–189 (2020).
6. Fried, M. & Duffy, P. E. Adherence of Plasmodium falciparum to Chondroitin Sulfate A in the Human Placenta. *Science* **272**, 1502 (1996).
7. Turner, L. *et al.* Severe malaria is associated with parasite binding to endothelial protein C receptor. *Nature* **498**, 502–505 (2013).

8. Heatwoie, M., Wertheimer, P., Hertfeldt, A., Peterson, D. S. & Ravetch, A. The Large Diverse Gene Family var Encodes Proteins Involved in Cytoadherence and Antigenic Variation of Plasmodium falciparum-Infected Erythrocytes. *Cell* **82**, 89-100 (1995).

9. McClure, N. S. & Day, T. A theoretical examination of the relative importance of evolution management and drug development for managing resistance. *Proc. R. Soc. B Biol. Sci.* **281**, 20141861 (2014).

10. Hetz, C., Zhang, K. & Kaufman, R. J. Mechanisms, regulation and functions of the unfolded protein response. *Nat. Rev. Mol. Cell Biol.* **21**, 421–438 (2020).

11. Smith, M. H., Ploegh, H. L. & Weissman, J. S. Road to Ruin: Targeting Proteins for Degradation in the Endoplasmic Reticulum. *Science* **334**, 1086–1090 (2011).

12. Harbut, M. B. *et al.* Targeting the ERAD pathway via inhibition of signal peptide peptidase for antiparasitic therapeutic design. *Proc. Natl. Acad. Sci.* **109**, 21486–21491 (2012).

13. Zhang, M. *et al.* PK4, a eukaryotic initiation factor 2 (eIF2) kinase, is essential for the development of the erythrocytic cycle of Plasmodium. *Proc. Natl. Acad. Sci.* **109**, 3956–3961 (2012).

14. Zhang, M. *et al.* Inhibiting the Plasmodium eIF2α Kinase PK4 Prevents Artemisinin-Induced Latency. *Cell Host Microbe* **22**, 766-776.e4 (2017).

15. Marti, M. Targeting Malaria Virulence and Remodeling Proteins to the Host Erythrocyte. *Science* **306**, 1930–1933 (2004).

16. Hiller, N. L. A Host-Targeting Signal in Virulence Proteins Reveals a Secretome in Malarial Infection. *Science* **306**, 1934–1937 (2004).

17. Klemba, M. & Goldberg, D. E. Characterization of plasmepsin V, a membrane-bound aspartic protease homolog in the endoplasmic reticulum of Plasmodium falciparum. *Mol. Biochem. Parasitol.* **143**, 183–191 (2005).

18. Russo, I. *et al.* Plasmepsin V licenses Plasmodium proteins for export into the host erythrocyte. *Nature* **463**, 632–636 (2010).

19. Boddey, J. A. *et al.* An aspartyl protease directs malaria effector proteins to the host cell. *Nature* **463**, 627–631 (2010).

20. Marapana, D. S. *et al.* Plasmepsin V cleaves malaria effector proteins in a distinct endoplasmic reticulum translocation interactome for export to the erythrocyte. *Nat. Microbiol.* **3**, 1010–1022 (2018).

21. Maier, A. G. *et al.* Exported proteins required for virulence and rigidity of Plasmodium falciparum-infected human erythrocytes. *Cell* **134**, 48–61 (2008).

22. Polino, A. J., Nasamu, A. S., Niles, J. C. & Goldberg, D. E. Assessment of Biological Role and Insight into Druggability of the Plasmodium falciparum Protease Plasmepsin V. *ACS Infect. Dis.* 9 (2020).

23. Sleebs, B. E. *et al.* Inhibition of Plasmepsin V Activity Demonstrates Its Essential Role in Protein Export, PfEMP1 Display, and Survival of Malaria Parasites. *PLOS Biol.* **12**, 16 (2014).

24. Boonyalai, N., Collins, C. R., Hackett, F., Withers-Martinez, C. & Blackman, M. J. Essentiality of Plasmodium falciparum plasmepsin V. *PloS One* **13**, e0207621–e0207621 (2018).

25. Riglar, D. T. *et al.* Spatial association with PTEX complexes defines regions for effector export into Plasmodium falciparum-infected erythrocytes. *Nat. Commun.* **4**, 1415 (2013).

26. de Koning-Ward, T. F. *et al.* A newly discovered protein export machine in malaria parasites. *Nature* **459**, 945–949 (2009).

27. Gehde, N. *et al.* Protein unfolding is an essential requirement for transport across the parasitophorous vacuolar membrane of *Plasmodium falciparum*. *Mol. Microbiol.* **71**, 613–628 (2009).

28. Ho, C.-M. *et al.* Malaria parasite translocon structure and mechanism of effector export. *Nature* **561**, 70–75 (2018).

29. Beck, J. R., Muralidharan, V., Oksman, A. & Goldberg, D. E. PTEX component HSP101 mediates export of diverse malaria effectors into host erythrocytes. *Nature* **511**, 592–595 (2014).

30. Elsworth, B. *et al.* PTEX is an essential nexus for protein export in malaria parasites. *Nature* **511**, 587–591 (2014).

31. Botha, M., Pesce, E.-R. & Blatch, G. L. The Hsp40 proteins of Plasmodium falciparum and other apicomplexa: Regulating chaperone power in the parasite and the host. *Int. J. Biochem. Cell Biol.* **39**, 1781–1803 (2007).

32. Külzer, S. *et al. Plasmodium falciparum* -encoded exported hsp70/hsp40 chaperone/co-chaperone complexes within the host erythrocyte: Chaperones in the *P. falciparum* -infected host cell. *Cell. Microbiol.* **14**, 1784–1795 (2012).

33. Külzer, S. *et al.* Parasite-encoded Hsp40 proteins define novel mobile structures in the cytosol of the P. falciparum-infected erythrocyte: Hsp40s in the P. falciparum-infected erythrocyte. *Cell. Microbiol.* **12**, 1398–1420 (2010).

34. Petersen, W. *et al.* J-dot targeting of an exported HSP40 in Plasmodium falciparum-infected erythrocytes. *Int. J. Parasitol.* **46**, 519–525 (2016).

35. Cobb, D. W. *et al.* The Exported Chaperone PfHsp70x Is Dispensable for the Plasmodium falciparum Intraerythrocytic Life Cycle. *mSphere* **2**, e00363-17 (2017).

36. Charnaud, S. C. *et al.* The exported chaperone Hsp70-x supports virulence functions for Plasmodium falciparum blood stage parasites. *PLOS ONE* **12**, e0181656 (2017).

37. Yeh, E. & DeRisi, J. L. Chemical Rescue of Malaria Parasites Lacking an Apicoplast Defines Organelle Function in Blood-Stage Plasmodium falciparum. *PLoS Biol.* **9**, e1001138 (2011).

38. Waller, R. F., Reed, M. B., Cowman, A. F. & McFadden, G. I. Protein trafficking to the plastid of Plasmodium falciparum is via the secretory pathway. *EMBO J.* **19**, 1794–1802 (2000).

39. Foth, B. J. *et al.* Dissecting Apicoplast Targeting in the Malaria Parasite *Plasmodium falciparum*. *Science* **299**, 705 (2003).

40. van Dooren, G. G., Su, V., D'Ombrain, M. C. & McFadden, G. I. Processing of an Apicoplast Leader Sequence in *Plasmodium falciparum* and the Identification of a Putative Leader Cleavage Enzyme. *J. Biol. Chem.* **277**, 23612–23619 (2002).

41. Klemba, M., Beatty, W., Gluzman, I. & Goldberg, D. E. Trafficking of plasmepsin II to the food vacuole of the malaria parasite Plasmodium falciparum. *J. Cell Biol.* **164**, 47–56 (2004).

42. Ehlgen, F., Pham, J. S., de Koning-Ward, T., Cowman, A. F. & Ralph, S. A. Investigation of the Plasmodium falciparum food vacuole through inducible expression of the chloroquine resistance transporter (PfCRT). *PloS One* **7**, e38781–e38781 (2012).

43. Florentin, A., Cobb, D. W., Kudyba, H. M. & Muralidharan, V. Directing Traffic: Chaperone-mediated protein transport in malaria parasites. *Cell. Microbiol.* (2020) doi:10.1111/cmi.13215.

44. Glushakova, S. *et al.* Cytoplasmic free Ca2+ is essential for multiple steps in malaria parasite egress from infected erythrocytes. *Malar. J.* **12**, 41–41 (2013).

45. Brochet, M. & Billker, O. Calcium signalling in malaria parasites: Calcium in malaria parasites. *Mol. Microbiol.* **100**, 397–408 (2016).

46. Arnou, B. *et al.* The Plasmodium falciparum Ca2+-ATPase PfATP6: insensitive to artemisinin, but a potential drug target. *Biochem. Soc. Trans.* **39**, 823–831 (2011).

47. Zhang, M. *et al.* Uncovering the essential genes of the human malaria parasite *Plasmodium falciparum* by saturation mutagenesis. *Science* **360**, eaap7847 (2018).

48. Coleman, R. Enzymes of triacylglycerol synthesis and their regulation. *Prog. Lipid Res.* **43**, 134–176 (2004).

49. Walther, T. C., Chung, J. & Farese, R. V. Lipid Droplet Biogenesis. *Annu. Rev. Cell Dev. Biol.* **33**, 491–510 (2017).

50. Palacpac, N. M. Q. Developmental-stage-specific triacylglycerol biosynthesis, degradation and trafficking as lipid bodies in Plasmodium falciparum-infected erythrocytes. *J. Cell Sci.* **117**, 1469–1480 (2004).

51. Vielemeyer, O., McIntosh, M. T., Joiner, K. A. & Coppens, I. Neutral lipid synthesis and storage in the intraerythrocytic stages of Plasmodium falciparum. *Mol. Biochem. Parasitol.* **135**, 197–209 (2004).

52. Gulati, S. *et al.* Profiling the Essential Nature of Lipid Metabolism in Asexual Blood and Gametocyte Stages of Plasmodium falciparum. *Cell Host Microbe* **18**, 371–381 (2015).

53. Santiago, T. C., Zufferey, R., Mehra, R. S., Coleman, R. A. & Mamoun, C. B. The *Plasmodium falciparum* PfGatp is an Endoplasmic Reticulum Membrane Protein Important for the Initial Step of Malarial Glycerolipid Synthesis. *J. Biol. Chem.* **279**, 9222–9232 (2004).

54. Lindner, S. E. *et al.* Enzymes involved in plastid-targeted phosphatidic acid synthesis are essential for *P lasmodium yoelii* liver-stage development: *Plasmodium* phosphatidic acid biosynthesis. *Mol. Microbiol.* **91**, 679–693 (2014).

55. Matsusaki, M. *et al.* The Protein Disulfide Isomerase Family: from proteostasis to pathogenesis. *Nov. Meas. Tech. Vis. Live Protein Mol.* **1864**, 129338 (2020).

56. Hatahet, F. & Ruddock, L. W. Protein Disulfide Isomerase: A Critical Evaluation of Its Function in Disulfide Bond Formation. *Antioxid. Redox Signal.* **11**, 2807–2850 (2009).

57. Bechtel, T. J. & Weerapana, E. From structure to redox: The diverse functional roles of disulfides and implications in disease. *PROTEOMICS* **17**, 1600391 (2017).

58. Mouray, E. *et al.* Biochemical properties and cellular localization of Plasmodium falciparum protein disulfide isomerase. *Biochimie* **89**, 337–346 (2007).

59. Mahajan, B. *et al.* Protein disulfide isomerase assisted protein folding in malaria parasites. *Int. J. Parasitol.* **36**, 1037–1048 (2006).

60. Cunnea, P. M. *et al.* ERdj5, an Endoplasmic Reticulum (ER)-resident Protein Containing DnaJ and Thioredoxin Domains, Is Expressed in Secretory Cells or following ER Stress. *J. Biol. Chem.* **278**, 1059–1066 (2003).

61. Ushioda, R. *et al.* ERdj5 Is Required as a Disulfide Reductase for Degradation of Misfolded Proteins in the ER. *Science* **321**, 569–572 (2008).

62. Oka, O. B. V., Pringle, M. A., Schopp, I. M., Braakman, I. & Bulleid, N. J. ERdj5 Is the ER Reductase that Catalyzes the Removal of Non-Native Disulfides and Correct Folding of the LDL Receptor. *Mol. Cell* **50**, 793–804 (2013).

63. Ushioda, R. *et al.* Redox-assisted regulation of Ca^{2+} homeostasis in the endoplasmic reticulum by disulfide reductase ERdj5. *Proc. Natl. Acad. Sci.* **113**, E6055–E6063 (2016).

64. Wang, J., Lee, J., Liem, D. & Ping, P. HSPA5 Gene encoding Hsp70 chaperone BiP in the endoplasmic reticulum. *Gene* **618**, 14–23 (2017).

65. Rudlaff, R. M., Kraemer, S., Marshman, J. & Dvorin, J. D. Three-dimensional ultrastructure of Plasmodium falciparum throughout cytokinesis. *PLOS Pathog.* **16**, e1008587 (2020).

66. Robert-Paganin, J. *et al.* Plasmodium myosin A drives parasite invasion by an atypical force generating mechanism. *Nat. Commun.* **10**, 3286 (2019).

67. Muralidharan, V., Oksman, A., Pal, P., Lindquist, S. & Goldberg, D. E. Plasmodium falciparum heat shock protein 110 stabilizes the asparagine repeat-rich parasite proteome during malarial fevers. *Nat. Commun.* **3**, 1310 (2012).

68. Hayward, J. A. & van Dooren, G. G. Same same, but different: Uncovering unique features of the mitochondrial respiratory chain of apicomplexans. *Mol. Biochem. Parasitol.* **232**, 111204 (2019).

69. Biagini, G. A. *et al.* Generation of quinolone antimalarials targeting the Plasmodium falciparum mitochondrial respiratory chain for the treatment and prophylaxis of malaria. *Proc. Natl. Acad. Sci.* **109**, 8298–8303 (2012).

70. Lu, K.-Y. *et al. Plasmodium* chaperonin TRiC/CCT identified as a target of the antihistamine clemastine using parallel chemoproteomic strategy. *Proc. Natl. Acad. Sci.* **117**, 5810–5817 (2020).

71. Baragaña, B. *et al.* A novel multiple-stage antimalarial agent that inhibits protein synthesis. *Nature* **522**, 315–320 (2015).

72. Baragaña, B. *et al.* Lysyl-tRNA synthetase as a drug target in malaria and cryptosporidiosis. *Proc. Natl. Acad. Sci.* **116**, 7015–7020 (2019).

73. Wong, W. *et al.* Mefloquine targets the Plasmodium falciparum 80S ribosome to inhibit protein synthesis. *Nat. Microbiol.* **2**, 17031 (2017).

74. Li, H. *et al.* Identification of Potent and Selective Non-covalent Inhibitors of the *Plasmodium falciparum* Proteasome. *J. Am. Chem. Soc.* **136**, 13562–13565 (2014).

75. Ng, C. L., Fidock, D. A. & Bogyo, M. Protein Degradation Systems as Antimalarial Therapeutic Targets. *Trends Parasitol.* **33**, 731–743 (2017).

76. Gantt, S. M. *et al.* Proteasome Inhibitors Block Development ofPlasmodium spp. *Antimicrob. Agents Chemother.* **42**, 2731–2738 (1998).

77. Czesny, B., Goshu, S., Cook, J. L. & Williamson, K. C. The Proteasome Inhibitor Epoxomicin Has Potent Plasmodium falciparum Gametocytocidal Activity. *Antimicrob. Agents Chemother.* **53**, 4080–4085 (2009).

78. Kaplan, A. *et al.* Small molecule-induced oxidation of protein disulfide isomerase is neuroprotective. *Proc. Natl. Acad. Sci.* **112**, E2245–E2252 (2015).

79. Hoffstrom, B. G. *et al.* Inhibitors of protein disulfide isomerase suppress apoptosis induced by misfolded proteins. *Nat. Chem. Biol.* **6**, 900–906 (2010).

80. Xu, S. *et al.* Discovery of an orally active small-molecule irreversible inhibitor of protein disulfide isomerase for ovarian cancer treatment. *Proc. Natl. Acad. Sci.* **109**, 16348–16353 (2012).

81. Vatolin, S. *et al.* Novel Protein Disulfide Isomerase Inhibitor with Anticancer Activity in Multiple Myeloma. *Cancer Res.* **76**, 3340–3350 (2016).

82. Lee, A. H., Symington, L. S. & Fidock, D. A. DNA Repair Mechanisms and Their Biological Roles in the Malaria Parasite Plasmodium falciparum. *Microbiol. Mol. Biol. Rev.* **78**, 469–486 (2014).

83. Maier, A. G., Braks, J. A. M., Waters, A. P. & Cowman, A. F. Negative selection using yeast cytosine deaminase/uracil phosphoribosyl transferase in Plasmodium falciparum for targeted gene deletion by double crossover recombination. *Mol. Biochem. Parasitol.* **150**, 118–121 (2006).

84. Duraisingh, M. T., Triglia, T. & Cowman, A. F. Negative selection of Plasmodium falciparum reveals targeted gene deletion by double crossover recombination. *Int. J. Parasitol.* **32**, 81–89 (2002).

85. Collins, C. R. *et al.* Robust inducible Cre recombinase activity in the human malaria parasite *Plasmodium falciparum* enables efficient gene deletion within a single asexual erythrocytic growth cycle: Conditional Cre in the human malaria parasite. *Mol. Microbiol.* **88**, 687–701 (2013).

86. Ganesan, S. M., Falla, A., Goldfless, S. J., Nasamu, A. S. & Niles, J. C. Synthetic RNA–protein modules integrated with native translation mechanisms to control gene expression in malaria parasites. *Nat. Commun.* **7**, 10727 (2016).

87. Prommana, P. *et al.* Inducible Knockdown of Plasmodium Gene Expression Using the glmS Ribozyme. *PLoS ONE* **8**, e73783 (2013).

88. Muralidharan, V., Oksman, A., Iwamoto, M., Wandless, T. J. & Goldberg, D. E. Asparagine repeat function in a Plasmodium falciparum protein assessed via a regulatable fluorescent affinity tag. *Proc. Natl. Acad. Sci.* **108**, 4411–4416 (2011).

89. Birnbaum, J. *et al.* A genetic system to study Plasmodium falciparum protein function. *Nat. Methods* **14**, 450–456 (2017).

90. Wagner, J. C., Platt, R. J., Goldfless, S. J., Zhang, F. & Niles, J. C. Efficient CRISPR-Cas9–mediated genome editing in Plasmodium falciparum. *Nat. Methods* **11**, 915–918 (2014).

91. Ghorbal, M. *et al.* Genome editing in the human malaria parasite Plasmodium falciparum using the CRISPR-Cas9 system. *Nat. Biotechnol.* **32**, 819–821 (2014).

92. Kudyba, H. M., Cobb, D. W., Florentin, A., Krakowiak, M. & Muralidharan, V. CRISPR/Cas9 Gene Editing to Make Conditional Mutants of Human Malaria Parasite P. falciparum. *J. Vis. Exp. JoVE* 57747 (2018) doi:10.3791/57747.

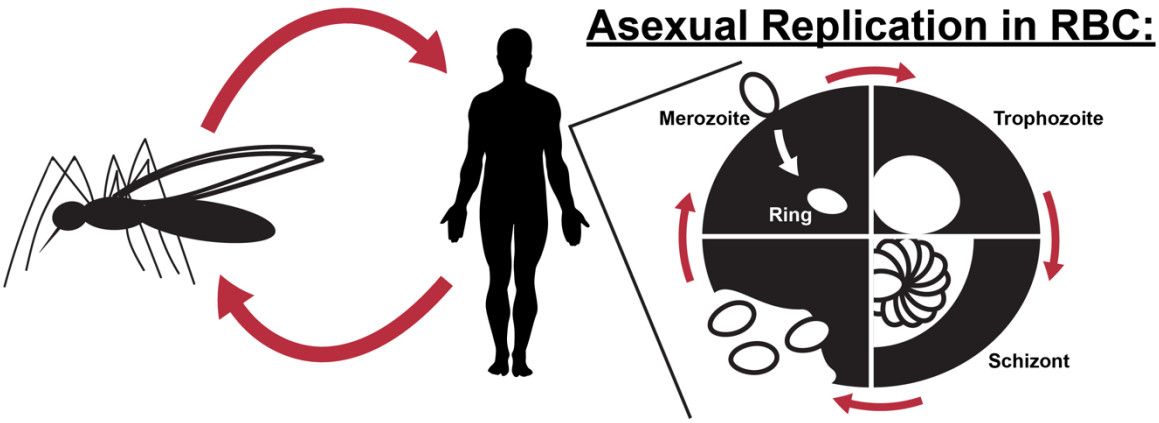

Figure 1.1. Asexual replication of *P. falciparum* inside of human RBCs. A merozoite invades a red blood cell (RBC), becoming a “Ring” stage parasite that transitions into the Trophozoite, which consumes the cytoplasm of the RBC. After the hemoglobin content of the RBC has been consumed by the Trophozoite, the parasite undergoes schizogony in the Schizont stage, replicating its genome and producing new daughter merozoites that egress and invade new host RBCs.

CHAPTER 2

CRISPR/CAS9 GENE EDITING TO MAKE CONDITIONAL MUTANTS OF HUMAN MALARIA PARASITE *P. FALCIPARUM*

David W. Cobb*, Heather M. Kudyba*, Anat Florentin, Michelle Krakowiak, Vasant Muralidharan. 2018. *Journal of Visualized Experiments*. (139): 57747. *Equal contributions. Reprinted here with permission of the publisher.

ABSTRACT

Malaria is a significant cause of morbidity and mortality worldwide. This disease, which primarily affects those living in tropical and subtropical regions, is caused by infection with *Plasmodium* parasites. The development of more effective drugs to combat malaria can be accelerated by improving our understanding of the biology of this complex parasite. Genetic manipulation of these parasites is key to understanding their biology; however, historically the genome of *P. falciparum* has been difficult to manipulate. Recently, CRISPR/Cas9 genome editing has been utilized in malaria parasites, allowing for easier protein tagging, generation of conditional protein knockdowns, and deletion of genes. CRISPR/Cas9 genome editing has proven to be a powerful tool for advancing the field of malaria research. Here, we describe a CRISPR/Cas9 method for generating *glmS*-based conditional knockdown mutants in *P. falciparum*. This method is highly adaptable to other types of genetic manipulations, including protein tagging and gene knockouts.

INTRODUCTION

Malaria is a devastating disease caused by protozoan parasites of the genus *Plasmodium*. *P. falciparum*, the most deadly human malaria parasite, causes approximately 445,000 deaths per year, mostly in children under the age of five[1]. *Plasmodium* parasites have an intricate life cycle involving a mosquito vector and a vertebrate host. Humans first become infected when an infected mosquito takes a blood meal. Then, the parasite invades the liver where it grows,

develops, and divides for approximately one week. After this process, the parasites are released into the bloodstream, where they undergo asexual replication in red blood cells (RBCs). Growth of the parasites within the RBCs are directly responsible for the clinical symptoms associated with malaria[2].

Until recently, production of transgenic *P. falciparum* was a laborious process, involving several rounds of drug selection that took many months and had a high failure rate. This time-consuming procedure relies on the generation of random DNA breaks in the region of interest and the endogenous ability of the parasite to mend its genome though homologous repair[3-6]. Recently, Clustered Regularly Interspaced Palindromic Repeat/Cas9 (CRISPR/Cas9) genome editing has been successfully utilized in *P. falciparum*[7,8]. The introduction of this new technology in malaria research has been critical for advancing understanding of the biology of these deadly *Plasmodium* parasites. CRISPR/Cas9 allows for specific targeting of genes through guide RNAs (gRNAs) that are homologous to the gene of interest. The gRNA/Cas9 complex recognizes the gene through the gRNA, and Cas9 then introduces a double-strand break, forcing the initiation of repair mechanisms in the organism[9,10]. Because *P. falciparum* lacks the machinery to repair DNA breaks through non-homologous end joining, it utilizes homologous recombination mechanisms and integrates transfected homologous DNA templates to repair the Cas9/gRNA-induced double-strand break[11,12].

Here, we present a protocol for the generation of conditional knockdown mutants in *P. falciparum* using CRISPR/Cas9 genome editing. The protocol demonstrates usage of the *glmS* ribozyme to conditionally knockdown protein

levels of *Pf*Hsp70x (PF3D7_0831700), a chaperone exported by *P. falciparum* into host RBCs[13,14]. The *glmS* ribozyme is activated by treatment with glucosamine (which is converted to glucosamine-6-phosphate in cells) to cleave its associated mRNA, leading to a reduction in the protein[14]. This protocol can be easily adapted to utilize other conditional knockdown tools, such as destabilization domains or RNA aptamers[4,5,15]. Our protocol details the generation of a repair plasmid consisting of a hemagglutinin (HA) tag and *glmS* ribozyme coding sequence flanked by sequences that are homologous to the *Pf*Hsp70x open reading frame (ORF) and 3'-UTR. We also describe the generation of a second plasmid to drive expression of the gRNA. These two plasmids, along with a third that drives expression of Cas9, are transfected into RBCs and used to modify the genome of *P. falciparum* parasites. Finally, we describe a polymerase chain reaction (PCR)-based technique to verify integration of the tag and *glmS* ribozyme. This protocol is highly adaptable for the modification or complete knockout of any *P. falciparum* genes, enhancing our ability to generate new insights into the biology of the malaria parasite.

PROTOCOL

Continuous culture of *P. falciparum* requires the use of human RBCs, and we utilized commercially purchased units of blood that were stripped of all identifiers and anonymized. The Institutional Review Board and the Office of Biosafety at the University of Georgia reviewed our protocols and approved all protocols used in our lab.

1. Choosing a gRNA Sequence

1.1. Go to CHOPCHOP (http://chopchop.cbu.uib.no/) and select Fasta Target. Under Target, paste the 200 base pairs from the 3' end of the open reading frame (ORF) of a gene and 200 base pairs from the start of the gene's 3'-UTR. Under In, select *P. falciparum* (3D7 v3.0), and select CRISPR/Cas9 under Using. Next, click Find Target Sites.

1.2. Select a gRNA sequence from the options presented, giving preference to the most efficient gRNA that is closest to the site of modification and that has the fewest off-target sites.

Note: Potential gRNA sequences are identified because they are immediately upstream of a Protospacer Adjacent Motif (PAM), which is required for recruitment of Cas9 to DNA. The sequence that is cloned into pMK-U6, the vector that drives gRNA expression, is the 20 bases immediately upstream of the PAM. The PAM specific for *S. pyogenes* Cas9 is the nucleotide sequence NGG and should not be included in the sequence that is cloned into pMK-U6.

Note: CHOPCHOP visually ranks the gRNA sequences, displaying the best options in green, the less ideal options in amber, and the worst options in red. CHOPCHOP gives each gRNA sequence an efficiency score that is calculated using the most up-to-date parameters found in the literature, and they predict off-

target sites that could be recognized by the gRNA. Two or three gRNA sequences may need to be attempted to find the gRNA best suited to a particular gene.

1.3. Purchase the gRNA sequence and its reverse-complement as Polyacrylamide Gel Electrophoresis-purified oligos. The gRNA sequence used to target *Pf*HSP70x can be found in **Figure 2.1B**.

Note: This oligo should include 15 base pairs homologous to the gRNA-expressing plasmid, which are necessary for sequence and ligation-independent cloning (SLIC) into the pMK-U6 vector[16].

2. Cloning the gRNA Sequence into pMK-U6

2.1. Digest the pMK-U6 with BtgZI.

2.1.1. Digest 10 µg of pMK-U6 with 5 µL of BtgZI enzyme (5000 units/mL) for 3 h at 60 °C. Follow the enzyme manufacturer's protocol for reaction conditions.

2.1.2. After the 3 h incubation period, add an additional 3 µL of BtgZI to the reaction to ensure complete digestion of the plasmid. Digest for an additional 3 h, still following the manufacturer's instructions for ensuring the correct reaction conditions.

2.1.3. To purify the digested pMK-U6 from the reaction, use a column-based PCR cleanup kit according to the manufacturer's instructions.

2.1.4. Separate the digested DNA using a 0.7% agarose gel and extract the 4,200-base pair band.

2.2. Anneal the oligos containing the gRNA sequence.

2.2.1. Reconstitute the PAGE-purified oligos to a concentration of 100 µM using nuclease-free water.

2.2.2. Combine 10 µL of each oligo with 2.2 µL of 10x buffer 2 (see **Table 2.1**). Ensure that the total reaction volume is 22.2 µL.

2.2.3. Run the gRNA annealing program in a thermocycler: Step 1- 95 °C, 10 min; step 2- 95 °C, 1 s, with a reduction in temperature of 0.6 °C/cycle; step 3- Go to step 2, 16 times; step 4- 85 °C, 1 min; step 5- 85 °C, 1 s, with a reduction in temperature of 0.6°C/cycle; step 6- Go to step 5, 16 times; step 7- 75 °C, 1 min; step 8- 75 °C, 1 s, with a reduction in temperature of 0.6 °C/cycle; step 9- Go to step 8, 16 times. Steps 10 to 21- Repeat the procedure used in Steps 4-9 until the temperature reaches 25 °C; step 22- 25 °C, 1 min.

2.3. Insert the annealed gRNA oligos into the BtgZI-digested and gel-purified pMK-U6 plasmid.

2.3.1. Combine 100 ng of digested pMK-U6 with 1 µL of 10x buffer 2.1 and 3 µL of annealed gRNA oligos. Increase the volume to 9.5 µL with nuclease-free water.

2.3.2. Add 0.5 µL of T4 polymerase and incubate the reaction at room temperature for 2.5 min.

2.3.3. Move the reaction to ice and incubate for 10 min.

2.3.4. Immediately transform 5 µL of the reaction into competent *E. coli* according to the bacteria supplier's instructions. Plate the bacteria on Lysogeny Broth (LB) agar plates containing 100 µg/mL Ampicillin.

2.3.5. Allow the transformed bacteria to grow at 37 °C overnight, then select colonies and extract DNA with a commercially available plasmid miniprep kit.

3. Designing Homology Regions of the Repair Template

3.1. Design shield mutations within the homology repair template to prevent re-cutting of the DNA that is integrated into the genome.

Note: A shield mutation typically consists of introducing a silent mutation to alter the PAM so that Cas9 will not induce a break in the repair template. The PAM required for the Cas9 used in this protocol is the nucleotide sequence “NGG”, where “N” is any nucleotide. If possible, change one of the G nucleotides to an A, C, or T.

3.1.1. If the PAM cannot be silently mutated, introduce at least 2 silent mutations into the 6 base pairs directly adjacent to the PAM[7,8].

Note: These mutations will prevent recognition of the repair template by the gRNA and prevent re-cutting of the repaired locus by the Cas9/gRNA complex. The shield mutations can be introduced into the homology region by amplifying the DNA with primers that contain the mutation.

3.2. Amplify the ORF homology region for the repair template.

3.2.1. Using PCR, amplify 800 base pairs from the 3’ end of the target gene’s ORF. Design the primers that will be used to exclude the stop codon from this amplicon.

3.2.2. Design the primers for insertion of this amplicon into the pHA-glmS that has been digested with SacII and AfeI through either a DNA ligation reaction or SLIC16.

3.3. Amplify the 3'-UTR homology region for the repair template.

3.3.1. Using PCR, amplify the 800 base pairs immediately following the stop codon of the target gene. Design primers for insertion of this amplicon into the pHA-glmS that has been digested with HindIII and NheI through either a DNA ligation reaction or SLIC[16].

Note: The high AT content of the *P. falciparum* genome can make amplification of regions such as UTRs difficult. An alternative approach to using PCR is synthesizing the homology regions.

4. Cloning Homology Regions into the Repair Plasmid

4.1. Insert the ORF homology region into the pHA-glmS.

4.1.1. Digest the pHA-glmS with SacII and AfeI, according to the enzyme manufacturer's instructions. Insert the ORF homology region PCR product into the digested plasmid using SLIC[16].

4.1.2. Transform into competent *E. coli* as performed in steps 2.3.4 and 2.3.5.

4.2. Insert the 3'-UTR homology region into a pHA-glmS plasmid that already contains the ORF homology region (see step 4.1).

4.2.1. Digest the plasmid with HindIII and NheI according to the enzyme manufacturer's instructions. Insert the 3'-UTR homology region amplicon into the digested plasmid using SLIC[16].

4.2.2. Transform into competent *E. coli* and extract the plasmid DNA (steps 2.3.4 and 2.3.5).

5. Precipitating DNA for Transfection

5.1. Add 40 µg each of pMK-U6, pUF1-Cas9, and pHA-glmS DNA (for a total of 120 µg of DNA) into a sterile 1.5 mL microcentrifuge tube.

5.2. Add 1/10th the volume of DNA of 3 M sodium acetate in water (pH 5.2) to the tube and mix it well using a vortex (e.g., if the volume in step 5.1 was 100 µL, add 10 µL of sodium acetate).

5.3. Add 2.5 times the volume of 100% ethanol to the tube and mix it well using a vortex for at least 30 s (e.g., if the volume in 5.1 was 100 µL, add 250 µL of 100% ethanol).

5.4. Place the tube on ice or at -20 °C for 30 min.

5.5. Centrifuge the tube at 18,300 x g for 30 min at 4 °C.

5.6. Carefully remove the supernatant from the tube. Do not disturb the pellet.

5.7. Add 3 times the volume of 70% ethanol to the tube and mix it briefly using a vortex (e.g., if the volume in 5.1 was 100 µL, add 300 µL of 70% ethanol).

5.8. Centrifuge the tube at 18,300 x g for 30 min at 4 °C.

Note: This step should be performed under sterile conditions in a biological safety cabinet.

5.9. Carefully remove the supernatant from the tube. Do not disturb the pellet. Leave the tube open and allow the pellet to air-dry for 15 min.

5.10. Store the precipitated DNA at -20 °C until it is needed for transfection.

6. Isolating Human RBCs from Whole Blood in Preparation for Transfection

6.1. Aliquot fresh blood into sterile 50 mL conical tubes (approximately 25 mL per tube).

6.2. Centrifuge the tubes at 1088 x g for 12 min, with centrifuge brakes set to 4.

6.3. Aspirate off the supernatant and buffy coat. Resuspend the RBC pellet with an equal volume of incomplete RPMI.

Note: Incomplete RPMI is prepared by supplementing RPMI 1640 with 10.32 μM thymidine, 110.2 μM hypoxanthine, 1 mM sodium pyruvate, 30 mM sodium bicarbonate, 5 mM HEPES, 11.1 mM glucose, and 0.02% (v/v) gentamicin.

6.4. Repeat steps 6.2-6.3 twice. After the last wash, resuspend the RBCs in an equal volume of incomplete RPMI and store the tubes at 4 °C.

7. Transfecting RBCs with the CRISPR/Cas9 Plasmids (to be done aseptically)

Note: *P. falciparum* cultures are maintained as described in other reports[17]. Maintain all the cultures at 37 °C under 3% O2, 3% CO2, and 94% N2 unless stated otherwise. Whenever blood is used in this protocol, it is referring to the pure red blood cells prepared in step 6. The blood used should not be older than 6 weeks, as there is typically a decrease in parasite proliferation in older blood. The following steps describe pre-loading RBCs with DNA and adding a parasite culture to the transfected cells. Other established transfection protocols are compatible with transfecting these constructs[18,19].

7.1. Prepare a 1x cytomix buffer in water (120 mM KCl, 0.15 mM CaCl2, 2 mM EGTA, 5 mM MgCl2, 10 mM K2HPO4, 25 mM HEPES, pH 7.6). Filter-sterilize the buffer using a 0.22 μm filter.

7.2. Add 380 μL of the 1x cytomix to the DNA precipitated in step 5, and vortex to dissolve. Allow the DNA to dissolve in the 1x cytomix for 10 minutes, vortexing every 3 min for 10 s.

7.3. In a sterile 15 mL conical tube, combine 300 μL of RBCs (50% hematocrit, from step 6) in the incomplete RPMI with 4 mL of 1x cytomix.

7.4. Centrifuge the RBCs from step 7.3 at 870 x g for 3 min, and then remove the supernatant from the RBC pellet.

7.5. Resuspend the RBC pellet with the DNA/cytomix mixture from step 6.2 and transfer to a 0.2 cm electroporation cuvette.

7.6. Electroporate the RBCs using the following conditions: 0.32kV, 925 μF, capacitance set to “High Cap”, and resistance set to “Infinite”.

7.7. Following electroporation, transfer the contents from the cuvette to a 15 mL conical containing 5 mL of complete RPMI (cRPMI). Centrifuge the tube at 870 x g for 3 min at 20 °C, and then decant the supernatant.

Note: cRPMI is prepared through the same method as incomplete RPMI with the addition of 0.25% (w/v) lipid-rich bovine serum albumin.

7.8. Resuspend the pellet in 4 mL of cRPMI and transfer to one well in a 6-well tissue culture plate. Add 400 µL of a high-schizont culture (7-10% schizont parasitemia is ideal) to the transfected RBCs.

Note: Parasitemia is defined as the percentage of parasite-infected RBCs.

7.9. The next day, wash the culture with 4 mL of cRPMI. Centrifuge the culture at 870 x g for 3 min and aspirate the supernatant. Resuspend the culture in 4 mL of cRPMI.

7.10. 48 h after completing step 7.6, wash the culture with 4 mL of cRPMI. Then resuspend the culture in cRPMI containing 1 µM DSM1 to select for the Cas9 plasmid.

7.11. Continue washing the cultures each day with cRPMI until parasites are no longer visible by blood smear. After this point, replace the culture medium with fresh cRPMI plus 1 µM DSM1 every 48 h.

7.11.1. To make a blood smear, pipette 150 µL of culture into a 0.6 mL centrifuge tube. Pellet the cells by centrifugation at 1700 x g for 30 s.

7.11.2. Aspirate off the supernatant. Use a pipette to transfer the pelleted cells to a glass slide. Using a second glass slide held at a 45° angle to the first slide, smear the blood droplet. Stain the slide using a commercially available staining kit according to the manufacturer's protocol.

7.11.3 View the parasites using a 100X oil immersion objective.

7.12. Beginning 5 days post-transfection (step 7.6), remove 2 mL of the culture with RBCs resuspended in the culture medium. Add back 2 mL of fresh medium (cRPMI plus 1 µM DSM1) and blood at 2% hematocrit. Add fresh blood in this manner once a week until parasites reappear, as determined by thin blood smear (step 7.11).

Note: If integration is successful, parasites generally reappear in the culture by one-month post-transfection.

7.13. Once parasites reemerge, remove DSM1 drug pressure. Alternatively, remove drug pressure after parasites have been cloned out.

8. Checking Parasites for Integration of the Repair Template

8.1. When parasites are visible again by thin blood smear, isolate DNA from the culture using an appropriate kit.

8.2. Use PCR to amplify the modified region of the genome to determine if the targeted locus has been successfully altered and if the unmodified wild-type locus (indicative of wild-type parasites) is detectable.

8.2.1. To detect parasites that have integrated the repair template, use a forward primer that sits at the beginning of the ORF, outside of the cloned homology region. Use a reverse primer that sits in the 3'-UTR.

Note: As this amplification includes the sequences of the HA tags and *glmS* ribozyme, amplicons from integrated parasites will be longer than the same region amplified in wild-type parasites.

9. Cloning Parasites by Limiting Dilution

9.1 Perform serial dilutions of the parasite culture from step 7.13 to achieve a final concentration of 0.5 parasites/200 µL. Add 200 µL of the diluted culture to the wells of a 96-well tissue culture plate.

Note: Because parasitemia is defined as the percentage of infected RBCs and the hematocrit is also a defined number (2%), the number of parasites per unit volume is easily inferred.

9.1.1. Prepare 1 mL of culture in cRPMI at 5% parasitemia and 2% hematocrit (at these parasitemia and hematocrit levels, the culture contains 1 x 10^7 parasites/mL).

9.1.2. Dilute this culture 1:100 with cRPMI. Dilute again 1:100 with cRPMI.

9.1.3. Dilute 1:400. Perform this dilution by adding 62.5 µL of culture to 25 mL of cRPMI and 1 mL of blood. This dilution results in the desired concentration of 0.5 parasites/200 µL.

9.2. Maintain the cloning plate until parasites are detectable in the wells.

9.2.1. Every 48 h, replace the medium in the 96-well plate with fresh medium.

9.2.2. Once a week, starting 5 days after beginning the cloning plate (step 9.1), remove 100 µL from each well and add back 100 µL of fresh medium + blood (2% hematocrit).

9.3. Identify any wells containing parasites.

9.3.1. Place the 96-well plate at a 45° angle for approximately 20 min, allowing the blood to settle at an angle within the plate.

9.3.2. Place the 96-well plate on a light box. Notice that the wells containing parasites contain media that is yellow in color, compared to the pink media of parasite-free wells, due to acidification of the medium by the parasites.

9.3.3. Using a serological pipette, move the contents of the parasite-containing wells to a 24-well tissue culture plate to allow expansion of the parasitemia.

9.3.4. Using PCR analysis as described in step 8, check these clonal parasite lines for correct integration.

10. Knockdown of the Protein by Treating Parasites with Glucosamine and Confirmation via Western Blot Analysis

10.1. Prepare a 0.5 M GlcN (glucosamine) stock solution, which can be stored at -20° C.

10.2. Add GlcN to the *glmS* parasite cultures and allow them to grow in the presence of GlcN.

Note: The final concentration and timing of GlcN treatment depends on the experiment and parasite line. GlcN can impact parasite growth, so the parental parasite strain should be exposed to a range of GlcN concentrations to determine its sensitivity to the compound. Often, a concentration of 2.0-7.5 mM GlcN is used[13,14,20].

10.3. Isolate protein samples from the GlcN-treated parasites[13].

10.4. Use protein samples for western blot analysis to detect reductions in the protein[13].

10.4.1. Use an anti-HA antibody according to the manufacturer's instructions to detect the HA-*glmS*-tagged protein. Compare the HA band to a loading control, such as *Pf*EF1α.

REPRESENTATIVE RESULTS

A schematic of the plasmids used in this method as well as an example of a shield mutation are shown in **Figure 2.1**. As an example of how to identify mutant parasites after transfection, results from PCRs for checking integration of the HA-*glmS* construct are shown in **Figure 2.2**. A representative image of a cloning plate is shown in **Figure 2.3** to demonstrate the color change of the medium in the presence of parasites. Results from an immunofluorescence assay and western blotting experiments are shown in **Figure 2.4** to demonstrate the

functionality of the HA tag and *glmS*-based reductions of proteins in the parasites. **Figure 2.5** demonstrates the inability of short homology arms on PCR products to modify the parasite genomes and obtain viable mutants.

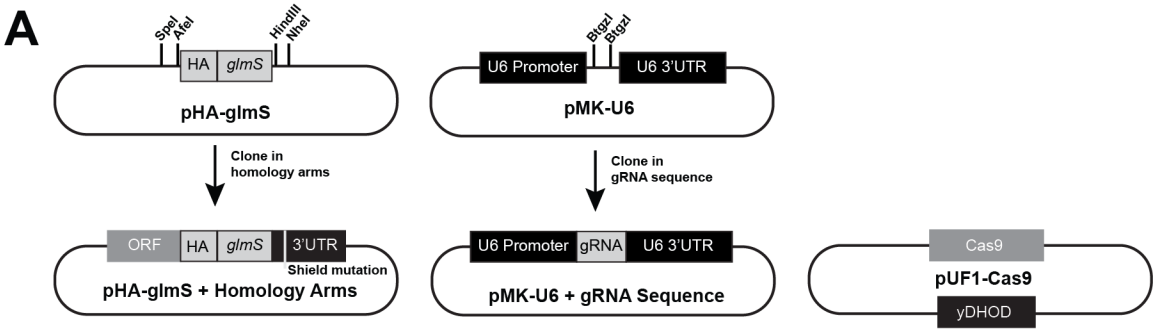

B **PfHsp70x gRNA oligo cloned into pMK-U6:**
5'-taagtatataatattTGCATTATTGTTGTATATTTgttttagagctagaa-3'

Genomic target of PfHsp70x gRNA + the PAM:
5'-TGCATTATTGTTGTATATTTTGG-3'
PAM

Genomic target of PfHsp70x gRNA + Shield Mutation in the PAM
5'-TGCATTATTGTTGTATATTTTCG-3'
Shield Mutation

Figure 2.1: Summary of our three-plasmid approach to CRISPR/Cas9 and examples of a gRNA oligo and shield mutation. (A) Schematics of empty pHA-glmS and pMK-U6 are shown with the restriction enzyme sites used for cloning. Also shown are pHA-glmS and pMK-U6 after the homology arms and gRNA sequences have been cloned into them, respectively. Finally, pUF1-Cas9 is shown. yDHOD = yeast dihydrofolate reductase, the resistance marker to DSM1. **(B)** The forward oligo used for cloning the *Pf*Hsp70x gRNA sequence into pMK-U6 is shown, with the gRNA sequence in capital letters and the pMK-U6

homology arms necessary for cloning in lowercase letters (top). The genomic target of the *Pf*Hsp70x gRNA is shown as the downstream PAM, in red (middle). The shield mutation in the *Pf*Hsp70x gRNA PAM is shown in red (bottom).

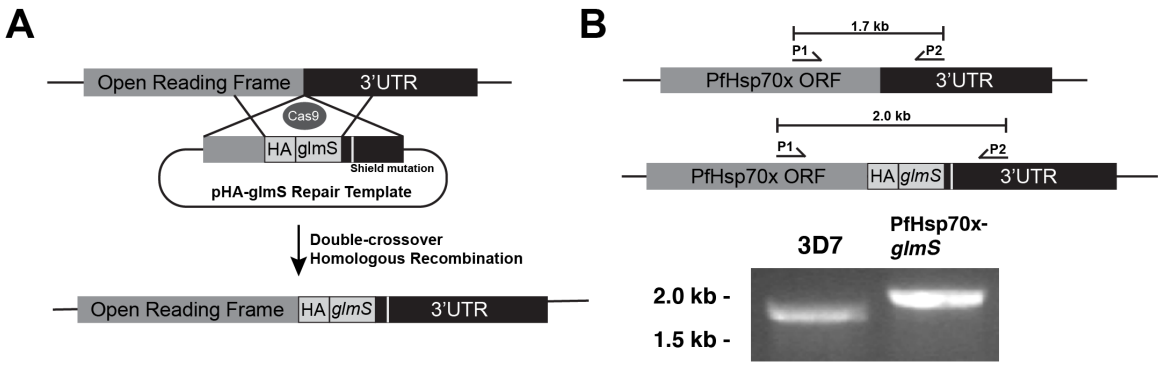

Figure 2.2: Schematic of CRISPR/Cas9 genome modification using pHA-glmS and a strategy for confirming integration. (A) Cas9, guided to a genomic locus by a gRNA, induces a double strand break in the DNA. The parasite repairs the damage through double crossover homologous repair, using the pHA-glmS plasmid as a template and introducing the HA-*glmS* sequence into the genome. **(B)** A PCR test to identify correct integration of the HA-*glmS* sequence. Using primers P1 and P2, the 3' ORF of wild-type *Pf*Hsp70x and *Pf*Hsp70x-glmS mutants are amplified[13]. The amplicon from *Pf*Hsp70x-*glmS* is longer than wild-type due to insertion of the HA-*glmS* sequence.

A

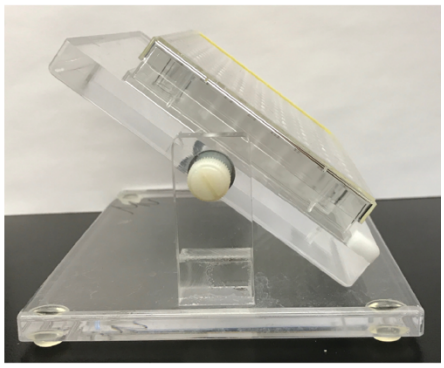

B

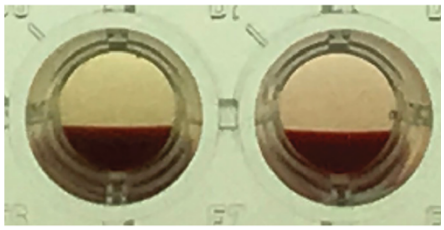

Figure 2.3: Identification of wells containing parasites in a 96-well cloning plate. (A) The 96-well plate is set at a 45° angle for approximately 20 minutes to allow the blood to settle at an angle in the plate. **(B)** The well on the left contains a parasite culture, indicated by the yellow color of the medium in comparison to the pink medium of the parasite-free well on the right.

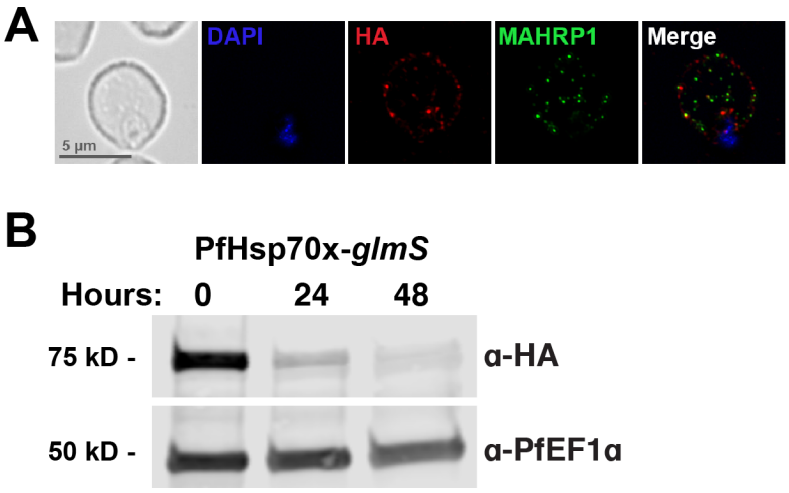

Figure 2.4: An immunofluorescence assay shows the correct HA-tagging of *Pf*Hsp70x and Western blotting shows reduction of *Pf*Hsp70x protein levels during treatment with glucosamine. (A) *Pf*Hsp70x-*glmS* parasites were fixed and stained with DAPI (nucleus marker) and antibodies to HA and MAHRP1 (Membrane Associated Histidine Rich Protein 1, a marker of protein export to the host RBC)[13]. **(B)** PfHsp70x-*glmS* parasites were treated with 7.5 mM glucosamine, and whole-parasite lysates were used for Western blotting analysis[13]. The membrane was probed with antibodies for HA and *Pf*EF1α as a loading control[13]. As expected, glucosamine treatment resulted in a reduction of the protein.

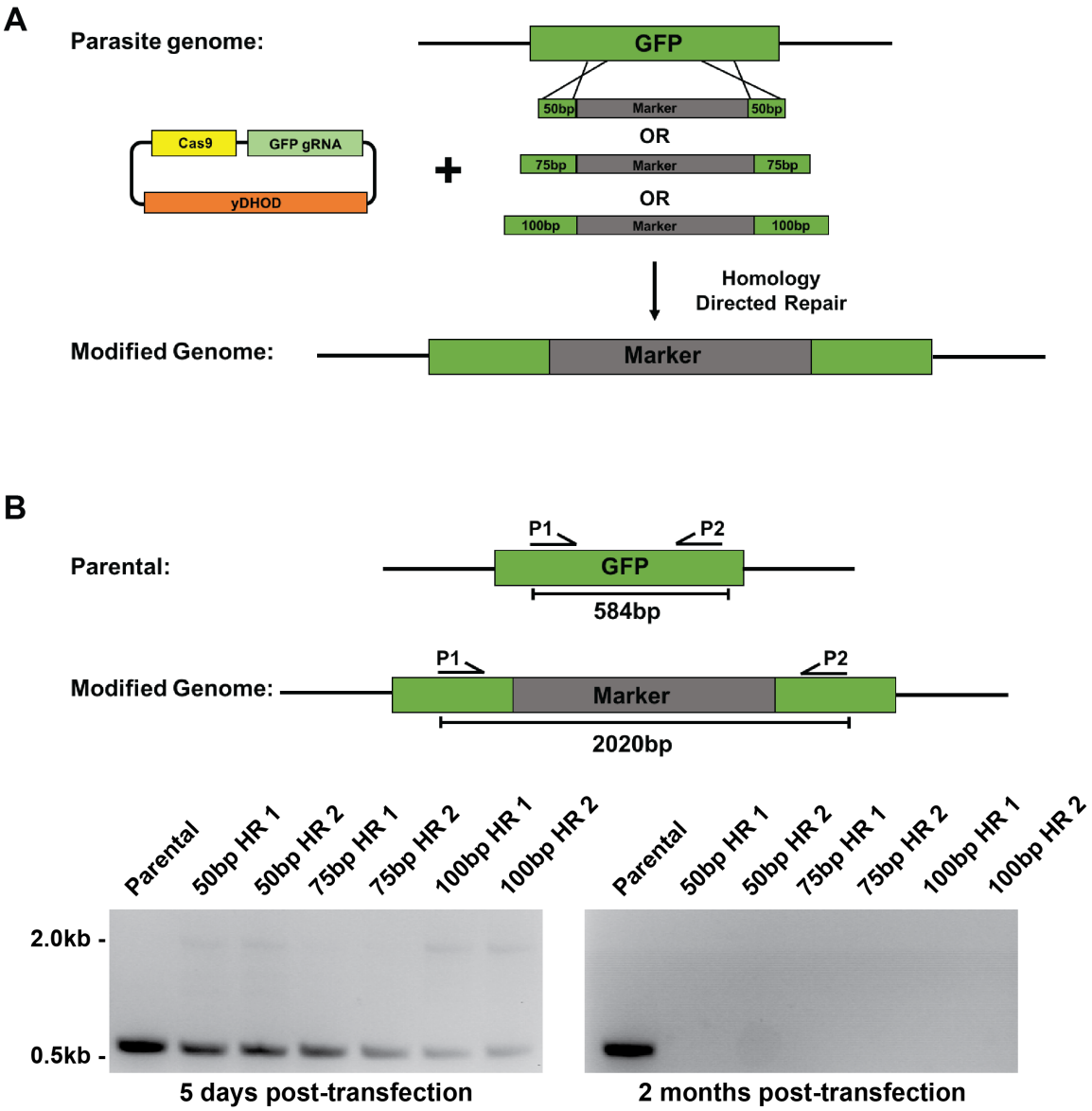

Figure 2.5: Using short homology sequences for repair. (A) Schematic representation showing knockout of GFP in B7 parasites[21]. B7 parasites are a derivative of 3D7 in which Plasmepsin II has been tagged with GFP. PCR products containing 50, 75, or 100 base pairs of GFP homology regions flanking a blasticidin S resistance cassette (labeled “marker”), along with pUF1-Cas9-eGFP-gRNA, a plasmid expressing Cas9 and a GFP gRNA, were transfected into B7 parasites. Each transfection was carried out twice. DSM1 drug pressure

was applied 2 days post-transfection. **(B)** Shown here are PCR tests on DNA isolated from transfected parasites 5 days post-transfection and 2 months post-transfection. Primers used to test integration of the BSD resistance cassette will yield a 584-base pair product for B7 parental parasites and a 2020-base pair product for parasites that have integrated the marker.

DISCUSSION

The implementation of CRISPR/Cas9 in *P. falciparum* has both increased the efficiency of and decreased the amount of time needed for modifying the parasite's genome, compared to previous methods of genetic manipulation. This comprehensive protocol outlines the steps necessary for generating conditional mutants using CRISPR/Cas9 in *P. falciparum*. While the method here is geared specifically for the generation of HA-*glmS* mutants, this strategy can be adapted for a variety of needs, including the tagging of genes, gene knockouts, and the introduction of point mutations.

A critical early step in this protocol is the selection of a gRNA sequence. When selecting a gRNA, there are several points to consider such as where the gRNA sits, how efficient it is, and whether or not it has the potential for off-target effects. The gRNA sequence should be as close as possible to the site of modification, ideally within 200 base pairs. This decreases the likelihood of the parasites using the repair template to fix their genome without integrating the tag. The tool used here to locate the gRNA was a free, online service called CHOPCHOP[22]. Another online tool, Eukaryotic Pathogen CRISPR guide

RNA/DNA Design Tool (EuPaGDT; http://grna.ctegd.uga.edu/), can also be used[23]. EuPaGDT provides additional characterization of gRNA sequences, including prediction of off-target hits and potential issues that may prevent transcription of the gRNA. EuPaGDT also has tools for batch processing of gRNAs to target multiple genes or whole genomes. The selected gRNA should be one that sits closest to the site of modification with the highest efficiency and minimal off-target hits. An important limitation of CRISPR/Cas9 gene editing that may arise is the inability to design a suitable gRNA to target the gene of interest. In such cases, a trial-and-error approach may be needed, using multiple sub-optimal gRNA sequences until the best option is found, and successful gene editing has occurred.

Another important factor to consider when generating *P. falciparum* mutants using CRISPR/Cas9 is the length of the homology regions used in the repair template. This protocol recommends that the homology regions should be approximately 800 base pairs each, but we have also been successful in using smaller regions numbering 500 base pairs[3]. Successful genome modification using CRISPR/Cas9 and short homology arms on PCR products have also been used in other protozoan parasites such as *Toxoplasma gondii* and *Trichomonas vaginalis*[24,25]. We tested the feasibility of using smaller homology arms on PCR products (50, 75, or 100 base pairs) by attempting to knockout GFP in B7 parasites using a blasticidin resistance cassette[21]. We saw some integration of the blasticidin resistance cassette at 5 days post transfection; however, these parasites never recovered from transfection. For these transfections, we selected

for the Cas9-expressing plasmid using DSM1. A different selection method, such as treating transfected cultures with blasticidin S alone or in combination with DSM1, may improve the chances of parasites reappearing when using shorter homology regions for repairing the Cas9/gRNA-induced breaks. In this case, we did not select with blasticidin S since we wanted to test if short homology arms could be used in instances where a drug resistance cassette is not being integrated into the genome, such as when a protein is being tagged.

The core components of CRISPR/Cas9 gene editing discussed are the Cas9 endonuclease, the gRNA, and the repair template. We describe a three-plasmid approach to introduce these components into the parasites, where Cas9, the gRNA, and the repair template are found in separate plasmids. In addition to this approach, our lab has been successful in using a two-plasmid approach in which Cas9 and gRNA expression are driven by a single plasmid and the repair template is found in a second plasmid[3]. Similar two-plasmid approaches have also been successfully employed by other labs to generate mutants[7,8,26-29]. Furthermore, several labs are using a strain of *Plasmodium* (NF54^{attB}) which constitutively expresses Cas9 and a T7 RNA polymerase to drive expression of gRNAs[30]. In this case, a single plasmid containing the repair template and the gRNA are transfected into NF54^{attB} parasites[31,32]. Finally, a plasmid-free approach utilizing a purified Cas9-gRNA ribonucleoprotein complex has been used to insert mutations into the genome, as well[33]. The success of these different approaches demonstrates flexibility of the methods in which researchers can introduce Cas9/gRNA components into the parasite.

Finally, the choice of drug pressure to apply to transfected parasites can be altered, depending on constructs used. Here, we show successful generation of mutants by transiently selecting for the Cas9-expressing plasmid using DSM1 until parasites reappear. To generate *Pf*Hsp70x knockout parasites, *pfhsp70x* was replaced with the human dihydrofolate reductase gene, and parasites were then selected using WR99210[13]. The recently described TetR-*Pf*DOZI knockdown system relies on integration of a plasmid containing a blasticidin S resistance gene, allowing for selection of parasites using blasticidin S[15,31].

Overall, CRISPR/Cas9 gene editing of *P. falciparum* has proven to be a powerful tool in malaria research, and the protocol here details the methods for generating conditional knockdown mutants[3,7,8,13,20,28]. This protocol is highly adaptable to individual research interests.

ACKNOWLEDGMENTS

We thank Muthugapatti Kandasamy at the University of Georgia (UGA) Biomedical Microscopy Core for technical assistance and Jose-Juan Lopez-Rubio for sharing the pUF1-Cas9 and pL6 plasmids. This work was supported by ARCS Foundation awards to D.W.C. and to H.M.K., UGA startup funds to V.M., grants from the March of Dimes Foundation (Basil O'Connor Starter Scholar Research Award) to V.M., and US National Institutes of Health grants (R00AI099156 and R01AI130139) to V.M. and (T32AI060546) to H.M.K.

DISCLOSURES

The authors have nothing to disclose.

REFERENCES

1. World Health Organization. *World Malaria Report*. World Health Organization, Geneva. (2017).
2. Miller, L. H., Baruch, D. I., Marsh, K., Doumbo, O. K. The pathogenic basis of malaria. *Nature*. 415 (6872), 673-679 (2002).
3. Florentin, A., et al. *Pf*ClpC Is an Essential Clp Chaperone Required for Plastid Integrity and Clp Protease Stability in *Plasmodium falciparum*. *Cell Reports*. 21 (7), 1746-1756 (2017).
4. Muralidharan, V., Oksman, A., Pal, P., Lindquist, S., Goldberg, D. E. *Plasmodium falciparum* heat shock protein 110 stabilizes the asparagine repeat-rich parasite proteome during malarial fevers. *Nature Communications*. 3, 1310-1310 (2012).
5. Muralidharan, V., Oksman, A., Iwamoto, M., Wandless, T. J., Goldberg, D. E. Asparagine repeat function in a *Plasmodium falciparum* protein assessed via a regulatable fluorescent affinity tag. *Proceedings of the National Academy of Sciences of the USA*. 108 (11), 4411-4416 (2011).
6. Beck, J. R., Muralidharan, V., Oksman, A., Goldberg, D. E. PTEX component HSP101 mediates export of diverse malaria effectors into host erythrocytes. *Nature*. 511 (7511), 592-595 (2014).
7. Ghorbal, M., et al. Genome editing in the human malaria parasite *Plasmodium*

falciparum using the CRISPR-Cas9 system. *Nature Biotec*hnology. 32 (8), 819-821 (2014).

8. Wagner, J. C., Platt, R. J., Goldfless, S. J., Zhang, F., Niles, J. C. Efficient CRISPR-Cas9-mediated genome editing in *Plasmodium falciparum*. *Nature Methods*. 11 (9), 915-918 (2014).

9. Doudna, J. A., Charpentier, E. Genome editing. The new frontier of genome engineering with CRISPR-Cas9. *Science*. 346 (6213), 1258096 (2014).

10. Wang, H., La Russa, M., Qi, L. S. CRISPR/Cas9 in Genome Editing and Beyond. *Annual Review of Biochemistry*. 85, 227-264 (2016).

11. Kirkman, L. A., Deitsch, K. W. Antigenic variation and the generation of diversity in malaria parasites. *Current Opinion in Microbiology*. 15 (4), 456-462 (2012).

12. Lee, A. H., Symington, L. S., Fidock, D. A. DNA Repair Mechanisms and Their Biological Roles in the Malaria Parasite *Plasmodium falciparum*. *Microbiology and Molecular Biology Reviews*. 78 (3), 469-486 (2014).

13. Cobb, D. W., et al. The Exported Chaperone *Pf*Hsp70x Is Dispensable for the *Plasmodium falciparum* Intraerythrocytic Life Cycle. *mSphere*. 2 (5), (2017).

14. Prommana, P., et al. Inducible knockdown of *Plasmodium* gene expression using the *glmS* ribozyme. *Public Library of Science One*. 8 (8), e73783 (2013).

15. Ganesan, S. M., Falla, A., Goldfless, S. J., Nasamu, A. S., Niles, J. C. Synthetic RNA-protein modules integrated with native translation

mechanisms to control gene expression in malaria parasites. *Nature Communications*. 7, 10727 (2016).

16. Li, M. Z., Elledge, S. J. Harnessing homologous recombination in vitro to generate recombinant DNA via SLIC. *Nature Methods*. 4 (3), 251-256 (2007).
17. Drew, M. E., et al. *Plasmodium* food vacuole plasmepsins are activated by falcipains. *Journal of Biological Chemistry*. 283 (19), 12870-12876 (2008).
18. Wu, Y., Sifri, C. D., Lei, H.-H., Su, X.-Z., Wellems, T. E. Transfection of *Plasmodium falciparum* within human red blood cells. *Proceedings of the National Academy of Sciences USA*. 92, 973-977 (1995).
19. Janse, C. J., et al. High efficiency transfection of *Plasmodium berghei* facilitates novel selection procedures. *Molecular and Biochemical Parasitology*. 145 (1), 60-70 (2006).
20. Counihan, N. A., et al. *Plasmodium falciparum* parasites deploy RhopH2 into the host erythrocyte to obtain nutrients, grow and replicate. *eLife*. 6, (2017).
21. Klemba, M., Beatty, W., Gluzman, I., Goldberg, D. E. Trafficking of plasmepsin II to the food vacuole of the malaria parasite *Plasmodium falciparum*. *Journal of Cell Biology*. 164 (1), 47-56 (2004).
22. Labun, K., Montague, T. G., Gagnon, J. A., Thyme, S. B., Valen, E. CHOPCHOP v2: a web tool for the next generation of CRISPR genome engineering. *Nucleic Acids Resesarch*. 44 (W1), W272-276 (2016).
23. Peng, D., Tarleton, R. EuPaGDT: a web tool tailored to design CRISPR guide

RNAs for eukaryotic pathogens. *Microbial Genomes*. 1 (4), e000033 (2015).

24. Shen, B., Brown, K. M., Lee, T. D., Sibley, L. D. Efficient Gene Disruption in Diverse Strains of *Toxoplasma gondii* Using CRISPR/CAS9. *mBio*. 5 (3), (2014).

25. Janssen, B. D., et al. CRISPR/Cas9-mediated gene modification and gene knock out in the human-infective parasite *Trichomonas vaginalis*. *Scientific Reports*. 8 (1), 270 (2018).

26. Spillman, N. J., Beck, J. R., Ganesan, S. M., Niles, J. C., Goldberg, D. E. The chaperonin TRiC forms an oligomeric complex in the malaria parasite cytosol. *Cellular Microbiology*. 19 (6), (2017).

27. Brancucci, N. M. B., et al. Lysophosphatidylcholine Regulates Sexual Stage Differentiation in the Human Malaria Parasite *Plasmodium falciparum*. *Cell*. 10.1016/j.cell.2017.10.020, (2017).

28. Ng, C. L., et al. CRISPR-Cas9-modified pfmdr1 protects *Plasmodium falciparum* asexual blood stages and gametocytes against a class of piperazine-containing compounds but potentiates artemisinin-based combination therapy partner drugs. *Molecular Microbiology.* 101 (3), 381-393 (2016).

29. Lim, M. Y., et al. UDP-galactose and acetyl-CoA transporters as *Plasmodium* multidrug resistance genes. *Nature Microbiology*. 10.1038/nmicrobiol.2016.166 16166, (2016).

30. Adjalley, S. H., et al. Quantitative assessment of *Plasmodium falciparum*

sexual development reveals potent transmission blocking activity by methylene blue. *Proceedings of the National Academy of Sciences USA*. 108 (47), E1214-E1223, (2011).

31. Sidik, S. M., et al. A Genome-wide CRISPR Screen in *Toxoplasma* Identifies Essential Apicomplexan Genes. *Cell*. 166 (6), e1412, 1423-1435 (2016).
32. Amberg-Johnson, K., et al. Small molecule inhibition of apicomplexan FtsH1 disrupts plastid biogenesis in human pathogens. *elife*. 6, (2017).
33. Crawford, E. D., et al. Plasmid-free CRISPR/Cas9 genome editing in *Plasmodium falciparum* confirms mutations conferring resistance to the dihydroisoquinolone clinical candidate SJ733. *Public Library of Science One*. 12 (5), e0178163 (2017).

Table 2.1 Materials Used for CRISPR/Cas9 Genome Editing in *P. falciparum*

Name of Material/ Equipment	Company	Catalog Number
Gene Pulser Xcell Electroporator	Bio-Rad	1652660
Gene Pulser®/MicroPulser Electroporation Cuvettes, 0.2 cm gap	Bio-Rad	165-2086
Sodium Acetate	Sigma-Aldrich	S2889-250g
DSM1	Gift from Akhil Vaidya lab	Ganesan et al. *Mol. Biochem. Parasitol.* 2011 177:29-34
TPP Tissue Culture 6 Well Plates	MIDSCI	TP92006
TPP 100mm Tissue Culture Dishes (12 mL Plate)	MIDSCI	TP93100
TPP Tissue Culture 96 Well Plates	MIDSCI	TP92096
TPP Tissue Culture 24 Well Plates	MIDSCI	TP92024
NEBuffer 2	New England Biolabs	#B7002S
NEBuffer 2.1	New England Biolabs	#B7202S
BtgZI	New England Biolabs	#R0703L
SacII	New England Biolabs	#R0157L
HindIII-HF	New England Biolabs	#R3104S
Afe1	New England Biolabs	#R0652S
Nhe1-HF	New England Biolabs	#R3131L
T4 DNA Polymerase	New England Biolabs	#M0203S
500 mL Steritop bottle top filter unit	Millipore	SCGPU10RE
EGTA	Sigma	E4378-100G
KCl	Sigma-Aldrich	P9333-500g
CaCl2	Sigma-Aldrich	C7902-500g
MgCl2	Sigma-Aldrich	M8266-100g
K2HPO4	Fisher	P288-500
HEPES	Sigma-Aldrich	H4034-500g
pMK-U6	Generated by the Muralidharan Lab	n/a
pHA-glmS	Generated by the Muralidharan Lab	n/a
pUF1-Cas9	Gift from the Jose-Juan Lopez-Rubio Lab	Ghorbal et al. *Nature Biotech* 2014

Glucose	Sigma-Aldrich	G7021-1KG
Sodium bicarbonate	Sigma-Aldrich	S5761-500G
Sodium pyruvate	Sigma-Aldrich	P5280-100G
Hypoxanthine	Sigma-Aldrich	H9636-25g
Gentamicin Reagent	Gibco	15710-064
Thymidine	Sigma-Aldrich	T1895-1G
PL6-eGFP BSD	Generated by the Muralidharan Lab	
Puf1-cas9 eGFP gRNA	Generated by the Muralidharan Lab	
NucleoSpin Gel and PCR Clean-up	Macherey-Nagel	740609.250
Albumax I	Life Technologies	N/A
Human Red Blood Cells	Interstate Blood Bank, Inc	Email or call them directly for ordering
3D7 parasite line	Available upon request	N/A
Lysogeny Broth (LB)	Fisher	BP1426-2
Ampicilin	Fisher	BP1760-25
PrimeSTAR® GXL DNA Polymerase	Clonetech	R050A
Anti-EF1alpha	Dr. Daniel Goldberg's Lab	Washington University in St. Louis
Rat Anti-HA Clone 3F10, monoclonal	Made by Roche, sold by Sigma	11867423001
0.6 mL tubes	Fisher	AB0350
Fisher HealthCare* PROTOCOL* Hema 3* Manual Staining System (Fixative+Solution I and II)	Fisher	22-122-911
Fisherfinest™ Premium Frosted Microscope Slides - Size: 3 x 1 in.	Fisher	12-544-3

CHAPTER 3

THE EXPORTED CHAPERONE *PF*HSP70X IS DISPENSABLE FOR THE *PLASMODIUM FALCIPARUM* INTRAERYTHROCYTIC LIFECYCLE

David W. Cobb*, Anat Florentin*, Manuel A. Fierro, Michelle Krakowiak, Julie M. Moore, Vasant Muralidharan. 2017. *mSphere*. 2(5):e00363-17. *Equal contributions. Reprinted here with permission of publisher.

.

Abstract

Export of parasite proteins into the host erythrocyte is essential for survival of *Plasmodium falciparum* during its asexual lifecycle. While several studies described key factors within the parasite that are involved in protein export, the mechanisms employed to traffic exported proteins within the host cell are currently unknown. Members of the Hsp70 family of chaperones, together with their Hsp40 co-chaperones, facilitate protein trafficking in other organisms, and are thus likely used by *P. falciparum* in the trafficking of its exported proteins. A large group of Hsp40 proteins is encoded by the parasite and exported to the host cell, but only one Hsp70, *Pf*Hsp70x, is exported with them. *Pf*Hsp70x is absent from most *Plasmodium* species and is found only in *P. falciparum* and closely-related species that infect Apes. Herein, we have utilized CRISPR/Cas9 genome editing in *P. falciparum* to investigate the essentiality of *Pf*Hsp70x. We show that parasitic growth was unaffected by knockdown of *Pf*Hsp70x using both the DHFR-based Destabilization Domain and the *glmS* ribozyme system. Similarly, a complete gene knockout of *Pf*Hsp70x did not affect the ability of *P. falciparum* to proceed through its intraerythrocytic lifecycle. The effect of *Pf*Hsp70x knockdown/knockout on the export of proteins to the host RBC, including the critical virulence factor *Pf*EMP1, was tested and we found that this process was unaffected. These data show that although *Pf*Hsp70x is the sole exported Hsp70, it is not essential for the asexual development of *P. falciparum*.

Importance

Half of the world's population lives at risk for malaria. The intraerythrocytic lifecycle of *Plasmodium* spp. is responsible for clinical manifestations of malaria; therefore, knowledge of the parasite's ability to survive within the erythrocyte is needed to combat the deadliest agent of malaria, *P. falciparum*. An outstanding question in the field is how P*. falciparum* undertakes the essential process of trafficking its proteins within the host cell. In most organisms, chaperones such as Hsp70 are employed in protein trafficking. Of the human-disease causing *Plasmodium* species, the chaperone *Pf*Hsp70x is unique to *P. falciparum*, and it is the only parasite protein of its kind exported to the host (1). This has placed *Pf*Hsp70x as an ideal target to inhibit protein trafficking and kill the parasite. However, we show that *Pf*Hsp70x is not required for export of parasite effectors nor is it essential for parasite survival inside of the RBC.

Introduction

Malaria is a profound killer worldwide. In 2015, 214 million cases of malaria resulted in 438,000 deaths, largely in Africa and Asia (2). Within malaria endemic countries, the disease targets the most vulnerable of the population, including children under five and pregnant women (2). The disease is caused by infection with eukaryotic parasites from the genus *Plasmodium*, but it is one species—*P. falciparum*—that is responsible for most of the malaria associated mortality. The clinical manifestations of malaria range from fever, headache, and muscle pains,

to severe anemia, coma, and respiratory distress (3). All of these symptoms are direct consequences of asexual replication of the parasite within the human red blood cell (RBC)(4). During this cycle of replication, *P. falciparum* invades the RBC and dramatically transforms its morphology and physiology. Alterations to the RBC include increased permeability, loss of cell deformability, and introduction of virulence-associated knobs at the RBC membrane (5, 6).

Remodeling of the RBC requires export of hundreds of parasite proteins into the host cell, a feat involving protein trafficking through multiple compartments before arriving at their final destinations in the host. The first phase of the journey begins in the parasite endoplasmic reticulum (ER). Many exported proteins contain an N-terminal signal motif termed the Host Targeting Signal or *Plasmodium* Export Element (PEXEL) (6, 7). A key step in the export of PEXEL-containing proteins is cleavage of the motif by the ER-resident aspartyl protease Plasmepsin V (8–10). A sub-group of exported proteins called PEXEL-Negative Exported Proteins (PNEPs) lack the motif, but their N-terminus is similarly necessary for export (12, 13). Aside from Plasmepsin V processing of PEXEL, mechanisms underlying the selection of host-destined proteins for exit from the ER remain unclear. Nonetheless, PEXEL-proteins and PNEPs continue their journey through the parasite's secretory pathway and are delivered to the parasitophorous vacuole (PV), a membranous structure within which the parasite resides. Previous studies have shown that proteins cross the parasitophorous vacuole membrane (PVM) through the Plasmodium Translocon of Exported Proteins (PTEX) (14–16). Once they are on the other side of the PVM, all classes

of proteins need to refold and find their specific subcellular localization, whether it is in the host cytoplasm, the host membrane, or parasite-induced structures such as knobs or Maurer's clefts. It is completely unknown how hundreds of proteins, within a short time period, cross through PTEX, refold to regain structure and function, and find their final destination in the host.

The process of protein export is essential for *P. falciparum* survival in the RBC, as blockage of protein export—whether at the parasite ER or at the PVM—results in parasite death. In the ER, overexpression of catalytically dead Plasmepsin V (PMV) results in impaired parasite growth, and inhibition of PMV with a PEXEL-mimetic impairs protein export and kills parasites during the transition to the trophozoite stage (10, 17, 18). Similarly, *P. falciparum* parasites are sensitive to interference of trafficking across the PVM. Conditional knockdown of PTEX components blocks protein export and kills the parasites (19, 20). As the parasites are susceptible to inhibition of trafficking in the ER and PV, interference in the trafficking process within the host may similarly impair parasite growth. The mechanisms of protein trafficking inside of the host cell remain unknown, but identification of essential components of this process will provide valuable targets for drug discovery programs.

Molecular chaperones are likely candidates in the search for key export and trafficking components. Indeed, PfHsp101 is an essential component of PTEX, and its inhibition results in accumulation of exported proteins within the PV (19). Furthermore, several parasite Hsp40s are exported to the RBC, but their function there is unknown (21). In other organisms Hsp40s serve as co-

chaperones for Hsp70s , but in contrast to the large number of exported Hsp40s, *Pf*Hsp70x (PF3D7_0831700) is the only parasite-encoded Hsp70 that is exported to host cell (1, 22). This chaperone is found only in *P. falciparum* and closely related species that cause malaria in apes such as *P. reichenowi*, but not in other *Plasmodium* species that infect humans, such as *P. vivax or P. knowlesi* (1). Within the *P. falciparum* infected RBC, *Pf*Hsp70x is localized to the PV and the host, where it associates with *Pf*Hsp40s in mobile structures termed J-dots (1). Given its status as sole exported Hsp70, we hypothesized that *Pf*Hsp70x is central to protein trafficking in the host cell, and thus essential to parasite viability. Indeed, studies focused on PTEX interactions have found *Pf*Hsp70x associated with the translocon, and it has been shown to co-localize with the critical virulence protein *Pf*EMP1 during its trafficking (1, 23, 24).

In this study, we took advantage of various genetic techniques to show that *Pf*Hsp70x is non-essential for protein export and parasite growth. We have used the DHFR-based destabilizing domain that has previously been used to inhibit chaperone function (19, 25). In addition, we have used the *glmS*-ribozyme system that inhibits translation via mRNA degradation (26). Mutants for both knockdown methods were successfully generated, but knockdown had no impact on parasite growth or protein export, including no discernible difference in the export of *Pf*EMP1. To confirm that the lack of a phenotype was not due to incomplete knockdown, we used CRISPR/Cas9 technology to generate a complete knockout of the *Pf*Hsp70x gene and found no defects in parasite proliferation or export. Our data demonstrate that *Pf*Hsp70x is not required for

protein export to the host RBC and not essential for the intraerythrocytic lifecycle of *P. falciparum*.

Results

Conditional mutants of *Pf*Hsp70x.

Previous work has shown that the DHFR-based destabilization domain (DDD) fusions can lead to the inhibition of protein-protein interactions (19, 25) or degradation of the DDD-tagged proteins (27–29). In the presence of the stabilizing ligand trimethoprim (TMP), the DDD is folded and the chaperone functions normally. However, upon TMP removal the DDD is unfolded and binds to its attached chaperone intramolecularly, thereby blocking interactions with the chaperone's client proteins and inhibiting normal chaperone function (**Figure 3.1A**). Relying on single-crossover homologous recombination, the *pfhsp70x* gene was modified with a triple-HA tag and the DDD, and integration at the *pfhsp70x* locus was confirmed via Southern blot analysis (**Figure 3.1A, B**). Consistent with the auto-inhibitory model of chaperone-DDD action, western blot analysis of parasite lysates following TMP removal showed that *Pf*Hsp70x protein levels remain consistent over time (**Figure 3.1C**). Isolation of the host cell cytoplasm using saponin lysis revealed that *Pf*Hsp70x-DDD is exported to the host cell (**Figure 3.1C**). Moreover, the persistence of *Pf*Hsp70x in the supernatant following TMP removal indicated that *Pf*Hsp70x is exported to the host cell even in its putative inhibited form. To assess the role of *Pf*Hsp70x in parasite proliferation, we removed TMP and measured asexual growth over a

course of several days and at least two replication cycles. We found that the absence of TMP had no effect on parasite proliferation (**Figure 3.2A**). It was previously reported that *Pf*Hsp70x, together with several other exported chaperones, localizes to specific punctate structures in the host cell termed J-dots. To test the effect of DDD-based inhibition on *Pf*Hsp70x localization, we performed immunofluorescence assays and found that *Pf*Hsp70x-DDD is trafficked to the expected punctate structures within the host cell, regardless of TMP presence (**Figure 3.2B**). These data suggest that unlike other chaperones, *Pf*Hsp70x activity was unaffected by the DDD fusion or that inhibition of *Pf*Hsp70x using the DDD system does not affect the asexual life cycle of the parasite. We therefore utilized alternative methods to reduce *Pf*Hsp70x protein levels in the parasite.

Next, we sought to conditionally knockdown *Pf*Hsp70x at the mRNA level using the *glmS* ribozyme (26). In this system, the *glmS* ribozyme sequence is inserted into the 3' end of the genomic locus of a gene and is transcribed with the gene as one mRNA. Addition of the small molecule glucosamine (GlcN) activates the *glmS* ribozyme, which cleaves itself from the mRNA, disconnecting the transcript from its polyA tail and leading to its degradation (**Figure 3.3A**). Using CRISPR/Cas9 genome engineering, we appended a triple HA tag to the C-terminus of *Pf*Hsp70x followed by the *glmS* ribozyme (**Figure 3.3A**) (30). A second cell line was generated in which the *pfhsp70x* locus was tagged with a mutant version of the ribozyme—termed M9—which is unresponsive to GlcN and serves as a control during GlcN treatment (26). Following transfection and drug

selection, *Pf*Hsp70x-*glmS* and PfHsp70x-M9 clones were isolated via limiting dilution. PCR analysis revealed the correct integration of the tag and ribozyme into the *pfhsp70x* gene in all clonal parasite lines (**Figure 3.3B**). Additionally, immunofluorescence assays confirmed that *Pf*Hsp70x-*glmS* is exported to the host cytoplasm, where it is found, as before, in punctate structures that are distinct from Maurer's clefts, suggestive of J-dot localization (**Figure 3.3C**).

Next, we tested the effect of reducing *Pf*Hsp70x levels on intraerythrocytic growth. To ensure that insertion of the ribozyme itself does not interfere with normal asexual growth, *Pf*Hsp70x-*glmS*, *Pf*Hsp70x-M9, and the parental line (3D7) were grown in the absence of GlcN. Indeed, we found that in the absence of GlcN, growth of both the *glmS* and M9 cell lines was comparable to 3D7 (**Figure 3.4A**). Next, *Pf*Hsp70x-*glmS* and *Pf*Hsp70x-M9 were cultured with GlcN and parasitemia was measured via flow cytometry. The growth of *Pf*Hsp70x-*glmS* and *Pf*Hsp70x-M9 was unaffected by treatment with 5 mM and 10 mM GlcN (**Figure 3.4B, C**). To confirm that *Pf*Hsp70x protein level is reduced in response to GlcN, schizont-stage parasites from the *glmS* and M9 cell lines were Percoll-purified and whole parasite lysates were used for western blotting. Using anti-HA antibody, we found that treatment with GlcN reduced protein levels in *Pf*Hsp70x-*glmS* but did not affect protein levels in *Pf*Hsp70x-M9 (**Figure 3.4D**). Together, these data show that we can efficiently reduce *Pf*Hsp70x levels using the *glmS* ribozyme but this has no effect on the asexual growth of the parasite within the RBC.

Protein export is unimpaired in *Pf*Hsp70x-knockdown parasites.

Although parasite growth was unaffected by *Pf*Hsp70x knockdown, we reasoned that it could nonetheless play a role in export of proteins to the host cell. In particular, we hypothesized that *Pf*Hsp70x is needed for the export of proteins known to mediate virulence of *P. falciparum* infection, as trafficking defects of these proteins would not manifest as arrest of the asexual lifecycle (21). Using immunofluorescence, we examined localization of specific virulence-associated proteins in *Pf*Hsp70x-M9 and *Pf*Hsp70x-*glmS* parasites after 72 hours of growth in GlcN-supplemented medium. First, the localization of the PEXEL-containing *Pf*FIKK4.2, an exported kinase associated with knob formation and infected RBC rigidity, is unchanged in control versus *Pf*Hsp70x-knockdown parasites (**Figure 3.5A**) (31). Next, we examined the localization of the PEXEL-containing protein KAHRP, which is essential for the formation of knobs on the surface of infected RBCs (32). Export of this protein was not inhibited in *Pf*Hsp70x-knockdown parasites (**Figure 3.5B**). Finally, we determined the localization of the PNEP MAHRP1, which has been implicated in the presentation of antigenically variant proteins, including *Pf*EMP1, at the RBC surface, and we found that its export is not impaired by the knockdown of *Pf*Hsp70x (**Figure 3.5C**) (33). As demonstrated by HA-staining in western blot and IFA (**Figures 3.4D, 3.5**), *Pf*Hsp70x is reduced, but not completely ablated, using the *glmS* ribozyme. We reasoned that the reduced level of *Pf*Hsp70x that is produced during GlcN treatment could be sufficient for parasite survival, and therefore endeavored next to knockout *pfhsp70x*.

Knockout of *pfhsp70x* does not affect parasite growth.

We utilized two different conditional knockdown systems to modify the *Pf*Hsp70x locus, but these approaches were insufficient to produce a growth defect in the parasites. Therefore, we sought to definitively test the essentiality of *Pf*Hsp70x via complete genomic knockout (termed *Pf*Hsp70x-KO). To this end, we employed CRISPR/Cas9 to interrupt the *Pf*Hsp70x ORF by inserting a human dihydrofolate reductase (hdhfr) drug resistance cassette (**Figure 3.6A**). Following transfection and selection with WR99210, *Pf*Hsp70x-KO parasites were cloned via limiting dilution. Southern blot analysis of genomic DNA isolated from the parental line and independent clones showed that the hdhfr cassette was inserted into the *pfhsp70x* gene via homology directed repair (**Figure 3.6B**). To verify that the null mutants do not express *Pf*Hsp70x, schizont-stage parasites from two independent knockout clones and the parental line were Percoll-purified, and whole parasite lysates were used for western blotting. Probing with anti-*Pf*Hsp70x shows that the knockout clones do not express *Pf*Hsp70x (**Figure 3.6C**). Intraerythrocytic growth of the *Pf*Hsp70x-KO clones was monitored over two replication cycles. In agreement with the lack of any growth phenotype in the conditional knockdown parasite lines, the *Pf*Hsp70x-KO parasites displayed wild-type level of proliferation in erythrocytes (**Figure 3.6D**). Finally, we measured the susceptibility of *Pf*Hsp70x-KO clones to heat shock stress by monitoring their growth after a heat shock (**Figure 3.7**). These data show that the *Pf*Hsp70x-KO parasites are able to deal with heat shock just as well as the wild type parasites (**Figure 3.7**). The normal growth in the complete absence of *Pf*Hsp70x

expression conclusively demonstrates that *Pf*Hsp70x activity is not essential for the asexual growth of the parasite within the RBC.

Protein export is unimpaired in *Pf*Hsp70x-KO parasites.

Using *Pf*Hsp70x-KO parasites, we next tested the hypothesis that the chaperone is required for export of virulence-associated proteins. Using immunofluorescence, we examined the export of the same proteins assayed with *Pf*Hsp70x-*glmS* parasites: *Pf*FIKK4.2, KAHRP, and MAHRP1 (31–33). Consistent with our observations using *Pf*Hsp70x-*glmS*, *pfhsp70x* knockout did not interrupt export of these proteins (**Figure 3.8**). These data show that the loss of *Pf*Hsp70x does not impede the parasite's ability to export virulence-associated proteins to the host cell.

Export of antigenic proteins to the host RBC is unaffected in PfHsp70x mutants.

*Pf*Hsp70x was shown to interact with the antigenically variant protein *Pf*EMP1, and recent data that identified proteins that interact with *Pf*EMP1 confirms these results (1). Therefore, we wanted to test how the export of *Pf*EMP1 is affected in our mutants. Utilizing immunofluorescence microscopy, we determined the localization of *Pf*EMP1 in 3D7 and *Pf*Hsp70x-KO parasites (**Figure 3.9**). Our data show that knockout of *Pf*Hsp70x does not prevent export of *Pf*EMP1 to the host cell (**Figure 3.9**). Next, we observed the export of *Pf*EMP1 in our *Pf*Hsp70x conditional mutants. Our data show that *Pf*EMP1 is exported equally well in both

*Pf*Hsp70x-M9 and *Pf*Hsp70x-*glmS* parasites under knockdown conditions (**Figure 3.10**). We quantified the amount of *Pf*Hsp70x-HA, as well as the amount of exported *Pf*EMP1, in these mutants and found no difference in regards to *Pf*EMP1, despite achieving significant reduction of *Pf*Hsp70x in the *glmS* parasite line (**Figure 3.10A, B**). Because MAHRP1 has been implicated in the trafficking of *Pf*EMP1, we also quantified the export of MAHRP1 in the *Pf*Hsp70x conditional mutants, and we found that knockdown of *Pf*Hsp70x does not affect MAHRP1 export (**Figure 3.10C**).

Next, we sought to investigate if there were any differences in the mutants in the export of antigenic parasite proteins that generate an immune response. We obtained pooled human sera collected from a malaria-endemic region (Kenya) as well as a non-endemic region (USA) (34). Uninfected RBCs, 3D7 parasites, and *Pf*Hsp70x-KO parasites were labeled with these sera and observed via flow cytometry (**Figure 3.11**). 3D7 and *Pf*Hsp70x-KO schizonts were synchronized and grown to the schizont stage, and cultures were brought to matching parasitemia prior to labeling with sera. Our data show that both 3D7 and *Pf*Hsp70x-KO parasites are labeled equally well by human sera collected from malaria-endemic regions but not by sera obtained from non-endemic regions, suggesting that the export of antigenic parasite proteins to the host RBC is unaffected by the loss of *Pf*Hsp70x (**Figure 3.11**).

Discussion

While this work was under review (and also available on the bioRxiv preprint server), another study was published showing that knockout of *Pf*Hsp70x did not affect parasite growth (35). In agreement with these data, our data also demonstrate that *Pf*Hsp70x is not required for intraerythrocytic growth, even though *Pf*Hsp70x is the only parasite-encoded Hsp70 that is exported to the RBC (**Figures 3.2A; 3.4A, B, C; 3.5D; 3.7D**). Using two different genetic approaches we demonstrate that the export of several parasite effectors are unaffected by the loss of *Pf*Hsp70x (**Figures 3.5, 3.8-11**). In the case of *Pf*EMP1, the newly published work suggests that knockout of *Pf*Hsp70x led to delays in its export and minor loss in cytoadherence, suggesting a role for *Pf*Hsp70x in parasite virulence (35). In this case, the data show that PfHsp70x knockout parasites over-express some exported proteins (35). This suggests that there may be compensatory mechanisms that are activated when *Pf*Hsp70x is knocked out and therefore lead to minor, if any, changes in the export of parasite virulence (35). However, this interpretation is clouded by the lack of a conditional mutant for *Pf*Hsp70x, which cannot compensate for the loss of *Pf*Hsp70x. The data described in this study show that in both *Pf*Hsp70x-KO and *Pf*Hsp70x-*glmS* mutants, export of parasite virulence factors is not affected (**Figure 3.5, 3.8-11**). We specifically tested the export of the antigenically variant protein, *Pf*EMP1, which is responsible for cytoadherence, and observed that the export of *Pf*EMP1 was unaffected in either the knockout or the conditional mutants of *Pf*Hsp70x

(**Figures 3.9-11**). Therefore, our data suggest a slightly different, though not mutually exclusive, model than the one proposed in Charnaud et al.

*Pf*Hsp70x is not the only Hsp70 found in infected RBCs. Several human chaperones, including Hsp70, are present in the erythrocyte cytoplasm (36). Thus, the role played by *Pf*Hsp70x in the parasite's biology could be redundant with the human Hsp70 that is already present in the host cell. In fact, infection with *P. falciparum* affects the normal localization of the human Hsp70, as the protein is soluble in non-parasitized RBCs but is found in detergent-resistant fractions following infection (37). Another paper published while this work was under review identified several interacting partners of *Pf*EMP1 using thorough proteomic and genetic data (38). They identified several human chaperones, specifically from the TRiC chaperonin complex, to interact with *Pf*EMP1. Together with our data, this suggests a model wherein *Pf*EMP1 export is aided both by *Pf*Hsp70x and by human chaperones present in the host RBCs. This further suggests that loss of either one of them may not be enough to derail the export of parasite virulence proteins to the host RBC. The methods used here to investigate the function of *Pf*Hsp70x, knockdown and complete genomic knockout, are more challenging to use for human chaperones such as Hsp70 or the TRiC chaperonin complex. The mature RBC cannot be genetically manipulated, and knockdown of human Hsp70 in hematopoietic stem cells abrogates RBC formation (39). Our data demonstrate that pooled human sera collected from malaria-endemic regions are unable to differentiate between wildtype and *Pf*Hsp70x-KO parasites, raising the possibility that *Pf*Hsp70x may

not be required in human infections (**Figure 3.11**). However, further detailed analysis of the *pfhsp70x* locus in strains isolated from the field may be informative about the essentiality of *Pf*Hsp70x in human infections. Overall, our data demonstrate that *Pf*Hsp70x is not required for export of *P. falciparum* effector proteins to the host, is dispensable for asexual growth within human RBCs, and suggest a model where both human chaperones and parasite chaperones act in a redundant manner to ensure export of parasite virulence factors to the host RBCs.

Materials and Methods

Plasmid construction. Genomic DNA was isolated from *P. falciparum* using the QIAamp DNA blood kit (QIAGEN). Constructs utilized in this study were confirmed by sequencing. PCR products were inserted into the respective plasmids using the In-Fusion cloning system (Clonetech) or using the SLIC method. Briefly, insert and cut vector were mixed with a T4 DNA polymerase and incubated for 2.5 minutes at room temperature, followed by 10 minutes incubation on ice and then transformed into bacteria. For generation of plasmid *Pf*Hsp70x-HADB, a 1-kb homologous sequence from the 3'-end of the *pfhsp70x* gene (not including the stop codon) was amplified by PCR using primers 5'-CACTATAGAACTCGAGGTGAAAAAGCTAAACGTGTATTATCATCATCCGCACAAGC-3' and 5'-CGTATGGGTACCTAGGATTTACTTCTTCAACGGTTGGTCCATTATTTTGTGC-

3’ and was inserted into pHADB (18) using restriction sites XhoI and AvrII (New England Biolabs).

For the generation of the glmS conditional mutants three plasmids were used; 1) pUF1-Cas9 (from J. J. Lopez-Rubio) was used to drive cas9 expression (30). 2) pMK-U6 was used to drive expression of the RNA guide. For this purpose, pL6 plasmid (from J. J. Lopez-Rubio, (30)) was digested with NotI and NcoI (New England Biolabs) and the fragment that contained the U6 RNA expression cassette was blunted and re-ligated to form the pMK-U6 plasmid. The guideRNA, oligos 5’-TAAGTATATAATATTTGCATTATTGTTGTATATTTGTTTTAGAGCTAGAA-3’ and 5’-TTCTAGCTCTAAAACAAATATACAACAATAATGCAAATATTATATACTTA-3’ were annealed and cloned into the RNA module in MK-U6 as previously described (30). Briefly, pMK-U6 was digested with BtgZI (New England Biolabs) and annealed oligos were inserted using In-Fusion HD Cloning Kit (Clontech). 3) pHA-glmS and pHA-M9 were used as donor DNA templates consisting of two homology regions flanking the HA tag and the *glmS* (or the M9) sequences. To generate the pHA-glmS and pHA-M9 plasmids, primers 5’-GAGCTCGCTAGCAAGCTTGCCGGCAAGATCATGTGATTTCTCTTTGTTCAAGGAGTC-3’ and 5’-TCCGCGGAGCGCTACTAGTTACCCATACGATGTTCCAGATTACGCTTACCCATACGATGTTCCAGATTACGCTTACCCATACGATGTTCCAGATTACGCTTAAATGTCCAGACCTGCAGTAATTATCCCGCCCGAACTAAGCGC-3’ were used to

amplify the *glmS* and M9 sequences from pGFP-*glmS* and pGFP-M9, respectively (from P.Shaw, (26)). PCR constructs were then inserted into a TOPO cloning vector (ThermoFisher). To allow efficient genomic integration of the pHA-glmS and pHA-M9 donor plasmids, 800bp sequences were used for each homology region. The C-terminus of the *pfhsp70x* coding region was PCR amplified form genomic DNA using primers 5'-AATTCGCCCTTCCGCGGGCTGTACAAGCAGCCATCTTATCAGGTGATCAATCATC-3' and 5'-ATCGTATGGGTAAGCGCTATTTACTTCTTCAACGGTTGGTCCATTATTTTGTGCTTC-3' and was inserted into pHA-glmS and pHA-M9 using restriction sites SacII and AfeI (New England Biolabs). The 3'UTR of *pfhsp70x* was pcr amplified from genomic DNA using primers 5'-ATGATCTTGCCGGCAAGCTTACGAAAATATACAACAATAATGCATAAAATAATAATAATT-3' and 5'-CCTTGAGCTCGCTAGCGCAATATAAATGGATTATTCCTTTTGTATATAATTTAAAATAAG-3' and was inserted into pHA-glmS and pHA-M9 (already containing the C-terminus homology region) using restriction sites HindIII and NheI (New England Biolabs).

For the generation of *pfhsp70x-ko* parasites two plasmids were used; 1) A cas9 expressing plasmid (as described above), and 2) pL7-*Pf*Hsp70x plasmid that is derived from the pL6 plasmid (from J. J. Lopez-Rubio, (30)). pL7-*Pf*Hsp70x contained the guide RNA and 800bp homology regions flanking a *hdhfr* gene that confers resistance to WR. The N-terminus of the *pfhsp70x* gene was amplified

via PCR from genomic DNA using primers 5'-cggggaggactagtATGAAGACAAAAATTTGTAGTTATATTCATTATATTG-3' and 5'-acaaaatgcttaagGGAAACATCTTTACCTCCATTTTTTTTTTTAAAATCTTGTAC-3' and was inserted into pL6 using restriction sites AflII and SpeI (New England Biolabs). The C-terminus of the *pfhsp70x* gene was pcr amplified from genomic DNA using primers 5'-taaatctagaattcTGATCAATCATCAGCTGTCAAAGACTTATTATTATTAGATG-3' and 5'-ttaccgttccatggTTAATTTACTTCTTCAACGGTTGGTCCATTATTTTGTGCTTC-3' and was inserted into pL6 (already containing the C-terminus homology region) using restriction sites NcoI and EcoRI (New England Biolabs). In order to insert the guide DNA sequence, oligos 5'-TAAGTATATAATATTGTACAAGCAGCCATCTTATCGTTTTAGAGCTAGAA-3' and 5'-TTCTAGCTCTAAAACGATAAGATGGCTGCTTGTACAATATTATATACTTA-3' were annealed and cloned into pL6 as previously described (30). Briefly, pL6 was digested with BtgZI (New England Biolabs) and annealed oligos were inserted using In-Fusion HD Cloning Kit (Clontech).

Cell culture and transfections. Parasites were cultured in RPMI medium supplemented with Albumax I (Gibco) and transfected as described earlier (40, 41). For generation of *Pf*Hsp70x-DDD parasites, *Pf*Hsp70x-HADB was transfected in duplicates into 3D7-derived parental strain PM1KO which contains

a hDHFR expression cassette conferring resistance to TMP (42). Selection and drug cycling were performed as described (25) in the presence of 10 μM of TMP (Sigma). Integration was detected after three rounds of drug cycling with blasticidin (Sigma).

For generation of *Pf*Hsp70x-*glmS* and *Pf*Hsp70x-M9 parasites, a mix of three plasmids (40 μg of each) was transfected in duplicates into 3D7 parasites. The plasmids mix contained pUF1-Cas9 (from J. J. Lopez-Rubio, (30)) which contains the DHOD resistance gene, pMK-U6-*Pf*Hsp70x, pHA-glmS-*Pf*Hsp70x or pHA-M9-*Pf*Hsp70x, which are all marker-free. Drug pressure was applied 48 hours post transfection, using 1 μM DSM1 (43), selecting only for Cas9 expression. Drug was removed from the culturing media once parasites became detectable in the culture, usually around 3 weeks post transfection.

For generation of *Pf*Hsp70x-KO parasites, a mix of pUF1-Cas9 (from J. J. Lopez-Rubio, (30)) and pL7-*Pf*Hsp70x (50 μg of each plasmid) was transfected in duplicates into 3D7 parasites. Drug pressure was applied 48 hours post transfection, using 2.5 nM WR99210 (Sigma), selecting for integration of the drug resistance cassette into the *pfhsp70x* gene.

Growth assays. For asynchronous growth assays of *Pf*Hsp70x-DDD lines, parasites were washed twice and incubated without TMP. For asynchronous growth assays of *Pf*Hsp70x-glmS and *Pf*Hsp70x-M9 parasites, 5 or 10 mM GlcN (Sigma) were added to the growth media. Asynchronous growth assays of *Pf*Hsp70x-KO parasites were performed in media containing

WR99210. Parasitemia was monitored every 24 hours via flow cytometry. For flow cytometry, aliquots of parasite cultures (5 µL) were stained with 1.5 mg/ml Acridine Orange (Molecular Probes) in PBS. The fluorescence profiles of infected erythrocytes were measured by flow cytometry on a CyAn ADP (Beckman Coulter) or CytoFLEX (Beckman Coulter) and analyzed by FlowJo software (Treestar, Inc.). Whenever required, parasites were sub-cultured to avoid high parasite density and relative parasitemia at each time point was back-calculated based on actual parasitemia multiplied by the relevant dilution factors. 100% parasitemia was determined as the highest relative parasitemia and was used to normalize parasite growth. Data were fit to exponential growth equations using Prism (GraphPad Software, Inc.)

Southern blotting. Southern blots were performed with genomic DNA isolated using the Qiagen Blood and Cell Culture kit. 10 µg of DNA was digested overnight with NcoI/XmnI for *Pf*Hsp70x-DDD and BamHI/ScaI for *Pf*Hsp70x-KO (New England Biolabs). Integrants were screened using biotin-labeled probes against the 3'-end (*Pf*Hsp70x-DDD parasites) or 5'-end (*Pf*Hsp70x-KO parasites) of the *pfhsp70x* ORF. Southern blot was performed as described earlier (44). The probe was labeled using biotinylated Biotin-16-dUTP (Sigma). The biotinylated probe was detected on blots using IRDye 800CW Streptavidin conjugated dye (LICOR Biosciences) and was imaged, processed and analyzed using the Odyssey infrared imaging system software (LICOR Biosciences).

Western blotting. Western blots were performed as described previously (27). Briefly, late-stage parasites were isolated on a percoll gradient (Genesee

Scientific). For *Pf*Hsp70x-DDD parasites, host RBCs were permeabilized selectively by treatment with ice-cold 0.04% saponin in PBS for 10 min. Supernatants were collected for detection of exported parasites proteins and pellets were collected for detection of proteins with the parasite. For *Pf*Hsp70x-KO, *Pf*Hsp70x-glmS and *Pf*Hsp70x-M9 parasites, whole parasite lysates, including the host RBC, were used to detect protein expression and export. The antibodies used in this study were rat anti-HA (3F10, Roche, 1:3000), rabbit anti-*Pf*EF1α (from D. Goldberg, 1: 2000), mouse anti-Plasmepsin V (From D. Goldberg, 1:400), rabbit anti-*Pf*Hsp70x (From J. Przyborski, 1:1000). The secondary antibodies that were used are IRDye 680CW goat anti-rabbit IgG and IRDye 800CW goat anti-mouse IgG (LICOR Biosciences, 1:20,000). The western blot images were processed and analyzed using the Odyssey infrared imaging system software (LICOR Biosciences).

Microscopy and image processing. For detection of HA-tags, *Pf*Hsp70x, *Pf*FIKK4.2, and MAHRP1, cells were smeared on a slide and acetone-fixed. For KAHRP detection, cells were fixed with paraformaldehyde and glutaraldehyde. *Pf*Hsp70x-HA was detected using rat anti-HA antibody (clone 3F10, Roche, 1:100). MAHRP1 was detected using rabbit anti-MAHRP1 (from Hans-Peter Beck, 1:500). *Pf*FIKK4.2 and KAHRP were detected using mouse anti-PfFIKK4.2 (1:1000) and mouse anti-KAHRP (1:1000 and 1:500, respectively. Both antibodies acquired from David Cavanagh and EMRR). *Pf*EMP1 was detected using mouse-anti-ATS (1B/98-6H1-1, 1:100, Alan Cowman). Secondary antibodies used were anti rat-AlexaFluor 488 or 594, anti rabbit-AlexaFluor 488,

and anti mouse-AlexaFluor 488 (Life Technologies, 1:100). Cells were mounted on ProLong Diamond with DAPI (Invitrogen) and were imaged using DeltaVision II microscope system with an Olympus IX-71 inverted microscope using a 100X objective. Image processing, analysis and display were preformed using SoftWorx and Adobe Photoshop. Adjustments to brightness and contrast were made for display purposes. For quantification of *Pf*Hsp70x-HA fluorescence, *Pf*EMP1 export, and MAHRP1 export, *Pf*Hsp70x-*glmS* and –M9 parasites were grown in the presence of 7.5 mM GlcN for 72 hours, then fixed and stained with anti-HA, anti-ATS, and anti-MAHRP1 as described above. Cells were imaged as described above. The mean fluorescence intensity (MFI) for each protein was calculated as described (10). Briefly, ImageJ was used to calculate MFI for the whole infected RBC (*Pf*Hsp70x) or the infected RBC minus the parasite in order to quantify the exported fraction (*Pf*EMP1and MAHRP1). DIC images were used to exclude the parasite from analysis when calculating the MFI of the *Pf*EMP1 and MAHRP1 exported fraction. Data were plotted using Prism (GraphPad Software, Inc.).

Human Sera Staining. 3D7 and PfHsp70x-KO parasites were synchronized to the ring stage by incubating infected RBCs with 5% D-sorbitol (Amresco, Inc.) for 10 minutes at 37 degrees Celsius. Parasites were washed 3 times with culture medium, then allowed to proceed through the lifecycle to the schizont stage. The cultures were incubated 1:10 with either pooled immune sera from Kenya or non-immune serum from the United States for 30 minutes at 37 degrees Celsius, shaking on an orbital shaker at 880 rpm. The serum was

washed from the parasites three times with culture medium, and goat-anti-human IgG Fc conjugated to PE was added to the parasites (1:500, Fisher Scientific, 50-112-8944). The secondary antibody was incubated with the parasites for 30 minutes at 37 degrees Celsius, shaking. Parasites were washed 3 times with culture medium, resuspended in PBS, and fluorescence was measured with a flow cytometer (CytoFLEX, Beckman Coulter) and data analyzed using FlowJo software (Treestar, Inc.). Immune serum samples were collected as described, and all samples have been de-identified (34, 45).

Acknowledgments

We thank Julie Nelson at the Center for Tropical and Emerging Global Diseases Cytometry Shared Resource Laboratory; Muthugapatti Kandasamy at the University of Georgia Biomedical Microscopy Core; Heather M. Bishop for technical assistance; Jose-Juan Lopez-Rubio for sharing the pUF1-Cas9 and pL6 plasmids; and Dan Goldberg (for anti-Plasmepsin V and anti-*Pf*EF1α), Hans-Peter Beck (for anti-MAHRP), Jude Przyborski (for anti-*Pf*Hsp70x), Alan Cowman (for anti-*Pf*EMP1), and David Cavanagh and EMRR (for anti-FIKK4.2 and anti-KAHRP). This work was supported by grants from the March of Dimes Foundation (Basil O'Connor Starter Scholar Research Award), and the US National Institutes of Health (R00AI099156) to V.M.

References

1. Külzer S, Charnaud S, Dagan T, Riedel J, Mandal P, Pesce ER, Blatch GL,

Crabb BS, Gilson PR, Przyborski JM. 2012. *Plasmodium falciparum*-encoded exported hsp70/hsp40 chaperone/co-chaperone complexes within the host erythrocyte. *Cell Microbiol* 14:1784–1795.

2. WHO. 2016. *World Malaria Report*. World Health Organization.

3. Cowman AF, Healer J, Marapana D, Marsh K. 2015. Malaria : Biology and Disease. *Cell* 167:610–624.

4. Nilsson SK, Childs LM, Buckee C, Marti M. 2015. Targeting Human Transmission Biology for Malaria Elimination. *PLoS Pathog* 11:e1004871.

5. Desai SA. 2014. Why do malaria parasites increase host erythrocyte permeability? *Trends Parasitol* 30:151–159.

6. Maier AG, Cooke BM, Cowman AF, Tilley L. 2009. Malaria parasite proteins that remodel the host erythrocyte. *Nat Rev Microbiol* 7:341–354.

7. Marti M, Good RT, Rug M, Knuepfer E, Cowman AF. 2004. Targeting Malaria Virulence and Remodeling Proteins to the Host Erythrocyte. *Science* 306:1930–1933.

8. Hiller NL, Bhattacharjee S, Ooij C Van, Liolios K, Harrison T, Lopez-estran C, Haldar K. 2004. A Host-Targeting Signal in Virulence Proteins Reveals a Secretome in Malarial Infection. *Science* 306:1934–1937.

9. Klemba M, Goldberg DE. 2005. Characterization of plasmepsin V, a membrane-bound aspartic protease homolog in the endoplasmic reticulum of *Plasmodium falciparum*. *Mol Biochem Parasitol* 143:183–191.

10. Russo I, Babbitt S, Muralidharan V, Butler T, Oksman A, Goldberg DE. 2010.

Plasmepsin V licenses *Plasmodium* proteins for export into the host erythrocyte. *Nature* 463:632–6.

11. Boddey J a, Hodder AN, Günther S, Gilson PR, Patsiouras H, Kapp E A, Pearce JA, de Koning-Ward TF, Simpson RJ, Crabb BS, Cowman AF. 2010. An aspartyl protease directs malaria effector proteins to the host cell. *Nature* 463:627–631.
12. Haase S, Herrmann S, Grüring C, Heiber A, Jansen PW, Langer C, Treeck M, Cabrera A, Bruns C, Struck NS, Kono M, Engelberg K, Ruch U, Stunnenberg HG, Gilberger TW, Spielmann T. 2009. Sequence requirements for the export of the *Plasmodium falciparum* Maurer's clefts protein REX2. *Mol Microbiol* 71:1003–1017.
13. Gruring C, Heiber A, Kruse F, Flemming S, Franci G, Colombo SF, Fasana E, Schoeler H, Borgese N, Stunnenberg HG, Przyborski JM, Gilberger TW, Spielmann T. 2012. Uncovering common principles in protein export of malaria parasites. *Cell Host Microbe* 12:717–729.
14. de Koning-Ward TF, Gilson PR, Boddey JA, Rug M, Smith BJ, Papenfuss AT, Sanders PR, Lundie RJ, Maier AG, Cowman AF, Crabb BS. 2009. A newly discovered protein export machine in malaria parasites. *Nature* 459:945–9.
15. Gehde N, Hinrichs C, Montilla I, Charpian S, Lingelbach K, Przyborski JM. 2009. Protein unfolding is an essential requirement for transport across the parasitophorous vacuolar membrane of *Plasmodium falciparum*. *Mol Microbiol* 71:613–628.

16. Riglar DT, Rogers KL, Hanssen E, Turnbull L, Bullen HE, Charnaud SC, Przyborski J, Gilson PR, Whitchurch CB, Crabb BS, Baum J, Cowman AF. 2013. Spatial association with PTEX complexes defines regions for effector export into *Plasmodium falciparum*-infected erythrocytes. *Nat Commun* 4:1415.

17. Boddey JA. 2014. Inhibition of Plasmepsin V activity demonstrates its essential role in protein export, PfEMP1 display, and survival of malaria parasites. *PLoS Biol* 12:e1001897.

18. Hodder AN, Sleebs BE, Czabotar PE, Gazdik M, Xu Y, O'Neill MT, Lopaticki S, Nebl T, Triglia T, Smith BJ, Lowes K, Boddey JA, Cowman AF. 2015. Structural basis for plasmepsin V inhibition that blocks export of malaria proteins to human erythrocytes. *Nat Struct Mol Biol* 22:590–596.

19. Beck JR, Muralidharan V, Oksman A, Goldberg DE. 2014. PTEX component HSP101 mediates export of diverse malaria effectors into host erythrocytes. *Nature* 511:592–5.

20. Elsworth B, Matthews K, Nie CQ, Kalanon M, Charnaud SC, Sanders PR, Chisholm SA, Counihan NA, Shaw PJ, Pino P, Chan J-A, Azevedo MF, Rogerson SJ, Beeson JG, Crabb BS, Gilson PR, de Koning-Ward TF. 2014. PTEX is an essential nexus for protein export in malaria parasites. Nature 511:587–91.

21. Maier AG, Rug M, O'Neill MT, Brown M, Chakravorty S, Szestak T, Chesson J, Wu Y, Hughes K, Coppel RL, Newbold C, Beeson JG, Craig A, Crabb BS, Cowman AF. 2008. Exported Proteins Required for Virulence and

Rigidity of *Plasmodium falciparum*-Infected Human Erythrocytes. *Cell* 134:48–61.

22. Rhiel M, Bittl V, Tribensky A, Charnaud SC, Strecker M, Müller S, Lanzer M, Sanchez C, Schaeffer-Reiss C, Westermann B, Crabb BS, Gilson PR, Külzer S, Przyborski JM. 2016. Trafficking of the exported *P. falciparum* chaperone *Pf*Hsp70x. *Sci Rep* 6:36174.
23. Mesen-Ramirez P, Reinsch F, Blancke Soares A, Bergmann B, Ullrich AK, Tenzer S, Spielmann T. 2016. Stable Translocation Intermediates Jam Global Protein Export in *Plasmodium falciparum* Parasites and Link the PTEX Component EXP2 with Translocation Activity. *PLoS Pathog* 12:1–28.
24. Elsworth B, Sanders PR, Nebl T, Batinovic S, Kalanon M, Nie CQ, Charnaud SC, Bullen HE, de Koning Ward TF, Tilley L, Crabb BS, Gilson PR. 2016. Proteomic analysis reveals novel proteins associated with the *Plasmodium* protein exporter PTEX and a loss of complex stability upon truncation of the core PTEX component, PTEX150. *Cell Microbiol*.
25. Muralidharan V, Oksman A, Pal P, Lindquist S, Goldberg DE. 2012. *Plasmodium falciparum* heat shock protein 110 stabilizes the asparagine repeat-rich parasite proteome during malarial fevers. *Nat Commun* 3:1310.
26. Prommana P, Uthaipibull C, Wongsombat C, Kamchonwongpaisan S, Yuthavong Y, Knuepfer E, Holder AA, Shaw PJ. 2013. Inducible Knockdown of *Plasmodium* Gene Expression Using the *glmS* Ribozyme.

PLoS One 8:1–10.

27. Muralidharan V, Oksman A, Iwamoto M, Wandless TJ, Goldberg DE. 2011. Asparagine repeat function in a *Plasmodium falciparum* protein assessed via a regulatable fluorescent affinity tag. *Proc Natl Acad Sci USA* 108:4411–6.
28. Pei Y, Miller JL, Lindner SE, Vaughan AM, Torii M, Kappe SHI. 2013. *Plasmodium yoelii* inhibitor of cysteine proteases is exported to exomembrane structures and interacts with yoelipain-2 during asexual blood-stage development. *Cell Microbiol* 15:1508–1526.
29. Nacer A, Claes A, Roberts A, Scheidig-Benatar C, Sakamoto H, Ghorbal M, Lopez-Rubio J-J, Mattei D. 2015. Discovery of a novel and conserved *Plasmodium falciparum* exported protein that is important for adhesion of *Pf*EMP1 at the surface of infected erythrocytes. *Cell Microbiol*.
30. Ghorbal M, Gorman M, Macpherson CR, Martins RM, Scherf A, Lopez-Rubio J-J. 2014. Genome editing in the human malaria parasite *Plasmodium falciparum* using the CRISPR-Cas9 system. *Nat Biotechnol* 32:819–21.
31. Kats LM, Fernandez KM, Glenister FK, Herrmann S, Buckingham DW, Siddiqui G, Sharma L, Bamert R, Lucet I, Guillotte M, Mercereau-Puijalon O, Cooke BM. 2014. An exported kinase (FIKK4.2) that mediates virulence-associated changes in *Plasmodium falciparum*-infected red blood cells. *Int J Parasitol* 44:319–328.
32. Watermeyer JM, Hale VL, Hackett F, Clare DK, Cutts EE, Vakonakis I, Fleck RA, Blackman MJ, Saibil HR. 2016. A spiral scaffold underlies

cytoadherent knobs in *Plasmodium falciparum*-infected erythrocytes. *Blood* 127:343–51.

33. Spycher C, Rug M, Pachlatko E, Hanssen E, Ferguson D, Cowman AF, Tilley L, Beck HP. 2008. The Maurer's cleft protein MAHRP1 is essential for trafficking of PfEMP1 to the surface of *Plasmodium falciparum*-infected erythrocytes. *Mol Microbiol* 68:1300–1314.
34. Perrault S, Hajek J, Zhong K, Owino S, Sichangi M, Smith G, Ping Shi Y, Moore J, Kain K. 2009. Human Immunodeficiency Virus Co-Infection Increased Placental Parasite Density and Transplacental Malaria Transmission in Western Kenya. *Am J Trop Med Hyg* 80:119–125.
35. Charnaud; SC, Dixon; MWA, Nie; CQ, Chappell; L, Sanders; PR, Nebl; T, Hanssen; E, Berriman; M, Chan; J-A, Blanch; AJ, Beeson; JG, Rayner; JC, Przyborski; JM, Tilley; L, Crabb; BS, Gilson; PR. 2017. The exported chaperone Hsp70-x supports virulence functions for *Plasmodium falciparum* blood stage parasites. *PLoS One* IN PRESS.
36. Pasini EME, Kirkegaard M, Mortensen P, Lutz HU, Thomas AW, Mann M. 2006. In-depth analysis of the membrane and cytosolic proteome of red blood cells. *Blood* 108:791–801.
37. Banumathy G, Singh V, Tatu U. 2002. Host chaperones are recruited in membrane-bound complexes by *Plasmodium falciparum*. *J Biol Chem* 277:3902–3912.
38. Batinovic S, McHugh E, Chisholm SA, Matthews K, Liu B, Dumont L, Charnaud SC, Schneider MP, Gilson PR, de Koning-Ward TF, Dixon

MWA, Tilley L. 2017. An exported protein-interacting complex involved in the trafficking of virulence determinants in *Plasmodium-infected* erythrocytes. *Nat Commun* 8:16044.

39. Egan ES, Jiang RHY, Moechtar MA, Barteneva NS, Weekes MP, Nobre L V, Gygi SP, Paulo JA, Frantzreb C, Tani Y, Takahashi J, Watanabe S, Goldberg J, Paul AS, Brugnara C, Root DE, Wiegand RC, Doench JG, Duraisingh MT. 2015. A forward genetic screen identifies erythrocyte CD55 as essential for *Plasmodium falciparum* invasion. *Science* 348:711–4.
40. Drew ME, Banerjee R, Uffman EW, Gilbertson S, Rosenthal PJ, Goldberg DE. 2008. *Plasmodium* food vacuole plasmepsins are activated by falcipains. *J Biol Chem* 283:12870–12876.
41. Russo I, Oksman A, Goldberg DE. 2009. Fatty acid acylation regulates trafficking of the unusual *Plasmodium falci*parum calpain to the nucleolus. *Mol Microbiol* 72:229–245.
42. Liu J, Gluzman IY, Drew ME, Goldberg DE. 2005. The role of *Plasmodium falciparum* food vacuole plasmepsins. *J Biol Chem* 280:1432–1437.
43. Ganesan SM, Morrisey JM, Ke H, Painter HJ, Laroiya K, Phillips MA, Rathod PK, Mather MW, Vaidya AB. 2011. Yeast dihydroorotate dehydrogenase as a new selectable marker for *Plasmodium falciparum* transfection. *Mol Biochem Parasitol* 177:29–34.
44. Klemba M, Gluzman I, Goldberg DE. 2004. A *Plasmodium falciparum* dipeptidyl aminopeptidase I participates in vacuolar hemoglobin

degradation. *J Biol Chem* 279:43000–43007.

45. Avery JW, Smith GM, Owino SO, Sarr D, Nagy T, Mwalimu S, Matthias J, Kelly LF, Poovassery JS, Middii JD, Abramowsky C, Moore JM. 2012. Maternal malaria induces a procoagulant and antifibrinolytic state that is embryotoxic but responsive to anticoagulant therapy. *PLoS One* 7:1–15.

Figures

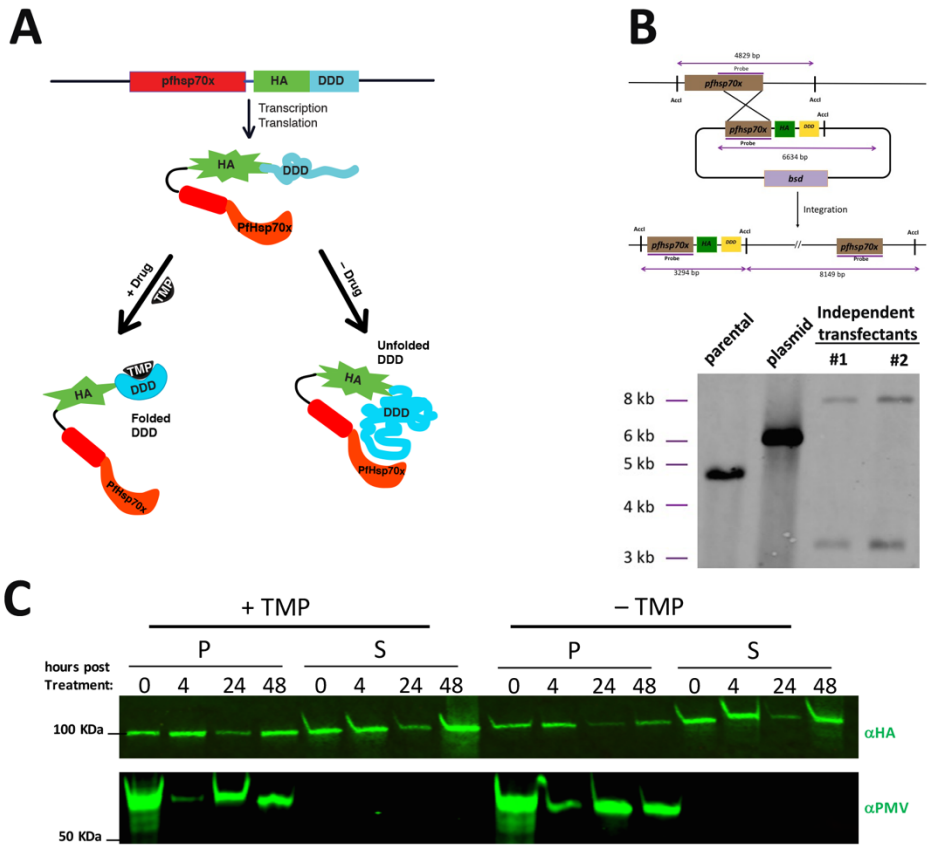

Figure 3.1. Generating *Pf*Hsp70x-DDD parasites. (A) Mechanism of *Pf*Hsp70x-DDD conditional inhibition. The *pfhsp70x* locus was modified to contain a triple hemagglutinin (HA) tag and a DHFR-based destabilization domain (DDD). In the presence of trimethoprim (TMP) the DDD is stable and the chaperone is active. Upon TMP removal the chaperone binds the DDD intra-molecularly and cannot interact with client proteins, inhibiting normal activity. **(B)** Single crossover homologous recombination enables the integration of the plasmid into the 3' end of the *pfhsp70x* gene (upper panel). Southern blot analysis of genomic DNA (bottom panel) isolated from parasite lines indicated above the lanes. The

genomic DNA was digested with AccI. Bands expected from integration of the plasmid into the 3' end of the *pfhsp70x* gene were observed in two independent transfections. A single band indicative of the parental allele was observed for the parental strain and it was absent in the integrant parasites. **(C)** *Pf*Hsp70x-DDD parasites were incubated without TMP, and Schizont stage parasites were purified on a percoll gradient. Host cell lysates together with exported proteins were isolated using 0.04% cold saponin and were then collected from the supernatant (S). Parasites cells with all non-exported proteins were collected from the pellet (P). Using western blot analysis, the two fractions were analyzed and probed for *Pf*Hsp70x expression and export. The membrane was probed with antibodies against HA (top) and Plasmepsin V (loading control, bottom). The protein marker sizes that co-migrated with the probed protein are shown on the left.

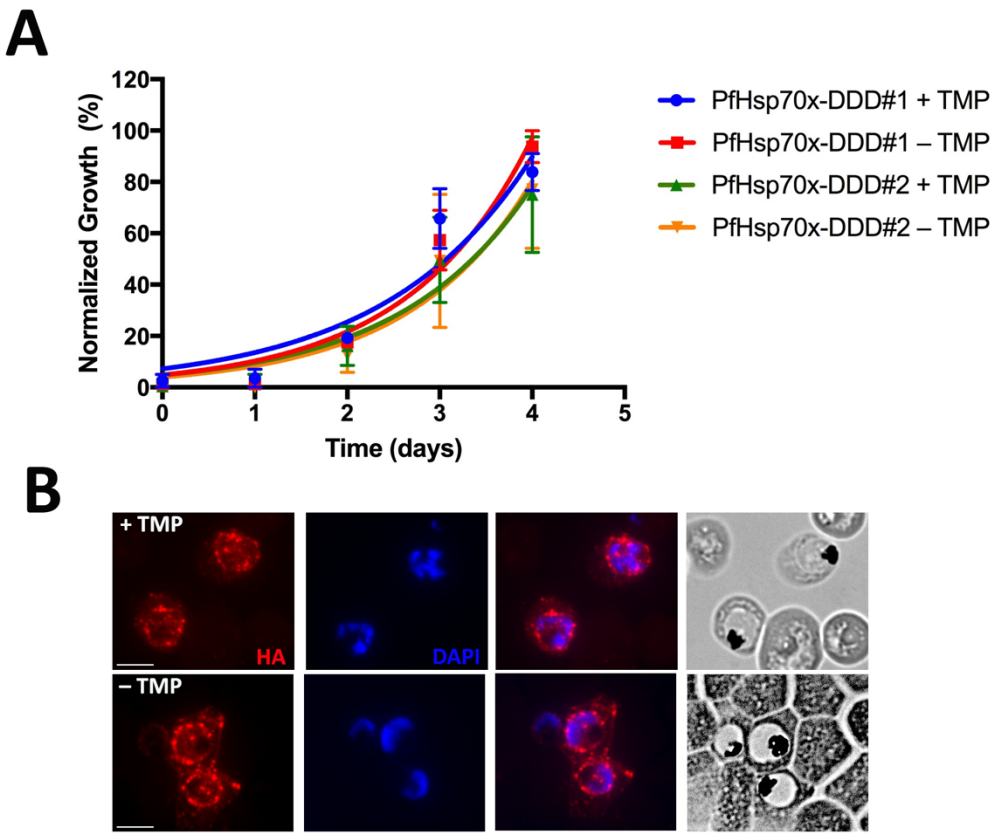

Figure 3.2. TMP removal does not affect parasite growth and *Pf*Hsp70x localization. (A) Asynchronous *Pf*Hsp70x-DDD parasites were grown with or without 10μM TMP and parasitemia was monitored every 24 hours over 5 days. Data are fit to an exponential growth equation and are represented as mean ± S.E.M. Experiments were done 3 times and biological replicates are shown. **(B)** Immunofluorescence imaging of acetone fixed *Pf*Hsp70x-DDD parasites stained with anti-HA (red) and DAPI (blue). Images from left to right are anti-HA (red), DAPI (blue), fluorescence merge, and phase. Scale bar, 5μm.

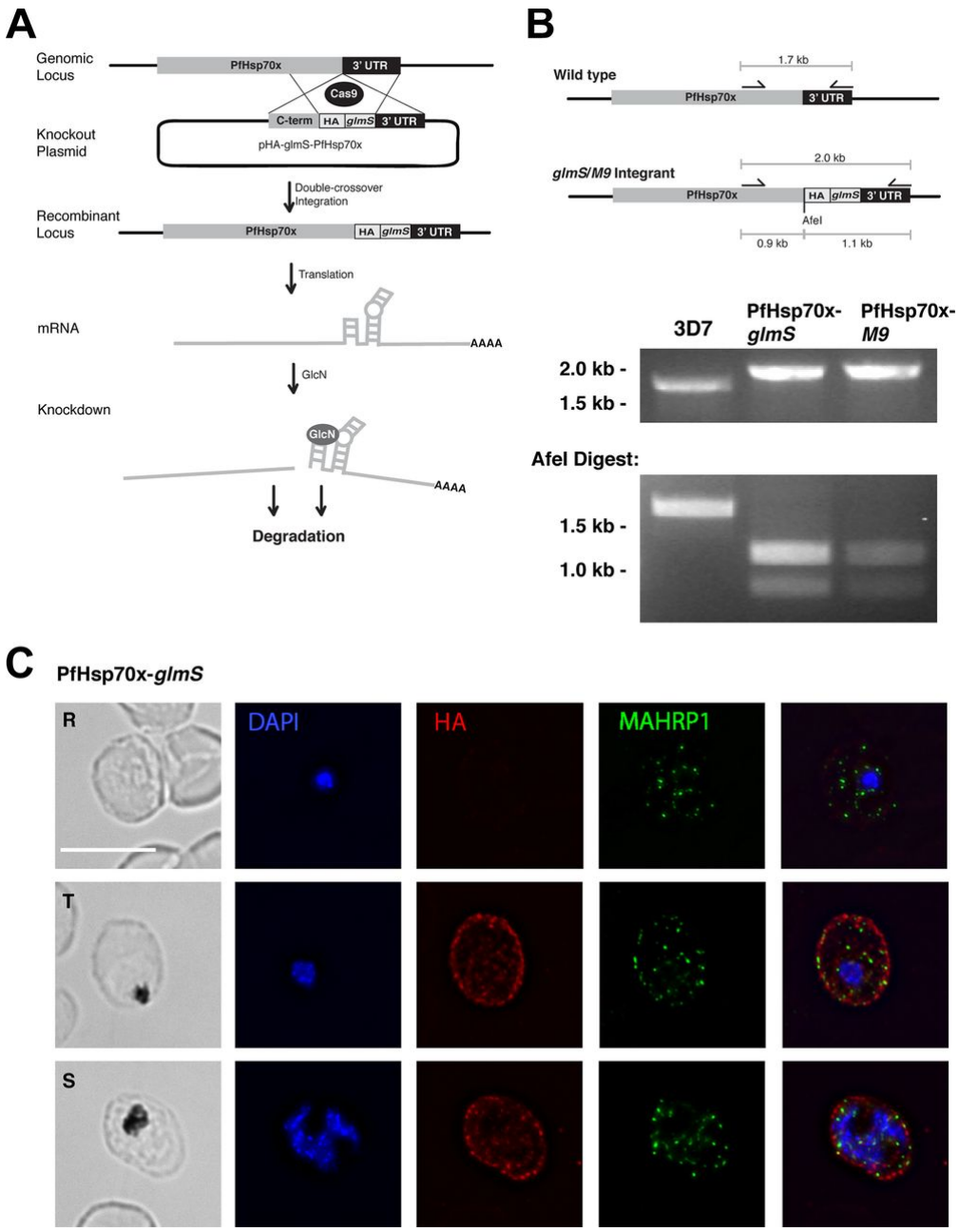

Figure 3.3. CRISPR/Cas9-mediated integration of HA-*glmS*/*M9* at *Pf*Hsp70x locus. (A) Diagram showing integration of 3xHA-ribozyme sequence and GlcN-induced degradation of mRNA. Cas9 introduces a double-stranded break at the beginning of the 3' UTR of the *pfhsp70x* locus. The repair plasmid provides homology regions for double-crossover homologous recombination, introducing a 3xHA tag and the ribozyme sequence. Following translation and addition of GlcN,

the *Pf*Hsp70x-*glmS* mRNA is cleaved by the ribozyme and is subject to degradation. **(B)** PCR test confirming integration at the *Pf*Hsp70x locus. DNA was purified from transfected, cloned parasites and primers were used to amplify the region between the C-terminus and 3'UTR of *pfhsp70x*. The PCR products were digested with AfeI, further confirming integration. **(C)** IFA showing export of HA-tagged *Pf*Hsp70x. Asynchronous *Pf*Hsp70x-*glmS* parasites were fixed with acetone and stained with specific antibodies. Images from left to right are phase, DAPI (parasite nucleus, blue), anti-HA (red), anti-MAHRP1 (green), and fluorescence merge. Scale bar represents 5 μm. (R) rings, (T) trophs and (S) schizont.

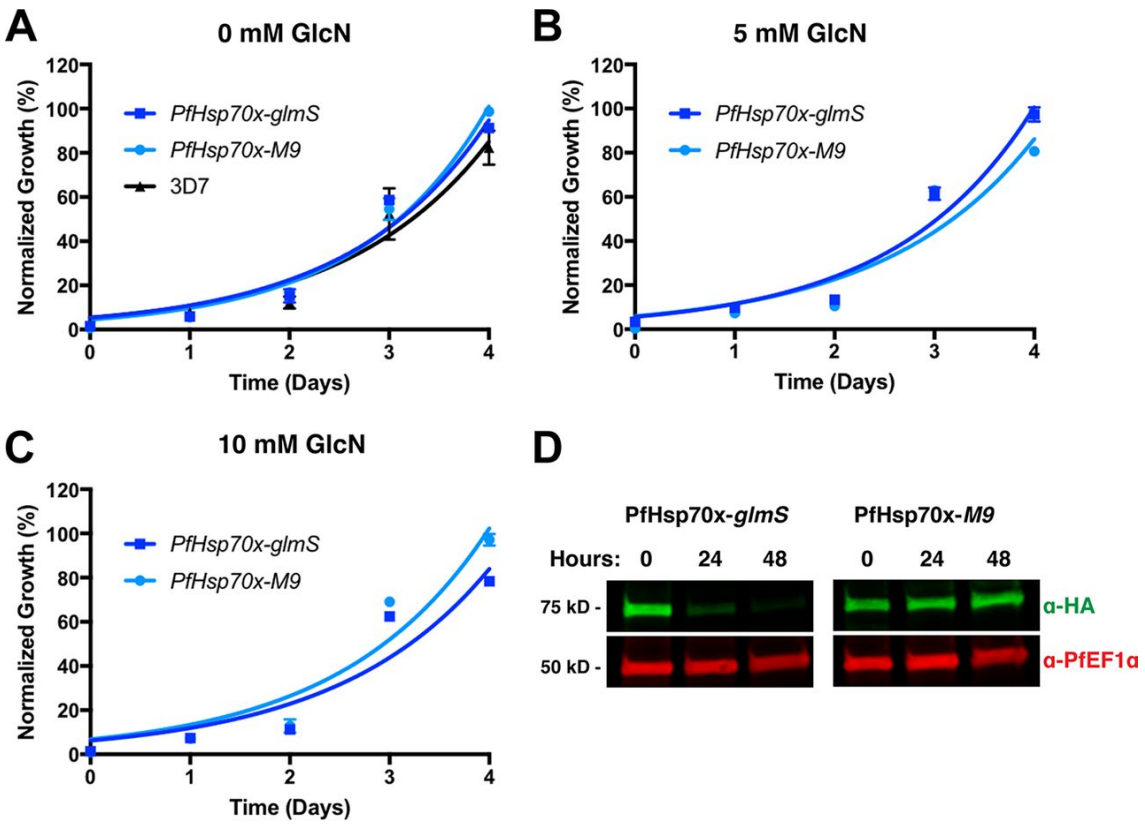

Figure 3.4. GlcN-induced knockdown of *Pf*Hsp70x does not affect intraerythrocytic growth. (A) *Pf*Hsp70x-*glmS*, *Pf*Hsp70x-*M9*, and 3D7 (parental line) were seeded at equal parasitemia in triplicate and grown in normal culturing media (complete RPMI). Parasitemia was measured every 24 hours using flow cytometry. Data are fit to an exponential growth equation and are represented as mean ± S.E.M. (n=3). **(B)** and **(C)** *Pf*Hsp70x-*glmS* and *Pf*Hsp70x-*M9* parasites were seeded at equal parasitemia in triplicate. Cultures were grown in the presence of either 5 mM **(B)** or 10 mM **(C)** GlcN. Parasitemia was measured every 24 hours using flow cytometry. Data are fit to an exponential growth equation and are represented as mean ± S.E.M. (n=3). **(D)** *Pf*Hsp70x-*glmS* and *Pf*Hsp70x-*M9* parasites were grown in the presence of 7.5 mM GlcN. Schizont-stage parasites were Percoll-purified every 24 hours, and whole parasite lysates

were used for western blot analysis. Membrane was probed with anti-HA, and anti-PfEF1α (loading control).

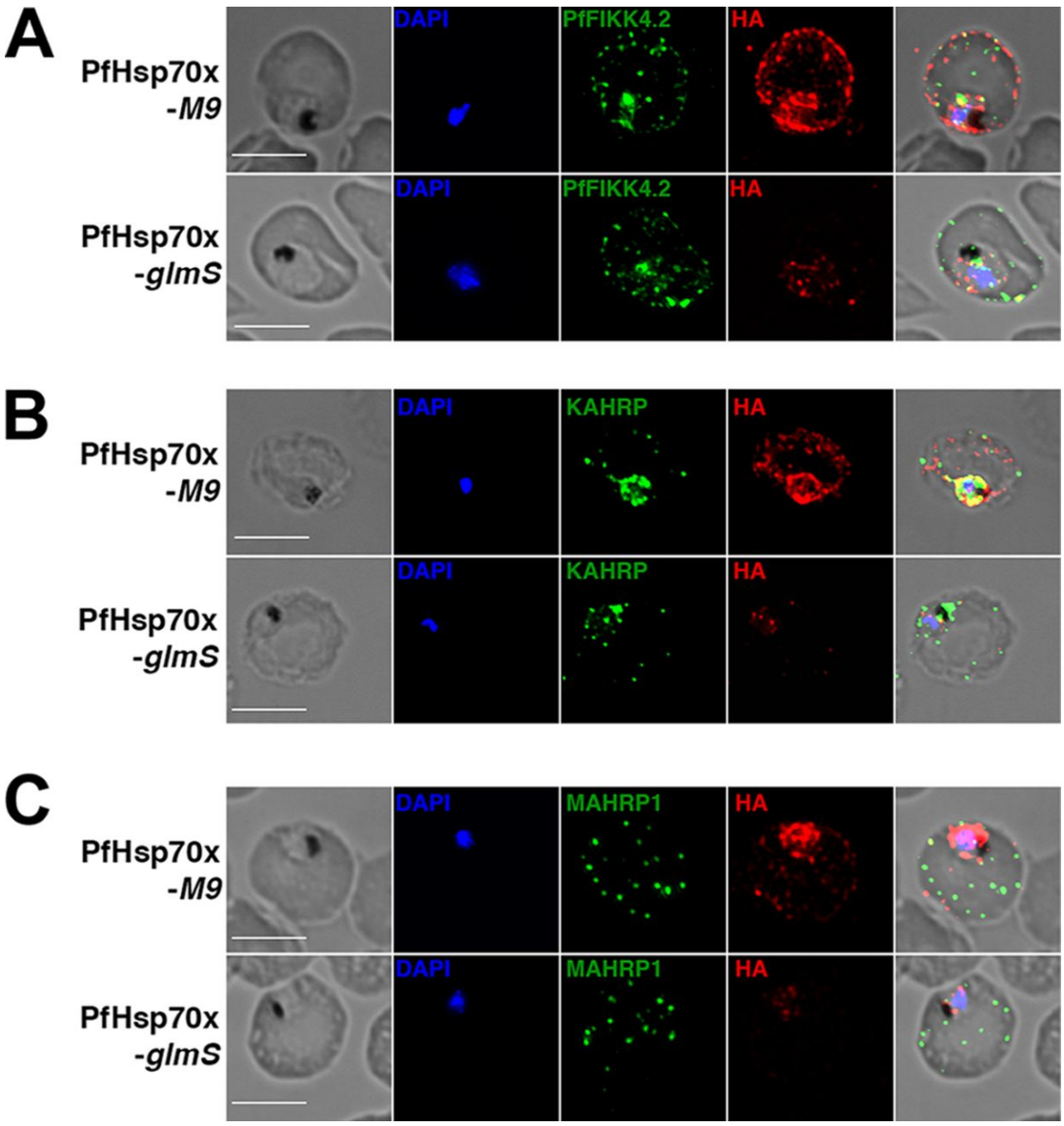

Figure 3.5. *Pf*Hsp70x knockdown does not inhibit export of virulence-associated proteins. Asynchronous *Pf*Hsp70x-*M9* and *Pf*Hsp70x-*glmS* parasites were fixed with acetone (PfFIKK4.2 and MAHRP1) or paraformaldehyde (KAHRP) and stained with antibodies against **(A)** PfFIKK4.2,

(B) KAHRP, or **(C)** MAHRP1. DAPI used to mark parasite cell nucleus. Scale bar represents 5µm. Images from left to right are phase, DAPI (blue), anti-exported protein (green), anti-HA (red), and fluorescence and phase merge. Representative images shown.

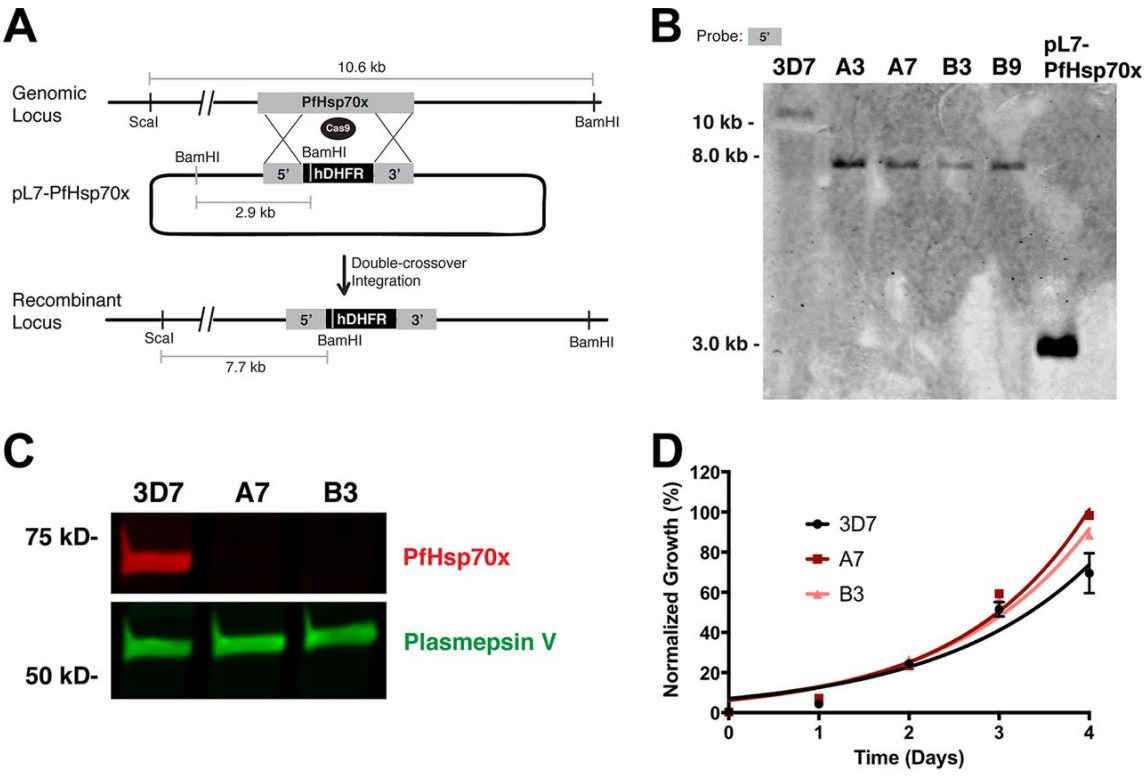

Figure 3.6. Knockout of *pfhsp70x* does not affect intraerythrocytic growth. **(A)** Schematic showing interruption of *Pf*Hsp70x ORF with *hDHFR* cassette. Cas9-mediated double-stranded break in the *pfhsp70x* ORF is repaired using homology regions on the template plasmid while inserting an *hDHFR* cassette into the locus. **(B)** Southern blot analysis confirming knockout of *Pf*Hsp70x. Genomic DNA from independent knockout clones (A3, A7, B3, and B9) was isolated and digested with BamHI and ScaI. Membrane was hybridized with a biotin-labeled probe complementary to the first 800 base pairs of the *pfhsp70x*

ORF. **(C)** Western blot analysis demonstrating loss of *Pf*Hsp70x protein expression in independent knockout clones. Schizont-stage parasites were Percoll-purified, and whole cell lysate was used for analysis. Membrane was probed with antibodies raised against *Pf*Hsp70x, and against Plasmepsin V as a loading control. **(D)** Parental lines and independent PfHsp70x-KO clones (A7 and B3) were seeded at equal parasitemia in triplicate. Parasitemia was measured every 24 hours using flow cytometry. Data are fit to an exponential growth equation and are represented as mean ± S.E.M. (n=3).

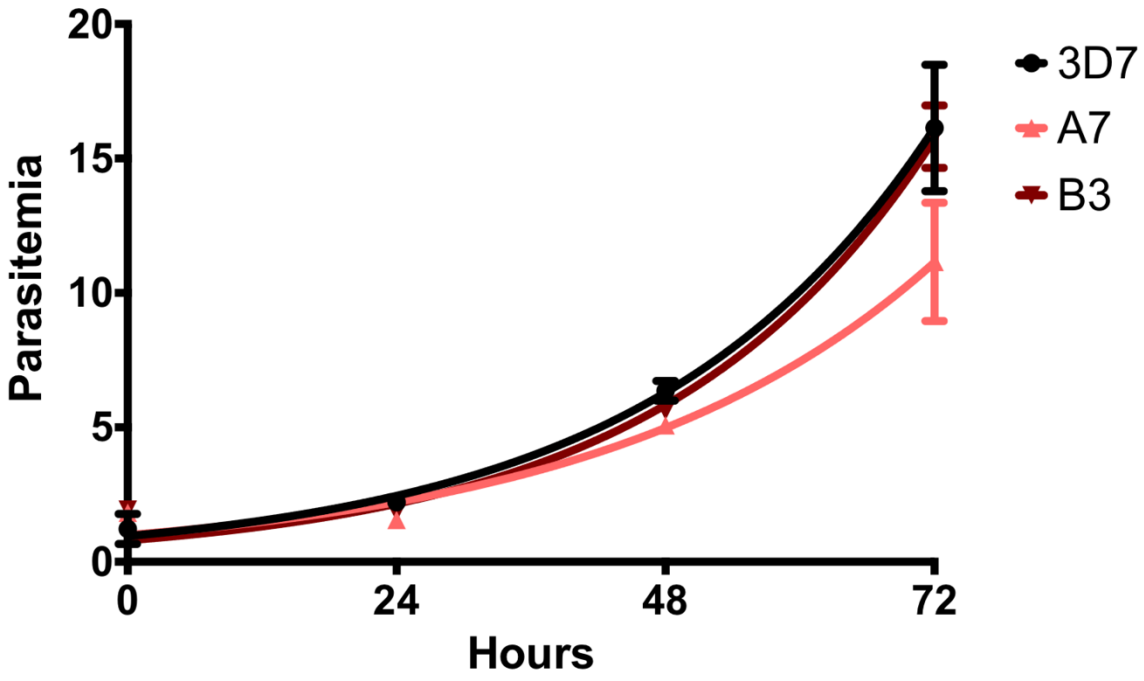

Figure 3.7. Heat shock does not inhibit the growth of PfHsp70x-KO parasites. 3D7 and *Pf*Hsp70x-KO clones A7 and B3 were subjected to 40 degree Celsius heat shock for 4 hours, and parasitemia was measured every 24

hours using flow cytometry. Data are fit to an exponential growth equation and are represented as mean ± S.E.M. (n=3).

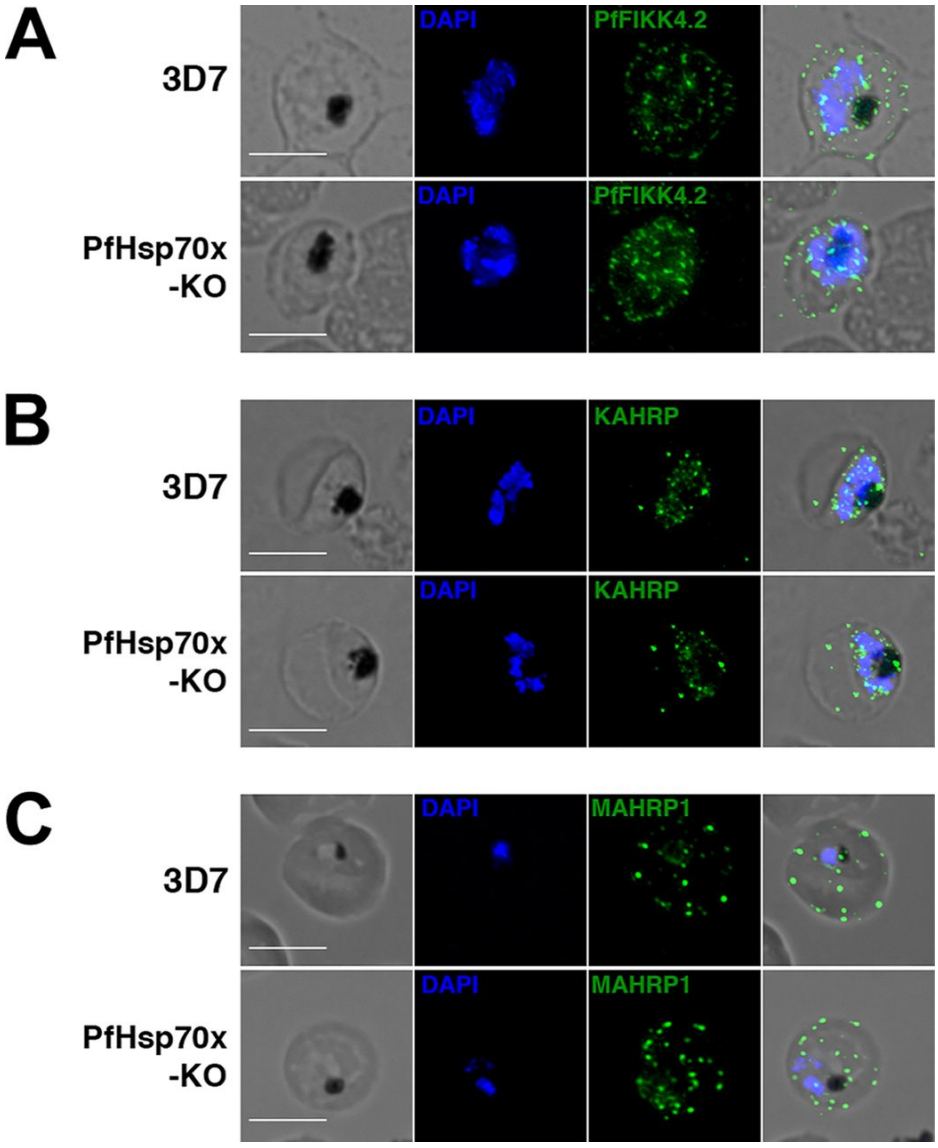

Figure 3.8. *Pf*Hsp70x knockout does not inhibit export of virulence-associated proteins. Asynchronous 3D7 and *Pf*Hsp70x-KO parasites were fixed with acetone (PfFIKK4.2 and MAHRP1) or paraformaldehyde (KAHRP) and stained with antibodies against **(A)** PfFIKK4.2, **(B)** KAHRP, or **(C)** MAHRP1.

DAPI used to mark parasite cell nucleus. Images from left to right are phase, DAPI (blue), anti-exported protein (green), and fluorescence and phase merge. Scale bar represents 5μm. Representative images shown.

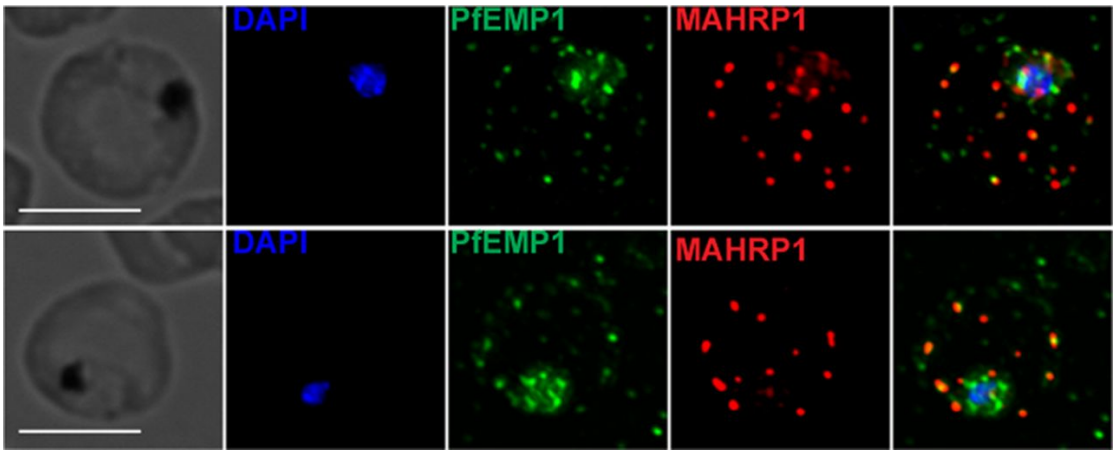

Figure 3.9. *Pf*Hsp70x knockout does not inhibit export of PfEMP1 to the host cell. Asynchronous 3D7 and *Pf*Hsp70x-KO parasites were fixed with acetone and stained with antibodies against the ATS domain of *Pf*EMP1 and MAHRP1. DAPI used to stain parasite cell nucleus. Images from left to right are phase, DAPI (Blue), PfEMP1 (green), MAHRP1 (red), and fluorescence merge. Representative images shown.

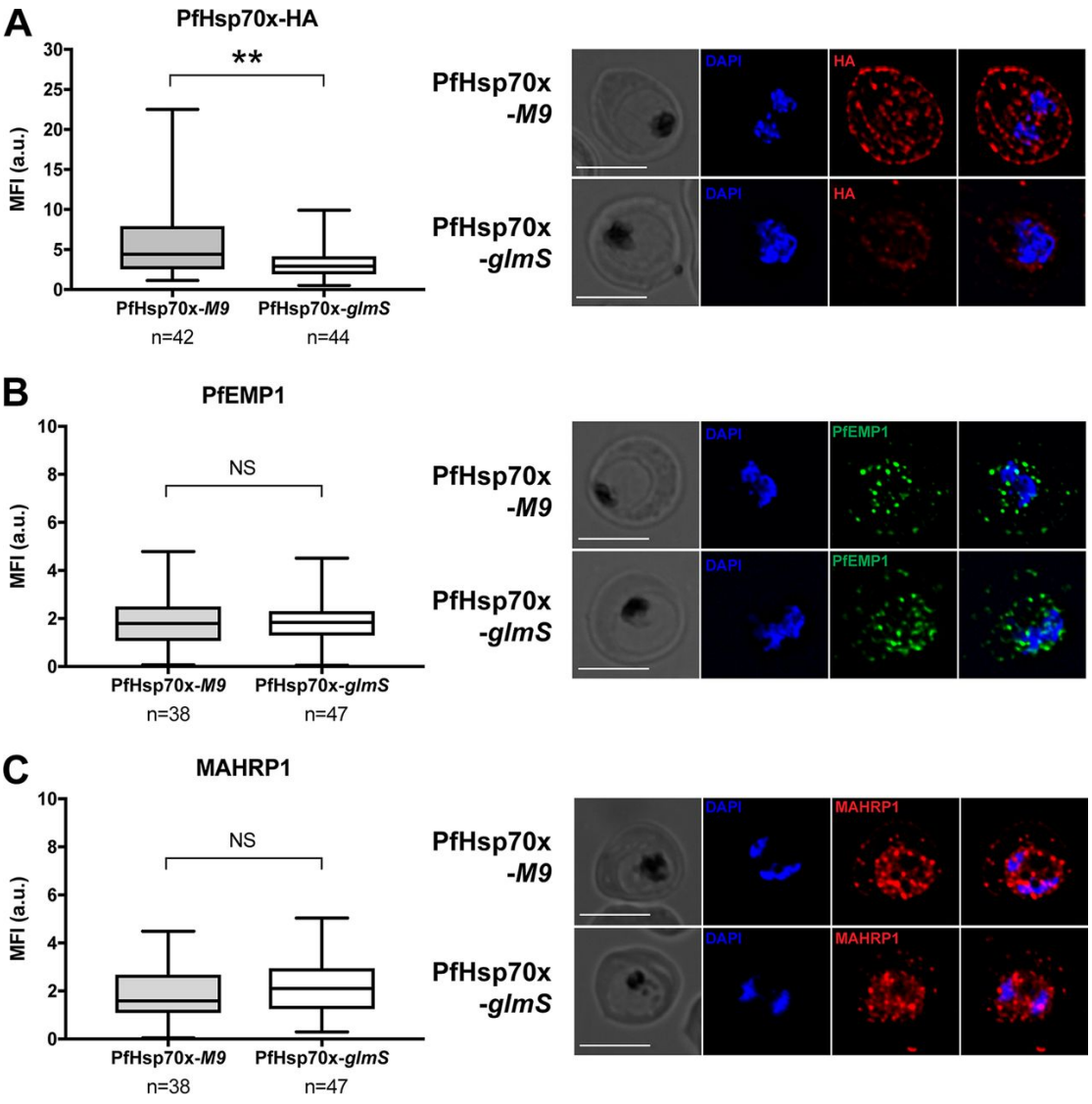

Figure 3.10. Knockdown of *Pf*Hsp70x does not inhibit export of *Pf*EMP1 to the host cell. *Pf*Hsp70x-*M9* and *Pf*Hsp70x-*glmS* parasites were fixed with acetone and stained with antibodies against **(A)** HA, **(B)** *Pf*EMP1, or **(C)** MAHRP1. DAPI used to mark parasite cell nucleus. Scale bar represents 5μm. Images from left to right are phase, DAPI, anti-HA or –exported protein, and fluorescence merge. Representative images shown. The mean fluorescence intensity (MFI) for each protein was calculated for individual cells and is shown as box-and-whisker plots, with whiskers representing the maximum and minimum

MFI. For HA, the MFI was calculated for the entire infected RBC. For *Pf*EMP1 and MAHRP1, MFI was calculated for the exported fraction only. Significance was determined using an unpaired t-test (**, P ≤ 0.01. NS = not significant).

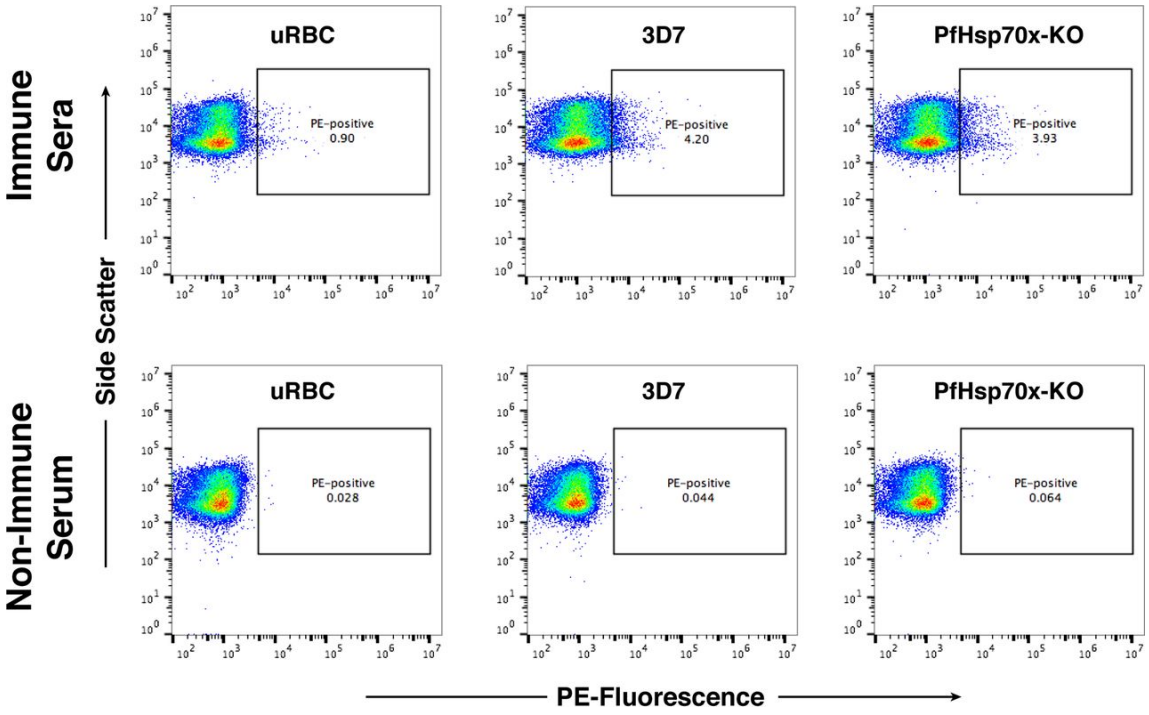

Figure 3.11. Human immune sera recognizes 3D7 and *Pf*Hsp70x-KO parasites. Synchronized 3D7 and *Pf*Hsp70x-KO parasites were incubated with either pooled human sera from malaria-endemic Kenya (top panels) or non-immune human serum from the United States. Recognition by the serum was determined using a PE-conjugated anti-human-IgG antibody and flow cytometry. Also assayed were uninfected red blood cells (uRBCs). Side-scatter shown on the Y axis, and PE fluorescence on the X axis.

CHAPTER 4

FUNCTION AND DRUGGABILITY OF THIOREDOXIN-DOMAIN PROTEINS IN THE ENDOPLASMIC RETICULUM OF HUMAN MALARIA PARASITES

David W. Cobb, Heather M. Kudyba, Alejandra Villegas, Michael R. Hoopmann, Rodrigo Baptista, Baylee Bruton, Michelle Krakowiak, Robert L. Moritz, Vasant Muralidharan. 2020. Submitted to *PLoS Pathogens*.

Abstract

Malaria remains a major global health problem, creating a constant need for research to identify druggable weaknesses in *P. falciparum* biology. As important components of cellular redox biology, members of the Thioredoxin (Trx) superfamily of proteins have received interest as potential drug targets in Apicomplexans. However, the function and essentiality of endoplasmic reticulum (ER)-localized Trx-domain proteins within *P. falciparum* has not been investigated. We generated conditional mutants of the protein *Pf*J2—an ER chaperone and member of the Trx superfamily—and show that it is essential for asexual parasite survival. Using a crosslinker specific for redox-active cysteines, we identified *Pf*J2 substrates as *Pf*PDI8 and *Pf*PDI11, both members of the Trx superfamily as well, which suggests a redox-regulatory role for *Pf*J2. Knockdown of these PDIs in *Pf*J2 conditional mutants show that *Pf*PDI11 may not be essential. However, *Pf*PDI8 is required for asexual growth and our data suggest it may work in a complex with *Pf*J2 and other ER chaperones. Finally, we show that the redox interactions between these Trx-domain proteins in the parasite ER and their substrates are sensitive to small molecule inhibition. Together these data build a model for how Trx-domain proteins in the *P. falciparum* ER work together to assist protein folding and demonstrate the suitability of ER-localized Trx-domain proteins for antimalarial drug development.

Introduction

Today, the majority of the world's population lives at risk for contracting malaria, a disease caused by eukaryotic parasites of the genus *Plasmodium*, with *P. falciparum* causing the most severe forms of the disease (World Heath Organization, 2019). In 2018, the world saw approximately 228 million cases of malaria resulting in more than 400,000 deaths. These numbers reflect a concerted effort to combat malaria in the past few decades, but progress has stagnated, with the numbers of malaria cases/deaths largely unchanged in recent years. A major impediment in the fight against malaria is the rise of drug-resistant—including multidrug-resistant—*P. falciparum* parasites, highlighting the continuous need for research into the biology of this major human pathogen and identification of promising drug targets.

The thioredoxin system and members of the Thioredoxin (Trx) superfamily of proteins have received interest as potential drug targets in Apicomplexan parasites, including in *Plasmodium* (Andricopulo et al., 2006; Becker et al., 2000; Biddau et al., 2018; Biddau & Sheiner, 2019). Members of the Trx superfamily typically contain at least one Trx domain with a "CXXC" active site. An oxidized Trx domain in which the active site cysteines have formed a disulfide bond can accept electrons to oxidize other proteins, and the sulfhydryl groups of a reduced Trx domain can donate electrons to reduce other proteins. As modulators of protein redox states, members of the Trx superfamily regulate diverse aspects of cellular biology. In *Plasmodium*, members of this superfamily are found in several cellular compartments (Kehr et al., 2010). Of these, the cytoplasmic Trx system

has been most characterized in *Plasmodium* (Krnajski et al., 2001). Within the parasite cytoplasm, Trx Reductase reduces Trx1, which in turn serves as a reductase for other proteins potentially involved in protein synthesis and folding, anti-oxidant stress response, carbohydrate and lipid metabolism, and several other processes (Kawazu et al., 2010; Sturm et al., 2009).

An important subset of Trx superfamily members that has received little study in *Plasmodium* are those that localize to the endoplasmic reticulum (ER). Classically, Trx domains in the ER are used to regulate the redox state of cysteines in other proteins, and to facilitate oxidative folding (the formation, reduction, and isomerization of disulfide bonds in newly synthesized proteins) (Hatahet & Ruddock, 2009). The *P. falciparum* ER functions in many essential processes during the asexual replication cycle—particularly by serving as the root of the parasite's complex secretory pathway—and ER-localized members of the Trx superfamily likely play critical roles in supporting these functions. *P. falciparum* encodes an ER-localized Hsp40 chaperone with a C-terminal Trx domain known as *Pf*J2 (Botha et al., 2007; Oehring et al., 2012). *Pf*J2 shares homology with the mammalian protein ERdj5, whose Trx domains serve the critical function of reducing other proteins' disulfide bonds within the oxidizing environment of the mammalian ER, which suggests *Pf*J2 may similarly act as a reductase in the *P. falciparum* ER (Cunnea et al., 2003; Oka et al., 2013; Ushioda et al., 2008). The P*. falciparum* genome also encodes four members of the Protein Disulfide Isomerase (PDI) family of proteins, which typically use their Trx domains as oxidoreductases to assist folding proteins form their correct

disulfide bonds (Mahajan et al., 2006). One member of the PDI family, *Pf*PDI8, has been localized to the ER and found able to form and reduce the disulfide bonds of proteins folding *in vitro*, including the parasite protein Erythrocyte-Binding Antigen 175 (EBA175) (Mahajan et al., 2006; Mouray et al., 2007). However, *Pf*J2 and the PDIs remain largely unstudied in the parasites, and their essentiality for *P. falciparum* survival within the host RBC and functions within the ER have not been investigated.

The ability to reduce disulfide bonds is critical within the oxidative environment of the ER, both for regulating protein function and for allowing correct disulfide pairs to form as proteins are folding (Ellgaard et al., 2018). We therefore chose the putative reductase *Pf*J2 for study, and we report here that *Pf*J2 is essential for the *P. falciparum* asexual lifecycle. We identify *Pf*J2 interacting partners and use a chemical biology approach to specifically identify those proteins which may be reduced by *Pf*J2. Surprisingly, these were found to be other Trx-domain proteins: *Pf*PDI8 and *Pf*PDI11. We demonstrate that *Pf*PDI8 is also essential for the asexual lifecycle, and our data suggests that *PfJ2 and Pf*PDI8 may work together with the Hsp70 *Pf*BiP to promote protein folding in the ER. Additionally, we demonstrate that the redox interactions between these essential proteins and their substrates are disrupted by a small molecule inhibitor. Together, these data suggest a model in *Plasmodium* for oxidative folding, in which Trx-domain proteins and *Pf*BiP cooperate to ensure proteins reach their native states, and we propose that the oxidative folding process of the *P. falciparum* ER is an exploitable drug target.

Results

*Pf*J2 is an essential, ER-resident Hsp40

*Pf*J2 is an ER-resident Hsp40 with a C-terminal thioredoxin (Trx) domain (**Figure 4.1A, B**). It has similarity to a reductase in the mammalian ER which has Trx domains following an Hsp40 J-domain, suggesting PfJ2 may catalyze disulfide bond reduction of client proteins (Cunnea et al., 2003; Oka et al., 2013; Ushioda et al., 2008). To investigate *Pf*J2 function and its potential role in *P. falciparum* oxidative folding, we generated a *Pf*J2 conditional knockdown parasite line using the TetR-*Pf*DOZI aptamer system (referred to as *Pf*J2^{apt} hereafter). In this knockdown system, protein expression is regulated by the presence of anhydrotetracycline (aTc), with knockdown induced by removal of aTc (Ganesan et al., 2016) (**Figure 4.1C**). Using CRISPR/Cas9 genome editing, we modified the *pfj2* locus to encode a 3xHA-tag immediately upstream of the ER-retention signal, as well as the regulatory aptamer sequences and a cassette to express the TetR-*Pf*DOZI fusion protein (**Figure 4.1D**). Correct integration of the construct into the *pfj2* locus was determined by PCR, and expression of HA-tagged *Pf*J2 was demonstrated via western blot (**Figure 4.1D**).

Using an immunofluorescence assay (IFA), we assessed the localization of *Pf*J2 throughout the asexual lifecycle (**Figure 4.2A**). Co-localization between *Pf*J2 and the ER-marker Plasmepsin V (*Pf*PMV) revealed that *Pf*J2 is in fact an ER-resident protein, consistent with the localization of exogenously overexpressed *Pf*J2 previously reported (**Figure 4.2A**) (Oehring et al., 2012).

Using highly synchronized parasites, we showed that *Pf*J2 is primarily expressed in the trophozoite and schizont stages, and that during knockdown conditions (removal of aTc), *Pf*J2 expression is reduced (**Figure 4.2B**). Importantly, knockdown of *Pf*J2 was found to inhibit expansion of parasites in culture (**Figure 4.2C**). Consistent with peak *Pf*J2 expression during the trophozoite/schizont stages, we observed normal development of knockdown parasites in the beginning of the asexual life cycle, but the development of these parasites began to slow in the trophozoite stage and they failed to complete schizogony and produce new daughter parasites (**Figure 4.3, Figure 4.2D**). These data demonstrate that *Pf*J2 is a *bona fide* ER-resident protein essential for progression through the *P. falciparum* asexual lifecycle.

*Pf*J2 interacts with essential ER chaperones and proteins in the secretory pathway

As a putative chaperone possibly involved in ER oxidative folding, we reasoned that the essentiality of *Pf*J2 is likely related to its ability to interact with other proteins in the ER. We therefore took a co-immunoprecipitation (coIP) approach to identify *Pf*J2 interacting partners. *Pf*J2 was immunoprecipitated from *Pf*J2^{apt} parasite lysates using anti-HA antibodies, and co-immunoprecipitating proteins were identified by tandem mass spectrometry (MS/MS) analysis. Control parental parasites (lacking HA-tagged *Pf*J2) were also used for immunoprecipitation and analyzed in the same manner. Each co-IP experiment was performed in triplicate, and the abundance of each identified protein was calculated by

summing the total MS1 intensities of all matched peptides for each selected protein, and normalizing by the total summed intensity of all matched peptides in the sample (**Figure 4.4A**) (Boucher et al., 2018; Florentin et al., 2020). Because *Pf*J2 is an ER-localized protein, we further narrowed our list of interacting partners to those containing a signal peptide and/or at least one transmembrane domain (i.e. proteins predicted to be within the ER or traffic through the secretory pathway). We identified a stringent list of high-confidence interacting partners as those proteins which were present in all three *Pf*J2^{apt} coIP experiments, and were at least 5-fold more abundant compared to the controls, as previously described (Florentin et al., 2020) (**Figure 4.4B, C**). A complete list of identified proteins is provided in **Appendix A**.

We identified other conserved proteins classically involved in essential ER processes—such as the Hsp70 Binding immunoglobulin Protein (BiP), the Hsp90 Endoplasmin, and the oxidoreductase Protein Disulfide Isomerase (PDI). We further identified proteins that are trafficked through the ER late in the parasite lifecycle and are required for egress and invasion, including *Pf*MSP1 and proteins destined for rhoptries (Das et al., 2015; Ito et al., 2017; Richard et al., 2009; Sherling et al., 2017). Nearly half of the identified proteins lack empirical evidence for their subcellular localization, and many have no known function. But, given the presence of a signal peptide and/or transmembrane domains, these proteins likely have localizations in the ER, parasite plasma membrane, apicoplast, and other destinations that are part of the secretory pathway. Also of note, approximately two-thirds of the identified proteins are predicted to have

essential functions (Zhang et al., 2018). These data together suggest that *Pf*J2 may work with other ER-resident chaperones to ensure proper folding/functioning of proteins that have essential roles throughout the parasite.

PfJ2 is a redox-active protein in the *P. falciparum* ER

We next sought to determine whether *Pf*J2 participates in disulfide exchanges with other proteins by chemically trapping these redox partnerships. To this end we employed the bifunctional, electrophilic crosslinker divinyl sulfone (DVSF), which shows remarkable specificity for nucleophilic cysteines, like those present in Trx domain active sites (West et al., 2011). In *Saccharomyces cerevisiae*, DVSF was used to specifically trap Thioredoxin to two proteins known to exchange electrons with its CXXC active site, validating the compound's ability to covalently and irreversibly trap Trx domains to their redox substrates (Naticchia et al., 2013). DVSF was subsequently used to identify substrates of other redox-active proteins containing hyper-reactive cysteines in *S. cerevisiae* and human cells (Allan et al., 2016; Araki et al., 2017). To determine whether DVSF was capable of trapping redox partnerships in *P. falciparum*, we treated *Pf*J2^{apt} parasite cultures with DVSF and isolated proteins for western blot analysis. In the absence of DVSF, *Pf*J2 was detected at approximately 50 kDa, while the addition of DVSF resulted in additional bands containing *Pf*J2 to appear between 100-150 kDa (**Figure 4.5A**). To demonstrate specificity of DVSF for nucleophilic cysteines participating in disulfide exchanges, the ER-resident protein *Pf*PMV—which contains 16 cysteines after its signal peptide—was probed for in the same

samples and its migration pattern was found to be unaffected by DVSF treatment (**Figure 4.5A**). As an additional control, *Pf*J2^{apt} parasite cultures were treated with the sulfhydryl-blocking compound N-ethylmaleimide (NEM) prior to the addition of DVSF. Pre-treatment with NEM resulted in the blockage of cross-linking between *Pf*J2 and its redox partners (**Figure 4.5B**). These results indicate that *Pf*J2 likely does participate in disulfide exchange, and that DVSF is a useful chemical tool for trapping redox interactions in the ER of *P. falciparum*.

*Pf*PDI8 and *Pf*PDI11 are *Pf*J2 redox partners

Having shown the redox activity of *Pf*J2, we next sought to specifically identify those redox partnerships. To identify the proteins trapped to *Pf*J2 by DVSF, cultures were treated with the compound and immunoprecipitation of *Pf*J2 was performed (**Figure 4.5C**). As a control, the immunoprecipitation was also performed in parallel using cultures that had not received DVSF treatment. The immunoprecipitated proteins were subjected to separation by SDS-PAGE and visualized using Coomassie (**Figure 4.5C**). Two bands between 100-150 kDa, corresponding to those previously detected by western blot, were extracted from the DVSF-treated sample, along with the corresponding areas of the gel in the untreated samples (**Figure 4.5C**, perforated boxes). Proteins present in these gel slices were identified via MS/MS analysis. By analyzing the untreated control samples, we were able to remove background proteins and found that the top gel slice primarily contained *Pf*J2, *Pf*PDI8, *Pf*PDI11 and *Pf*BiP, and the bottom slice contained *Pf*J2, *Pf*PDI8, and *Pf*PDI11 (**Figure 4.5C**, table). The complete list of

proteins identified in all samples can be found in **Appendix B**. Because alterations to *Pf*BiP migration during SDS-PAGE after DVSF treatment were not detected (**Figure 4.6**), we chose to focus our attentions on *Pf*PDI8 and -11.

*Pf*PDI8 and *Pf*PDI11 are redox-active ER proteins

Like *Pf*J2, *Pf*PDI8 and -11 are both predicted members of the Trx superfamily (**Figure 4.7A**). *Pf*PDI8 appears to be a canonical PDI, with two Trx domains containing CXXC active sites that likely allow it to carry out disulfide oxidoreductase/isomerase activity. PfPDI11 also has two Trx domains, but each contains an unusual CXXS active site. *Pf*PDI8 has been characterized recombinantly *in vitro*, but the functions of both *Pf*PDI8 and -11 remain unstudied in parasites (Mahajan et al., 2006; Mouray et al., 2007). In order to validate interaction between these PDIs and *Pf*J2, and to understand their roles in the *P. falciparum* ER, we used the *glmS* ribozyme to create conditional knockdown parasite lines for each protein in the background of *Pf*J2^{apt} parasites (Prommana et al., 2013) (**Figure 4.7B**). Using CRISPR/Cas9 genome editing, we introduced sequences for a 3xV5 tag and the *glmS* ribozyme into the *pfpdi8* or the *pfpdi11* locus (*Pf*J2^{apt}-PDI8^{glmS} and *Pf*J2^{apt}-PDI11^{glmS}, respectively) (**Figure 4.7C**). Correct modifications of the loci were validated by PCR integration test, and V5-tagged proteins were visualized by western blot (**Figure 4.7D, E**).

The subcellular localizations of *Pf*PDI8 and -11 were determined by IFA, and both proteins were found to co-localize with *Pf*J2 in the ER (**Figure 4.8A**). To test the functionality of the *glmS* ribozyme knockdown system, each parasite line

was treated with glucosamine (GlcN), and samples were taken for western blot analysis over the course of the parasite lifecycle. Compared to untreated control samples, protein levels were found to be reduced during GlcN treatment (**Figure 4.9**). In order to determine the effect that PDI knockdown had on parasite growth, each cell line was treated with GlcN and parasite growth was measured over the course of two life cycles. We observed dramatic inhibition of parasite growth during *Pf*PDI8 knockdown, but no growth defects were observed when *Pf*PDI11 was knocked down (**Figure 4.8B**). These results demonstrate that *Pf*PDI8 is essential for the asexual lifecycle and suggest that *Pf*PDI11 may be dispensable. Both conclusions are supported by a genome-wide essentiality screen performed in *P. falciparum* (Zhang et al., 2018).

*Pf*PDI8 contains two thioredoxin domains with classical CXXC active site cysteines, allowing the protein to function in oxidative folding as an oxidoreductase/isomerase (Mahajan et al., 2006; Mouray et al., 2007). *Pf*PDI11 has two thioredoxin domains containing noncanonical CXXS active sites, but likely maintains the ability to form mixed disulfide bonds with client proteins through the conserved cysteine residues (Anelli, 2003; Fomenko & Gladyshev, 2009; Park et al., 2009). To determine whether we could trap redox interactions between these PDIs and their substrates, *Pf*J2^{apt}-PDI8^{glmS} and *Pf*J2^{apt}-PDI11^{glmS} cultures were treated with DVSF, and protein lysates were collected for western blot analysis. Several high molecular weight bands containing *Pf*PDI8 appear following DVSF treatment, indicating that multiple substrates rely on the oxidoreductase activity of *Pf*PDI8, in contrast to *Pf*J2, whose western blot shows

a narrower set of redox substrates (**Figure 4.8C**). Similar results were observed for PfPDI11 (**Figure 4.8C**).

We next sought to confirm that DVSF crosslinking occurs through Trx-domain cysteines. To do this, we attempted to generate parasites overexpressing either wild-type copies of *Pf*J2, *Pf*PDI8, *Pf*PDI11, or overexpressing these proteins with cysteine-to-alanine mutations in the Trx domain active sites. These types of mutations abolish DVSF-crosslinking in Trx proteins of model organisms (Araki et al., 2017; Naticchia et al., 2013). We were unable to generate parasites overexpressing wild-type or mutant copies of *Pf*J2. We were also unable to generate parasites overexpressing a mutant version of *Pf*PDI8, but were successful in creating parasites overexpressing the wild-type protein; characterization of that parasite line revealed mislocalization of the overexpressed *Pf*PDI8 (**Figure 4.10**). Given the essential nature of *Pf*J2 and *Pf*PDI8, we concluded that the parasites may be sensitive to their overexpression and to mutations in their Trx domains.

In contrast, we were successfully able to generate both wild-type and cysteine-to-alanine *Pf*PDI11 overexpression mutants (*Pf*PDI11^{wt} and *Pf*PDI11^{mut}, respectively) (**Figure 4.11**). Both parasite lines displayed the expected ER co-localization with PfJ2 (**Figure 4.11**). Importantly, treatment of these parasites with DVSF revealed extensive crosslinking between *Pf*PDI11 and substrates in the wild-type parasites, but crosslinking is abolished in parasites with cysteine-to-alanine mutations in the Trx domain (**Figure 4.11**). These data demonstrated the specificity of DVSF for trapping redox partnerships in *P. falciparum*.

Given the unusual nature of the *Pf*PDI11 CXXS Trx-domain active site, we took advantage of these overexpression parasites to further investigate *Pf*PDI11 function. Trx-domain-proteins with CXXS active sites are largely under-studied in all organisms (Anelli, 2003; Fomenko & Gladyshev, 2009; Park et al., 2009). It is possible that the remaining active-site cysteines in *Pf*PDI11 forms mixed disulfides that may serve to retain proteins the in ER, prevent their aggregation, and/or block cysteines from non-productive bond formation as they fold (Anelli, 2003; Park et al., 2009). Therefore, we hypothesized that we would be able to detect the mixed *Pf*PDI11-substrate disulfide bonds by non-reducing SDS-PAGE and western blotting. Indeed, we were able to detect high-molecular-weight species of *Pf*PDI11 when *Pf*PDI11^{wt} parasite lysates were used for western blotting under non-reducing conditions (**Figure 4.12**). In contrast, these species were missing when *Pf*PDI11^{mut} parasite lysates were used (**Figure 4.12**).

The *Pf*BiP-*Pf*J2-*Pf*PDI8 oxidative folding complex

Having shown that *Pf*J2 and *Pf*PDI8 are redox partners and that both proteins are essential for the *P. falciparum* asexual lifecycle, we decided to focus on their interaction and what roles they may play together in the ER. To confirm the interaction between *Pf*J2 and *Pf*PDI8, *Pf*J2 was immunoprecipitated from *Pf*J2^{apt}-PDI8^{glmS} parasites, and *Pf*PDI8 was found to co-immunoprecipitate (**Figure 4.13A**). When performing the reciprocal co-IP, we were unable to detect *Pf*J2 pulling down with *Pf*PDI8, perhaps due to inefficiency of the anti-V5 IP (**Figure 4.14**). However, we were able to detect a band of overlapping *Pf*J2/*Pf*PDI8 signal

when the *Pf*PDI8 IP was performed on cultures treated with DVSF, showing that the two proteins are interacting, redox partners (**Figure 4.13B**).

Our observations using the redox crosslinker DVSF showed that *Pf*PDI8 is a major redox partner for *Pf*J2, whereas *Pf*PDI8 has multiple other redox partnerships (**Figures 4.5C, 4.8D**). One explanation for this observation is that *Pf*J2 may work upstream to prime *Pf*PDI8 for interaction with its substrates. Therefore, we asked whether we could detect *Pf*PDI8+substrates co-immunoprecipitating with *Pf*J2. When *Pf*J2 was immunoprecipitated from *Pf*J2^{apt}-PDI8^{glmS} parasites treated with DVSF, we were able to detect *Pf*PDI8 trapped to other substrates, indicated by smearing of the *Pf*PDI8 signal above 150 kDa (**Figure 4.13C**). Together, these results confirm the interaction between *Pf*J2 and *Pf*PDI8 and suggest that *Pf*J2 may be part of a complex including *Pf*PDI8 and its substrates.

Oxidative folding in the ER, mediated by proteins such as *Pf*J2 and *Pf*PDI8, is only one aspect of protein folding in the ER, and likely works in conjunction with other folding determinants, such as the Hsp70 BiP. *Pf*J2 is an ER Hsp40—a class of co-chaperones that interact with the Hsp70 BiP—and BiP is likely involved in the folding of the same substrates that interact with *Pf*PDI8. Such cooperation between BiP and mediators of oxidative folding has not received much investigation in any organism, to our knowledge. Therefore, we next asked whether *Pf*BiP interacts with *Pf*J2 and/or *Pf*PDI8.

Western blot analysis of proteins co-immunoprecipitating with *Pf*J2 revealed that *Pf*BiP does interact with *Pf*J2, consistent with our *Pf*J2 co-IP

experiments and the proteins' predicted chaperone/co-chaperone roles (**Figure 4.4, Figure 4.13D**, top). Lack of a suitable antibody precluded reciprocal *Pf*BiP immunoprecipitation to probe for *Pf*J2. However, as a control we showed that *Pf*BiP is not detected when wild-type parasites (lacking HA-tagged *Pf*J2) are subjected to anti-HA immunoprecipitation, ruling out nonspecific binding during the co-IP experiment (**Figure 4.15**).

Next, we found that when *Pf*PDI8 was immunoprecipitated, *Pf*BiP was detected (**Figure 4.13D**, bottom). We further reasoned that because the same substrates may rely on both *Pf*PDI8 and *Pf*BiP to achieve their native state, trapping the *Pf*PDI8-substrate interaction with DVSF may increase the amount of *Pf*BiP co-immunoprecipitating with *Pf*PDI8. To test this hypothesis, parasite cultures were equally split into +/- DVSF treated aliquots, *Pf*PDI8 was immunoprecipitated, and lysates probed for *Pf*PDI8 and *Pf*BiP. Consistent with our hypothesis, we detected a two-fold increase in the amount of *Pf*BiP that pulled down with *Pf*PDI8 crosslinked to its substrates, with no significant difference in the starting amount of *Pf*BiP detected in the sample prior to immunoprecipitation (**Figure 4.13E**). Together, these results suggest that *Pf*J2 and *Pf*PDI8 work together with the major ER folding chaperone *Pf*BiP to help substrates reach their native states.

ER redox interactions are druggable

Our data have shown that *Pf*J2 and *Pf*PDI8, which participate in ER redox partnerships with each other as well as other substrates, are essential proteins in

the *P. falciparum* asexual lifecycle. These proteins, through inhibition of their redox interactions, may represent unexploited targets for antimalarials. Further, our data show that DVSF can target these redox partners, suggesting that these proteins may be druggable. Consistent with the idea of targeting ER redox proteins in disease, high-throughput drug screens have identified potent inhibitors of human PDI in an effort to combat upregulation that is associated with some cancers and neurodegenerative diseases (Hoffstrom et al., 2010; Kaplan et al., 2015; Vatolin et al., 2016; Xu et al., 2012).

We tested four of these commercially available PDI inhibitors—16F16, LOC14, CCF642, and PACMA31—for activity against cultured asexual *P. falciparum* parasites. In contrast to their reported, highly potent activity against human cells, we observed a wide range of IC_{50} values for *P. falciparum* (**Figure 4.16**). The compound with the best anti-*Plasmodium* activity was 16F16, with an IC_{50} value of approximately 4 μM (**Figure 4.17A**) (Harbut et al., 2012).

16F16 inhibits human PDI function by covalently binding the cysteines of the Trx domain active sites, thereby blocking their ability to catalyze oxidative folding (Hoffstrom et al., 2010; Kaplan et al., 2015). If 16F16 behaves similarly in *P. falciparum*, we reasoned that treatment of cultures with 16F16 prior to performing redox crosslinking with DVSF would prevent crosslinking from occurring, as both compounds rely on the same cysteine residues for their activity. Indeed, pre-treatment with increasing amounts of 16F16 significantly and reproducibly decreased the amount of crosslinked *Pf*J2 detected by western blot (**Figure 4.17B**). Our data indicate that DVSF treatment crosslinks *Pf*J2 to *Pf*PDI8

and *Pf*PDI11 (**Figure 4.5**). Therefore, the observed reduction in *Pf*J2 crosslinking likely occurs due to direct reaction of 16F16 with the *Pf*J2 Trx-domain active site and/or the *Pf*PDI8 and -11 active sites. Similar experiments showed that pre-treatment of cultures with 16F16 also blocked crosslinking of *Pf*PDI8 and -11 with their substrates, though to a lesser extent than what was observed for PfJ2 (**Figure 4.17C, D**).

These data demonstrate that redox interactions within the *P. falciparum* ER, occurring between essential proteins like *Pf*J2 and *Pf*PDI8 and their substrates, are sensitive to small molecule inhibition. Additionally, the disparity in activity observed for the PDI inhibitors against human and *P. falciparum* cell lines suggest that development of *Plasmodium*-specific inhibitors is likely possible (**Figure 4.16**).

Discussion

The ability to conduct oxidative folding likely underlies the diverse functions of the *P. falciparum* ER. The oxidizing environment of the ER encourages disulfide bond formation, but only the correct bonds allow proteins to reach their native states. Therefore, organisms must maintain a way to reduce/isomerize nonproductive disulfides. We have used CRISPR/Cas9 genome editing and conditional knockdown to show here that a putative disulfide reductase in the *P. falciparum* ER—*Pf*J2—Is essential for the parasite asexual lifecycle (**Figure 4.1, 4.2**).

A co-IP/mass spectroscopy approach with stringent parameters for identifying interacting partners places *Pf*J2 in the broader context of ER biology, revealing that *Pf*J2 interacts with other folding determinants, such as BiP and Endoplasmin, as well as other members of the Thioredoxin superfamily, such as PDIs. The remaining proteins that were identified, most with unknown localization throughout the secretory pathway and many with no known function, may represent substrates that rely on *Pf*J2 and these other chaperones for their folding and/or trafficking. Among the proteins identified were large, complex proteins such as *Pf*MSP1 and *Pf*RhopH3 (**Figure 4.4**). Both proteins have numerous cysteine residues that must navigate oxidative folding when they are synthesized into the ER, likely relying on *Pf*J2 and *Pf*PDIs to do so correctly. Consistent with this hypothesis, a recent study identified *Pf*J2, *Pf*PDI11, and *Pf*Endoplasmin as potential contributors to folding and trafficking of *Pf*EMP1, a cysteine-rich transmembrane protein that serves as the major *P. falciparum* virulence factor (Batinovic et al., 2017). Our analysis of the proteins identified by mass spectroscopy predicted interactions between *Pf*J2 and *Pf*BiP, and between *Pf*J2 and *Pf*PDI8. We confirmed these interactions via co-immunoprecipitation and western blot experiments. Notably, we also demonstrated an interaction between *Pf*J2 and *Pf*PDI11, a protein which was identified by mass spectroscopy (**Appendix A**) but did not meet our 5-fold enrichment criteria, suggesting that our parameters err on the side of caution to reduce false-positives.

One major *Pf*J2 redox substrate—*Pf*PDI8—was identified using a chemical biology approach. DVSF is a redox-specific crosslinker that has been

used to identify redox partnerships between Thioredoxin proteins in the cytoplasm of model organisms (Allan et al., 2016; Araki et al., 2017; Naticchia et al., 2013). To our knowledge, this compound had not yet been used to trap and define redox partnerships in *Plasmodium*, nor in the ER of any organism. We demonstrate its utility in the *Plasmodium* ER, using it to identify the redox partnership between *Pf*J2, *Pf*PDI8 and *Pf*PDI11 (**Figure 4.5**). Double conditional *P. falciparum* mutants showed that *Pf*PDI8 is also an essential, ER-resident protein and allowed us to probe more deeply the relationship between *Pf*J2 and *Pf*PDI8 (**Figures 4.7, 4.8, 4.13**). *Pf*J2 likely acts as a reductase, and previous *in vitro* characterization of *Pf*PDI8 revealed that it behaves like a classical PDI, capable of both forming and reducing disulfide bonds (Cunnea et al., 2003; Mahajan et al., 2006; Mouray et al., 2007; Oka et al., 2013; Ushioda et al., 2008).The propensity for *Pf*PDI8 to use its Trx domains either for oxidation of cysteines or reduction of disulfides likely depends on the oxidation state of its own active site (i.e. reduced *Pf*PDI8 can act as a reductase). One explanation for the redox partnership between *Pf*J2 and *Pf*PDI8 is that *Pf*J2 primes *Pf*PDI8 to act as a reductase for some or all of the numerous substrates we visualized using DVSF (**Figure 4.8D**). Consistent with this hypothesis, immunoprecipitation experiments showed that *Pf*PDI8+substrates pull down with *Pf*J2 (**Figure 4.13C**). We also found that *Pf*J2 and *Pf*PDI8 both interact with the Hsp70 *Pf*BiP, and detection of that interaction increases for *Pf*PDI8 when it is trapped to its substrates (**Figure 4.13D, E**). These data suggest a model in which *Pf*J2, *Pf*PDI8, and *Pf*BiP cooperate to ensure substrates in the ER correctly navigate

the oxidative folding process to achieve their native states (**Figure 4.18**). As a predicted Hsp40 with an Hsp70-interacting J-domain, one of PfJ2's roles in this complex may be to recruit PfBiP to into a possible folding complex.

We also identified *Pf*PDI11 as a redox substrate of *Pf*J2 (**Figure 4.5**). Our data demonstrate that *Pf*PDI11 retains the ability to form mixed disulfides with client proteins despite the unusual CXXS Trx-domain active site (**Figures 4.8, 4.11, 4.12**). Typically, the second cysteine of the Trx-domain active site is used to resolve enzyme-substrate mixed disulfides (Hatahet & Ruddock, 2009). Therefore, the mechanisms used to resolve mixed disulfides between CXXS active sites and their substrates remains unclear, both in *P. falciparum* and other organisms. We propose that an ER-resident reductase such as *Pf*J2 helps resolve mixed disulfides, which would explain why *Pf*J2 and *Pf*PDI11 were found to be redox partners.

Collectively, our data also demonstrate the power and specificity of using DVSF for trapping redox interactions between proteins with Trx domains and their substrates in *P. falciparum*. We showed that DVSF does not crosslink *Pf*PMV or *Pf*BiP to other proteins, despite the presence of numerous cysteine residues in the former, and that using NEM to block sulfhydryl groups in the parasite prevents crosslinking between *Pf*J2 and its substrates (**Figure 4.5, 4.6**). Furthermore, we showed that DVSF traps *Pf*PDI11 to its substrates, but cysteine-to-alanine mutations in the *Pf*PDI11 Trx domain active sites abolish this crosslinking (**Figure 4.11**). These data are consistent with observations in yeast and mammalian cells, in which DVSF has been validated to trap Trx-domain

proteins to the substrates with which they exchange disulfide bonds (Allan et al., 2016; Araki et al., 2017; Naticchia et al., 2013).

Importantly, given the recent stagnation observed in malaria elimination efforts, which is coincident with increasing cases of antimalarial resistance, we not only identified two proteins with essential functions; we further demonstrated that the redox partnerships of these proteins are sensitive to disruption by small molecule inhibition (**Figure 4.17**). 16F16 is a covalent inhibitor that blocks Trx-domain cysteines (Hoffstrom et al., 2010; Kaplan et al., 2015). Such a compound, if specific for *P. falciparum*, could be expected to cripple oxidative folding in the ER and kill the parasite. Recently, interest in covalent inhibitors for treatment of human disease has renewed, with several covalent inhibitors approved for use by the United States Food and Drug Administration (Ghosh et al., 2019). One particular concern with covalent inhibitors is the fact that mutagenesis of the target residue would result in resistance, but mutagenesis of Trx-domain cysteines would lead to loss of function in and of itself, presumably making this type of resistance harder to evolve.

Another concern is whether proteins with such conserved active sites and roles in biology would make appropriate drug targets. In reality, conserved proteins have given the field many of its validated and proposed drug targets. For example, the widely-used anti-malarial drug atovaquone targets Complex III of the mitochondrial electron transport chain (Hayward & van Dooren, 2019). Some other conserved proteins/complexes that have been proposed as anti-malarial drug targets include Cytochrome B, the TCP-1 Ring Complex chaperone, and the

proteasome (Biagini et al., 2012; Li et al., 2014; Lu et al., 2020; Ng et al., 2017). The precedence for targeting proteins that participate in conserved biology exists. Interest in targeting the *P. falciparum* proteasome began with observations that mammalian proteasome inhibitors have anti-malarial activity, which subsequently spurred development of *Plasmodium*-specific inhibitors (Czesny et al., 2009; Gantt et al., 1998; Li et al., 2014). Similarly, 16F16 likely targets many Trx-domains within the parasite, but we have used it to show that the redox interactions between *Pf*J2, *Pf*PDI8, and their substrates can be disrupted with a small molecule, and development of a *Plasmodium*-specific inhibitor may be possible. In fact, given the disparity in activity observed for the PDI inhibitors against human cell lines and *P. falciparum*, enough diversity likely exists between these conserved proteins that *Plasmodium*-specific inhibitors could be developed (**Figure 4.16**). Therefore, essential Trx-domain proteins in the parasite ER—like *Pf*J2 and *Pf*PDI8—represent a class of proteins and a pathway in the ER that is apt for antimalarial drug development.

Materials and Methods

Construction of Plasmids

Parasite genomic DNA was isolate from 3D7 parasites using QIAamp DNA blood kit (QIAGEN). All constructs utilized in this study were confirmed by sequencing. Plasmids were constructed using the Sequence and Ligation Independent Cloning (SLIC) method. Plasmids to express Cas9 and gRNAs were constructed using pUF1-Cas9 as previously described (Cobb et al., 2017; Ghorbal et al.,

2014; Kudyba et al., 2018). All primers used in this study are listed in **Appendix C**. pfpdi8 cDNA was prepared using TRIzol-extracted mRNA and reverse transcription with primer P20 (SuperScript III, Invitrogen). All restriction enzymes used in plasmid construction were purchased from New England Biolabs.

To generate pMG74-PfJ2, approximately 500 bp of the sequence encoding the *Pf*J2 C-terminus was amplified using primers P1 and P2, and approximately 500 bp from the pfj2 3'UTR were amplified using P3 and P4. The two amplicons were joined together via PCR sewing using P1 and P4, then inserted into pMG74 (Ganesan et al., 2016) digested with AflII and AatII. For expression of a *Pf*J2 gRNA, oligos P31 and P32 were inserted into pUF1-Cas9.

To generate pV5-glmS-PDI8, approximately 500 bp of the sequence encoding the *Pf*PDI8 C-terminus was amplified using primers P5 and P6. The 3x V5 tag was added to this amplicon via PCR sewing using a linearized plasmid encoding the 3xV5 sequence and primers P5 and P7. The glmS ribozyme sequence was amplified from pHA-glmS (Prommana et al., 2013) using P8 and P9, then added to the *Pf*PDI8 C-terminus+V5 amplicon via PCR sewing using P5 and P9. The resulting amplicon was inserted into pHA-glmS that had been digested with AfeI and NheI, creating pPDI8-Cterm. Approximately 500 bp of the *pfpdi8* 3'UTR was amplified using P10 and P11, then inserted into pPDI8-Cterm that had been digested with HindIII and NotI, creating pV5-glmS-PDI8. For expression of a *Pf*PDI8 gRNA, oligos P33 and P34 were inserted into pUF1-Cas9.

To generate pV5-glmS-PDI11, approximately 500 bp of the sequence encoding the *Pf*PDI11 C-terminus was amplified using primers P12 and P13. The 3x V5 tag was added to this amplicon via PCR sewing using a linearized plasmid encoding the 3xV5 sequence and primers P12 and P14. The glmS ribozyme sequence was amplified from pHA-glmS (Prommana et al., 2013) using 15 and P16, then added to the *Pf*PDI8 C-terminus+V5 amplicon via PCR sewing using P12 and P16. The resulting amplicon was inserted into pHA-glmS that had been digested with AfeI and NheI, creating pPDI11-Cterm. Approximately 500 bp of the *pfpdi11* 3'UTR was amplified using P17 and P18, then inserted into pPDI11-Cterm that had been digested with HindIII and NotI, creating pV5-glmS-PDI11. For expression of a *Pf*PDI11 gRNA, oligos P35 and P36 were inserted into pUF1-Cas9.

*Pf*PDI8 and *Pf*PDI11 overexpression was carried out by using CRISPR/Cas9 to insert the open reading frame (ORF) of the tagged genes into the *pfhsp110c* locus. pUC57-Hsp110, the repair plasmid targeting *pfhsp110*, includes the last 429 bp encoding the PfHsp110c (PF3D7_0708800) C-terminus, a 2A skip peptide sequence, sequences for various peptide tags, then the first 400 bp from the *pfhsp110c* 3'UTR. This plasmid was synthesized by GeneScript. For expression of a *Pf*Hsp110c gRNA, oligos P37 and P38 were inserted into pUF1-Cas9.

To generate pUC57-Hsp110-PDI8^{wt}, the *Pf*PDI8 ORF was amplified from cDNA using P19 and P20. A sequence encoding the 3xV5 was attached to this amplicon via PCR sewing using a linearized plasmid encoding the tag and

primers P19 and P21. The resulting amplicon was inserted into pUC57-Hsp110 digested with MfeI and SpeI.

To generate pUC57-Hsp110-PDI11^{wt}, the *Pf*PDI11 ORF was amplified using P22 and P23. A sequence encoding the 3xV5 was attached to this amplicon via PCR sewing using a linearized plasmid encoding the tag and primers P22 and P24. The resulting amplicon was inserted into pUC57-Hsp110 digested with MfeI and SpeI.

To generate pUC57-Hsp110-PDI11^{mut}, which required mutagenesis of the 2 Trx-domain active site, the PfPDI11 ORF was amplified in 3 parts. Part 1 was amplified using P25 and P26. Part 2 was amplified using P27 and P28. Part 3 was amplified using P29 and P30. Parts 1+2 were joined together using PCR sewing and primers P25 and P28. The resulting amplicon was attached to Part 3 using PCR sewing and primers P25 and P30. A sequence encoding the 3xV5 was attached to this amplicon via PCR sewing using a linearized plasmid encoding the tag and primers P25 and P24. The resulting amplicon was inserted into pUC57-Hsp110 digested with MfeI and SpeI.

Parasite Culture and Transfection

P. falciparum asexual parasites were cultured in RPMI 1640 medium supplemented with AlbuMAX I (Gibco) and transfected as described earlier (Drew et al., 2008; Russo et al., 2009).

To generate the *Pf*J2^{apt} parasite line, RBCs were transfected with 20 µg pMG74-PfJ2 (linearized prior to transfection using EcoRV) and 50 µg pUF1-

Cas9-PfJ2, then fed to 3D7 parasites. Drug pressure was applied 48 hours after transfection, selecting for integration using 0.5 μM aTc and 2.5 μg/mL Blasticidin. After parasites grew back up from transfection and were cloned using limiting dilution, clones were maintained in medium containing 10 nM aTc and 2.5 μg/mL Blasticidin. Unless started otherwise, all +/- aTc growth experiments were conducted in medium containing 10 nM aTc and 2.5 μg/mL Blasticidin or medium containing only 2.5 μg/mL Blasticidin.

To generate the *Pf*J2^{apt}-PDI8^{glms} parasite line, RBCs were transfected with 50 μg pV5-glmS-PDI8 and 50 μg pUF1-Cas9-PDI8, then fed to *Pf*J2^{apt} parasites. Drug pressure was applied 48 hours after transfection, selecting with 0.5 μM aTc, 2.5 μg/mL Blasticidin, and 1 μM Drug Selectable Marker 1 (DSM1) (Ghorbal et al., 2014). After parasites grew back up from transfection and were cloned using limiting dilution, clones were maintained in medium containing 50 nM aTc and 2.5 μg/mL Blasticidin. *Pf*J2^{apt}-PDI11^{glms} parasites were generated in the same manner, using 50 μg pV5-glmS-PDI11 and 50 μg pUF1-Cas9-PDI11.

To generate the *Pf*PDI8^{wt} overexpression parasite line, RBCs were transfected with 50 μg pUC57-Hsp110-PDI8^{wt} and 50 μg pUF1-Cas9-Hsp110, then fed to *Pf*J2^{apt} parasites. Drug pressure was applied 48 hours after transfection, selecting with 0.5 μM aTc, 2.5 μg/mL Blasticidin, and 1 μM Drug Selectable Marker 1 (DSM1) (Ghorbal et al., 2014). After parasites grew back up from transfection and were cloned using limiting dilution, clones were maintained in medium containing 10 nM aTc and 2.5 μg/mL Blasticidin. *Pf*PDI11^{wt} and

*Pf*PDI11^{mut} parasites were generated in the same manner, using pUC57-Hsp110-PDI11^{wt} and pUC57-Hsp110-PD11^{mut}, respectively.

Parasite synchronization was carried out as described (Kudyba et al., 2019).

Western Blotting

Western blots were performed as previously described (Muralidharan et al., 2011). Briefly, ice-cold 0.04% saponin in 1x PBS was used to isolate parasites from host cells. Parasite pellets were subsequently solubilized in protein loading dye to which Beta-mercaptoethanol had been added (LI-COR Biosciences) and used for SDS-PAGE. Primary antibodies used in this study were rat-anti-HA 3F10 (Roche, 1:3000), mouse-anti-HA 6E2 (Cell Signaling Technology, 1:1000), rabbit-anti-HA 715500 (Thermofisher, 1:100), mouse-anti-V5 TCM5 (eBioscence, 1:1000), rabbit-anti-V5 D3H8Q (Cell Signaling Technology, 1:1000), rabbit anti-*Pf*BiP MRA-1246 (BEI resources, 1:500), rabbit-anti-*Pf*EF1α (from D. Goldberg, 1:2000), and mouse-anti-*Pf*PMV (from D. Goldberg 1:400). Secondary antibodies used were IRDye 680CW goat-anti-rabbit IgG and IRDye 800CW goat-anti-mouse IgG (Li-COR Biosciences, 1:20,000). Membranes were imaged using the Odyssey Clx Li-COR infrared imaging system (Li-COR Biosciences). Images of membranes were processed using ImageStudio, the Odyssey Clx Li-COR infrared imaging system software (Li-COR Biosciences). Densitometry analysis of western blot signal was also performed using ImageStudio (Li-COR Biosciences).

Microscopy and Image Analysis

Parasites were fixed for IFA using 4% Paraformaldehyde and 0.03% glutaraldehyde, then permeabilized with 0.1% Triton-X100. Primary antibodies used were rat-anti-HA 3F10 (Roche, 1:100), mouse-anti-HA 6E2 (Cell Signaling Technology, 1:100), mouse-anti-V5 TCM5 (eBioscence, 1:100), rabbit-anti-V5 D3H8Q (Cell Signaling Technology, 1:100), and mouse-anti-*Pf*PMV (from D. Goldberg 1:1). Secondary antibodies used were Alexa Fluor 488 and Alexa Fluor 546 (Life Technologies, 1:100). Cells were mounted to slides using ProLong Diamond with DAPI (Invitrogen). Fixed and stained cells were imaged using a DeltaVision II microscope system with an Olympus IX-71 inverted microscope. Images were collected as a Z-stack and deconvolved using SoftWorx, then displayed as a maximum intensity projection. Images were processed using Adobe Photoshop, with adjustments made to brightness and contrast for display purposes.

For imaging of parasite cultures using light microscopy, aliquots of culture were smeared onto glass slides and field-stained using Hema3 Fixative and Solutions (Fisher Healthcare), which is comparable to Wright-Giemsa staining. Slides were imaged using a Nikon Eclipse E400 microscope with a Nikon DS-L1-5M imaging camera. To measure parasite size, images were taken and parasites measured using ImageJ (NIH).

Growth Assays using Flow Cytometry

Aliquots of parasites culture were incubated in 8 μM Hoescht 33342 (Thermofisher Scientific) for 20 minutes at room temperature, then fluorescence was measured using a CytoFlex S (Beckman Coulter, Hialeah, Florida). Flow cytometry data were analyzed using FlowJo software(Treestar, Inc., Ashland, Oregon). For IC_{50} experiments, data were analyzed using the 4-parameter dose-response-curve function of Prism (GraphPad Software, Inc.).

Immunoprecipitation Assays

Anti-HA immunoprecipitation (IP) assays were performed as previously described, using anti-HA magnetic beads (Pierce) (Fierro et al., 2020). Anti-V5 IP assays were performed in the same manner as with anti-HA, but anti-V5 magnetic beads were used according to manufacturer instructions (MBL International Corporation).

Mass Spectrometry and Data Analysis

CoIP samples were sent to Emory University Integrated Proteomics Core and analyzed using a Fusion Orbitrap mass spectrometer, or to the proteomics core at the Fred Hutchinson Cancer Research Center, where samples were analyzed using an OrbiTrap Elite. Data were searched using Proteome Discoverer 2.2 with UP000001450 *Plasmodium falciparum* (Uniprot Nov 2018) as the background database. The validation also included Sequest HT and Percolator to search for common contaminants. Results consisted of high confidence data with a 1%

false discovery rate. Protein abundance was calculated by summing the total intensities (MS1 values) of all matched peptides for each selected protein, and normalizing by the total summed intensity of all matched peptides in the sample, as previously described (Boucher et al., 2018).

Identification of PfJ2 Redox Partners

*Pf*J2^{apt} parasites were incubated with 3 mM divinyl sulfone (DVSF, Fisher Scientific) in 1x PBS for 30 minutes at 37°C, then used for anti-HA immunoprecipitation as described above. Immunoprecipitated proteins were separated by SDS-PAGE. Polyacrylamide gel slices corresponding to the protein molecular weights of interest were excised and the peptides extracted by in-gel enzymatic digestion. The gel slices were dehydrated in 100% acetonitrile and dried using a speed vac. The proteins were then reduced by rehydrating the gel slices in 10mM dithiothreitol in 100mM ammonium bicarbonate solution, and alkylated in 50mM iodoacetamide in 100 mM ammonium bicarbonate solution. The gel slices were then washed in 50% acetonitrile in 50mM ammonium bicarbonate solution before being dehydrated and dried again using 100% acetonitrile and a speed vac. Proteins were then digested in-gel by rehydrating the gel slices in trypsin enzyme solution consisting of 6ng/µl trypsin (Promega) in 50mM ammonium bicarbonate solution. Digestion was performed at 37°C overnight. Peptides were extracted through stepwise incubations with 2% acetonitrile and 1% formic acid solution, 60% acetonitrile and 0.5% formic acid

solution, and 100% acetonitrile solution. Supernatants were combined and dried in a speed vac before resuspension in 20 µl water with 0.1% formic acid.

LC-MS/MS analysis was performed using a 50 cm fused silica capillary (75 µm ID) packed with C18 (2 µm, Dr. Maisch GmbH), and heated to 50°C. Prior to loading the column, sample was loaded onto a 2 cm Acclaim PepMap 100 (Thermo Fisher Scientific) trap (75 µm ID, C18 3 µm). For each sample injection, 5 µl of sample was loaded onto the trap using an Easy nLC-1000 (Thermo Fisher Scientific). Each sample was separated using the Easy nLC-1000 with a binary mobile phase gradient to elute the peptides. Mobile phase A consisted of 0.1% formic acid in water, and mobile phase B consisted of 0.1% formic acid in acetonitrile. The gradient program consisted of three steps at a flow rate of 0.3 µL/min: (1) a linear gradient from 5% to 40% mobile phase B over two hours, (2) a 10 minute column wash at 80% mobile phase B, and (3) column re-equilibration for 20 minutes at 5% mobile phase B.

Mass spectra were acquired on a Fusion Lumos Tribrid (Thermo Fisher Scientific) mass spectrometer operated by data dependent acquisition (DDA) using a top 15 selection count. Precursor ion scans were performed at 120,000 resolution over a range from 375 to 1375 m/z. DDA was performed with charge exclusion of 1 and greater than 8, with isotope exclusion, and dynamic exclusion set to 10 seconds. MS/MS was performed using an isolation window of 1.6 m/z for selection, normalized collision energy (NCE) of 28, and higher energy collision induced dissociation (HCD). MS/MS spectra were acquired at 15000

resolution with an automatic gain control (AGC) target of 70,000 and maximum injection time of 50 ms.

Mass spectra (.raw files) were converted to mzML format using MSConvert (version 3.0.1908) (Adusumilli & Mallick, 2017) and peptide sequences were identified using database searching with Comet (Eng et al., 2013) (version 2016.01 rev 2). Spectra were searched against a subset of *P. falciparum* secretory proteins, common laboratory contaminants, and an equal number of randomized decoy sequences (4386 total protein sequence). Comet parameters included variable modifications of +57.021464 Da or +118.0089 Da on cysteine and a variable modification of +15.994915 Da on methionine or tryptophan. Precursor mass tolerance was set to 25 ppm and a fragment_bin_tolerance of 0.02 and fragment_bin_offset of 0 were used. Full-tryptic enzymatic cleavage was set, allowing for up to 3 missed cleavages. Peptide spectrum matches (PSM) were analyzed using the Trans-Proteomic Pipeline (Deutsch et al., 2015) (TPP, version 5.0.0 Typhoon), to assign peptide and protein probabilities using PeptideProphet (Keller et al., 2002) and iProphet (Shteynberg et al., 2011), respectively. Spectral counts and precursor ion intensities were exported for each non-redundant PSM at a 1% false discovery rate (FDR). Protein inference was performed with ProteinProphet (Nesvizhskii et al., 2003), using a 1% FDR. The mass spectrometry proteomics data have been deposited to the ProteomeXchange Consortium via the PRIDE partner repository (Vizcaıno et al., n.d.) with dataset identifier PXD019100.

Acknowledgements

We thank Dan Goldberg for antibodies against *Pf*PMV and *Pf*EF1α; Julie Nelson at the CTEGD Cytometry Shared Resource Laboratory for help with flow cytometry and analysis; and Muthugapatti Kandasamy at the Biomedical Microscopy Core at the University of Georgia for help with microscopy. We acknowledge assistance of the Proteomics Resource at Fred Hutchinson Cancer Research Center and the Emory University Integrated Proteomics Core for mass spectrometry and data analysis. This work was supported by awards from the ARCS Foundation to D.W.C., and the US National Institutes of Health (R01AI130139) to V.M. and (T32AI060546) to D.W.C. and A.V. We are grateful for support from the National Institutes of Health from the Office of The Director, under award number S10OD026936, and by National Institute of General Medical Sciences under award numbers R01GM087221 and P41GM103533.

Competing Interests

The authors declare no competing interests.

References

Adusumilli, R., & Mallick, P. (2017). Data Conversion with ProteoWizard msConvert. In L. Comai, J. E. Katz, & P. Mallick (Eds.), *Proteomics: Methods and Protocols* (pp. 339–368). Springer New York. https://doi.org/10.1007/978-1-4939-6747-6_23

Allan, K. M., Loberg, M. A., Chepngeno, J., Hurtig, J. E., Tripathi, S., Kang, M. G., Allotey, J. K., Widdershins, A. H., Pilat, J. M., Sizek, H. J., Murphy, W. J., Naticchia, M. R., David, J. B., Morano, K. A., & West, J. D. (2016). Trapping redox partnerships in oxidant-sensitive proteins with a small, thiol-reactive cross-linker. *Free Radical Biology & Medicine*, *101*, 356–366. PubMed. https://doi.org/10.1016/j.freeradbiomed.2016.10.506

Andricopulo, A. D., Akoachere, M. B., Krogh, R., Nickel, C., McLeish, M. J., Kenyon, G. L., Arscott, L. D., Williams, C. H., Davioud-Charvet, E., & Becker, K. (2006). Specific inhibitors of Plasmodium falciparum thioredoxin reductase as potential antimalarial agents. *Bioorganic & Medicinal Chemistry Letters*, *16*(8), 2283–2292. https://doi.org/10.1016/j.bmcl.2006.01.027

Anelli, T. (2003). Thiol-mediated protein retention in the endoplasmic reticulum: The role of ERp44. *The EMBO Journal*, *22*(19), 5015–5022. https://doi.org/10.1093/emboj/cdg491

Araki, K., Ushioda, R., Kusano, H., Tanaka, R., Hatta, T., Fukui, K., Nagata, K., & Natsume, T. (2017). A crosslinker-based identification of redox relay targets. *Analytical Biochemistry*, *520*, 22–26. https://doi.org/10.1016/j.ab.2016.12.025

Batinovic, S., McHugh, E., Chisholm, S. A., Matthews, K., Liu, B., Dumont, L., Charnaud, S. C., Schneider, M. P., Gilson, P. R., de Koning-Ward, T. F., Dixon, M. W. A., & Tilley, L. (2017). An exported protein-interacting complex involved in the trafficking of virulence determinants in

Plasmodium-infected erythrocytes. *Nature Communications*, *8*(1), 16044. https://doi.org/10.1038/ncomms16044

Becker, K., Gromer, S., Schirmer, R. H., & Müller, S. (2000). Thioredoxin reductase as a pathophysiological factor and drug target: Thioredoxin reductase in medicine and parasitology. *European Journal of Biochemistry*, *267*(20), 6118–6125. https://doi.org/10.1046/j.1432-1327.2000.01703.x

Biagini, G. A., Fisher, N., Shone, A. E., Mubaraki, M. A., Srivastava, A., Hill, A., Antoine, T., Warman, A. J., Davies, J., Pidathala, C., Amewu, R. K., Leung, S. C., Sharma, R., Gibbons, P., Hong, D. W., Pacorel, B., Lawrenson, A. S., Charoensutthivarakul, S., Taylor, L., … Ward, S. A. (2012). Generation of quinolone antimalarials targeting the Plasmodium falciparum mitochondrial respiratory chain for the treatment and prophylaxis of malaria. *Proceedings of the National Academy of Sciences*, *109*(21), 8298–8303. https://doi.org/10.1073/pnas.1205651109

Biddau, M., Bouchut, A., Major, J., Saveria, T., Tottey, J., Oka, O., van-Lith, M., Jennings, K. E., Ovciarikova, J., DeRocher, A., Striepen, B., Waller, R. F., Parsons, M., & Sheiner, L. (2018). Two essential Thioredoxins mediate apicoplast biogenesis, protein import, and gene expression in Toxoplasma gondii. *PLOS Pathogens*, *14*(2), e1006836. https://doi.org/10.1371/journal.ppat.1006836

Biddau, M., & Sheiner, L. (2019). Targeting the apicoplast in malaria. *Biochemical Society Transactions*, *47*(4), 973–983. https://doi.org/10.1042/BST20170563

Botha, M., Pesce, E.-R., & Blatch, G. L. (2007). The Hsp40 proteins of Plasmodium falciparum and other apicomplexa: Regulating chaperone power in the parasite and the host. *The International Journal of Biochemistry & Cell Biology*, *39*(10), 1781–1803. https://doi.org/10.1016/j.biocel.2007.02.011

Boucher, M. J., Ghosh, S., Zhang, L., Lal, A., Jang, S. W., Ju, A., Zhang, S., Wang, X., Ralph, S. A., Zou, J., Elias, J. E., & Yeh, E. (2018). Integrative proteomics and bioinformatic prediction enable a high-confidence apicoplast proteome in malaria parasites. *PLOS Biology*, *16*(9), e2005895. https://doi.org/10.1371/journal.pbio.2005895

Cobb, D. W., Florentin, A., Fierro, M. A., Krakowiak, M., Moore, J. M., & Muralidharan, V. (2017). The Exported Chaperone PfHsp70x Is Dispensable for the Plasmodium falciparum Intraerythrocytic Life Cycle. *MSphere*, *2*(5), e00363-17. PubMed. https://doi.org/10.1128/mSphere.00363-17

Cunnea, P. M., Miranda-Vizuete, A., Bertoli, G., Simmen, T., Damdimopoulos, A. E., Hermann, S., Leinonen, S., Huikko, M. P., Gustafsson, J.-Å., Sitia, R., & Spyrou, G. (2003). ERdj5, an Endoplasmic Reticulum (ER)-resident Protein Containing DnaJ and Thioredoxin Domains, Is Expressed in

Secretory Cells or following ER Stress. *Journal of Biological Chemistry*, *278*(2), 1059–1066. https://doi.org/10.1074/jbc.M206995200

Czesny, B., Goshu, S., Cook, J. L., & Williamson, K. C. (2009). The Proteasome Inhibitor Epoxomicin Has Potent Plasmodium falciparum Gametocytocidal Activity. *Antimicrobial Agents and Chemotherapy*, *53*(10), 4080–4085. https://doi.org/10.1128/AAC.00088-09

Das, S., Hertrich, N., Perrin, A. J., Withers-Martinez, C., Collins, C. R., Jones, M. L., Watermeyer, J. M., Fobes, E. T., Martin, S. R., Saibil, H. R., Wright, G. J., Treeck, M., Epp, C., & Blackman, M. J. (2015). Processing of Plasmodium falciparum Merozoite Surface Protein MSP1 Activates a Spectrin-Binding Function Enabling Parasite Egress from RBCs. *Cell Host & Microbe*, *18*(4), 433–444. PubMed. https://doi.org/10.1016/j.chom.2015.09.007

Deutsch, E. W., Mendoza, L., Shteynberg, D., Slagel, J., Sun, Z., & Moritz, R. L. (2015). Trans-Proteomic Pipeline, a standardized data processing pipeline for large-scale reproducible proteomics informatics. *PROTEOMICS - Clinical Applications*, *9*(7–8), 745–754. https://doi.org/10.1002/prca.201400164

Drew, M. E., Banerjee, R., Uffman, E. W., Gilbertson, S., Rosenthal, P. J., & Goldberg, D. E. (2008). Plasmodium Food Vacuole Plasmepsins Are Activated by Falcipains. *Journal of Biological Chemistry*, *283*(19), 12870–12876. https://doi.org/10.1074/jbc.M708949200

Ellgaard, L., Sevier, C. S., & Bulleid, N. J. (2018). How Are Proteins Reduced in the Endoplasmic Reticulum? *Trends in Biochemical Sciences*, *43*(1), 32–43. https://doi.org/10.1016/j.tibs.2017.10.006

Eng, J. K., Jahan, T. A., & Hoopmann, M. R. (2013). Comet: An open-source MS/MS sequence database search tool. *PROTEOMICS*, *13*(1), 22–24. https://doi.org/10.1002/pmic.201200439

Fierro, M. A., Asady, B., Brooks, C. F., Cobb, D. W., Villegas, A., Moreno, S. N. J., & Muralidharan, V. (2020). An Endoplasmic Reticulum CREC Family Protein Regulates the Egress Proteolytic Cascade in Malaria Parasites. *MBio*, *11*(1), e03078-19, /mbio/11/1/mBio.03078-19.atom. https://doi.org/10.1128/mBio.03078-19

Florentin, A., Stephens, D. R., Brooks, C. F., Baptista, R. P., & Muralidharan, V. (2020). Plastid biogenesis in malaria parasites requires the interactions and catalytic activity of the Clp proteolytic system. *Proceedings of the National Academy of Sciences*, *117*(24), 13719. https://doi.org/10.1073/pnas.1919501117

Fomenko, D. E., & Gladyshev, V. N. (2009). CxxS: Fold-independent redox motif revealed by genome-wide searches for thiol/disulfide oxidoreductase function. *Protein Science*, *11*(10), 2285–2296. https://doi.org/10.1110/ps.0218302

Ganesan, S. M., Falla, A., Goldfless, S. J., Nasamu, A. S., & Niles, J. C. (2016). Synthetic RNA–protein modules integrated with native translation

mechanisms to control gene expression in malaria parasites. *Nature Communications*, *7*(1), 10727. https://doi.org/10.1038/ncomms10727

Gantt, S. M., Myung, J. M., Briones, M. R. S., Li, W. D., Corey, E. J., Omura, S., Nussenzweig, V., & Sinnis, P. (1998). Proteasome Inhibitors Block Development ofPlasmodium spp. *Antimicrobial Agents and Chemotherapy*, *42*(10), 2731–2738. https://doi.org/10.1128/AAC.42.10.2731

Ghorbal, M., Gorman, M., Macpherson, C. R., Martins, R. M., Scherf, A., & Lopez-Rubio, J.-J. (2014). Genome editing in the human malaria parasite Plasmodium falciparum using the CRISPR-Cas9 system. *Nature Biotechnology*, *32*(8), 819–821. https://doi.org/10.1038/nbt.2925

Ghosh, A. K., Samanta, I., Mondal, A., & Liu, W. R. (2019). Covalent Inhibition in Drug Discovery. *ChemMedChem*, *14*(9), 889–906. PubMed. https://doi.org/10.1002/cmdc.201900107

Harbut, M. B., Patel, B. A., Yeung, B. K. S., McNamara, C. W., Bright, A. T., Ballard, J., Supek, F., Golde, T. E., Winzeler, E. A., Diagana, T. T., & Greenbaum, D. C. (2012). Targeting the ERAD pathway via inhibition of signal peptide peptidase for antiparasitic therapeutic design. *Proceedings of the National Academy of Sciences*, *109*(52), 21486–21491. https://doi.org/10.1073/pnas.1216016110

Hatahet, F., & Ruddock, L. W. (2009). Protein Disulfide Isomerase: A Critical Evaluation of Its Function in Disulfide Bond Formation. *Antioxidants &*

Redox Signaling, *11*(11), 2807–2850. https://doi.org/10.1089/ars.2009.2466

Hayward, J. A., & van Dooren, G. G. (2019). Same same, but different: Uncovering unique features of the mitochondrial respiratory chain of apicomplexans. *Molecular and Biochemical Parasitology*, *232*, 111204. https://doi.org/10.1016/j.molbiopara.2019.111204

Hoffstrom, B. G., Kaplan, A., Letso, R., Schmid, R. S., Turmel, G. J., Lo, D. C., & Stockwell, B. R. (2010). Inhibitors of protein disulfide isomerase suppress apoptosis induced by misfolded proteins. *Nature Chemical Biology*, *6*(12), 900–906. https://doi.org/10.1038/nchembio.467

Ito, D., Schureck, M. A., & Desai, S. A. (2017). An essential dual-function complex mediates erythrocyte invasion and channel-mediated nutrient uptake in malaria parasites. *ELife*, *6*, e23485. https://doi.org/10.7554/eLife.23485

Kaplan, A., Gaschler, M. M., Dunn, D. E., Colligan, R., Brown, L. M., Palmer, A. G., Lo, D. C., & Stockwell, B. R. (2015). Small molecule-induced oxidation of protein disulfide isomerase is neuroprotective. *Proceedings of the National Academy of Sciences*, *112*(17), E2245–E2252. https://doi.org/10.1073/pnas.1500439112

Kawazu, S., Takemae, H., Komaki-Yasuda, K., & Kano, S. (2010). Target proteins of the cytosolic thioredoxin in Plasmodium falciparum. *Parasitology International*, *59*(2), 298–302. https://doi.org/10.1016/j.parint.2010.03.005

Kehr, S., Sturm, N., Rahlfs, S., Przyborski, J. M., & Becker, K. (2010). Compartmentation of Redox Metabolism in Malaria Parasites. *PLoS Pathogens*, *6*(12), e1001242. https://doi.org/10.1371/journal.ppat.1001242

Keller, A., Nesvizhskii, A. I., Kolker, E., & Aebersold, R. (2002). Empirical Statistical Model To Estimate the Accuracy of Peptide Identifications Made by MS/MS and Database Search. *Analytical Chemistry*, *74*(20), 5383–5392. https://doi.org/10.1021/ac025747h

Krnajski, Z., Gilberger, T.-W., Walter, R. D., & Müller, S. (2001). The malaria parasite Plasmodium falciparum possesses a functional thioredoxin system. *Molecular and Biochemical Parasitology*, *112*(2), 219–228. https://doi.org/10.1016/S0166-6851(00)00372-8

Kudyba, H. M., Cobb, D. W., Fierro, M. A., Florentin, A., Ljolje, D., Singh, B., Lucchi, N. W., & Muralidharan, V. (2019). The endoplasmic reticulum chaperone PfGRP170 is essential for asexual development and is linked to stress response in malaria parasites. *Cellular Microbiology*, *21*(9). https://doi.org/10.1111/cmi.13042

Kudyba, H. M., Cobb, D. W., Florentin, A., Krakowiak, M., & Muralidharan, V. (2018). CRISPR/Cas9 Gene Editing to Make Conditional Mutants of Human Malaria Parasite P. falciparum. *Journal of Visualized Experiments : JoVE*, *139*, 57747. PubMed. https://doi.org/10.3791/57747

Li, H., Tsu, C., Blackburn, C., Li, G., Hales, P., Dick, L., & Bogyo, M. (2014). Identification of Potent and Selective Non-covalent Inhibitors of the

Plasmodium falciparum Proteasome. *Journal of the American Chemical Society*, *136*(39), 13562–13565. https://doi.org/10.1021/ja507692y

Lu, K.-Y., Quan, B., Sylvester, K., Srivastava, T., Fitzgerald, M. C., & Derbyshire, E. R. (2020). *Plasmodium* chaperonin TRiC/CCT identified as a target of the antihistamine clemastine using parallel chemoproteomic strategy. *Proceedings of the National Academy of Sciences*, *117*(11), 5810–5817. https://doi.org/10.1073/pnas.1913525117

Mahajan, B., Noiva, R., Yadava, A., Zheng, H., Majam, V., Mohan, K. V. K., Moch, J. K., Haynes, J. D., Nakhasi, H., & Kumar, S. (2006). Protein disulfide isomerase assisted protein folding in malaria parasites. *International Journal for Parasitology*, *36*(9), 1037–1048. https://doi.org/10.1016/j.ijpara.2006.04.012

Mouray, E., Moutiez, M., Girault, S., Sergheraert, C., Florent, I., & Grellier, P. (2007). Biochemical properties and cellular localization of Plasmodium falciparum protein disulfide isomerase. *Biochimie*, *89*(3), 337–346. https://doi.org/10.1016/j.biochi.2006.11.001

Muralidharan, V., Oksman, A., Iwamoto, M., Wandless, T. J., & Goldberg, D. E. (2011). Asparagine repeat function in a Plasmodium falciparum protein assessed via a regulatable fluorescent affinity tag. *Proceedings of the National Academy of Sciences*, *108*(11), 4411–4416. https://doi.org/10.1073/pnas.1018449108

Naticchia, M. R., Brown, H. A., Garcia, F. J., Lamade, A. M., Justice, S. L., Herrin, R. P., Morano, K. A., & West, J. D. (2013). Bifunctional

electrophiles cross-link thioredoxins with redox relay partners in cells. *Chemical Research in Toxicology*, *26*(3), 490–497. PubMed. https://doi.org/10.1021/tx4000123

Nesvizhskii, A. I., Keller, A., Kolker, E., & Aebersold, R. (2003). A Statistical Model for Identifying Proteins by Tandem Mass Spectrometry. *Analytical Chemistry*, *75*(17), 4646–4658. https://doi.org/10.1021/ac0341261

Ng, C. L., Fidock, D. A., & Bogyo, M. (2017). Protein Degradation Systems as Antimalarial Therapeutic Targets. *Trends in Parasitology*, *33*(9), 731–743. https://doi.org/10.1016/j.pt.2017.05.009

Oehring, S. C., Woodcroft, B. J., Moes, S., Wetzel, J., Dietz, O., Pulfer, A., Dekiwadia, C., Maeser, P., Flueck, C., Witmer, K., Brancucci, N. M., Niederwieser, I., Jenoe, P., Ralph, S. A., & Voss, T. S. (2012). Organellar proteomics reveals hundreds of novel nuclear proteins in the malaria parasite Plasmodium falciparum. *Genome Biology*, *13*(11), R108. https://doi.org/10.1186/gb-2012-13-11-r108

Oka, O. B. V., Pringle, M. A., Schopp, I. M., Braakman, I., & Bulleid, N. J. (2013). ERdj5 Is the ER Reductase that Catalyzes the Removal of Non-Native Disulfides and Correct Folding of the LDL Receptor. *Molecular Cell*, *50*(6), 793–804. https://doi.org/10.1016/j.molcel.2013.05.014

Park, S.-W., Zhen, G., Verhaeghe, C., Nakagami, Y., Nguyenvu, L. T., Barczak, A. J., Killeen, N., & Erle, D. J. (2009). The protein disulfide isomerase AGR2 is essential for production of intestinal mucus. *Proceedings of the*

National Academy of Sciences, *106*(17), 6950–6955. https://doi.org/10.1073/pnas.0808722106

Prommana, P., Uthaipibull, C., Wongsombat, C., Kamchonwongpaisan, S., Yuthavong, Y., Knuepfer, E., Holder, A. A., & Shaw, P. J. (2013). Inducible Knockdown of Plasmodium Gene Expression Using the glmS Ribozyme. *PLoS ONE*, *8*(8), e73783. https://doi.org/10.1371/journal.pone.0073783

Richard, D., Kats, L. M., Langer, C., Black, C. G., Mitri, K., Boddey, J. A., Cowman, A. F., & Coppel, R. L. (2009). Identification of Rhoptry Trafficking Determinants and Evidence for a Novel Sorting Mechanism in the Malaria Parasite Plasmodium falciparum. *PLoS Pathogens*, *5*(3), e1000328. https://doi.org/10.1371/journal.ppat.1000328

Russo, I., Oksman, A., Vaupel, B., & Goldberg, D. E. (2009). A calpain unique to alveolates is essential in Plasmodium falciparum and its knockdown reveals an involvement in pre-S-phase development. *Proceedings of the National Academy of Sciences*, *106*(5), 1554–1559. https://doi.org/10.1073/pnas.0806926106

Sherling, E. S., Knuepfer, E., Brzostowski, J. A., Miller, L. H., Blackman, M. J., & Ooij, C. van. (2017). The Plasmodium falciparum rhoptry protein RhopH3 plays essential roles in host cell invasion and nutrient uptake. *ELife*, *6*, e23239. https://doi.org/10.7554/eLife.23239

Shteynberg, D., Deutsch, E. W., Lam, H., Eng, J. K., Sun, Z., Tasman, N., Mendoza, L., Moritz, R. L., Aebersold, R., & Nesvizhskii, A. I. (2011). iProphet: Multi-level Integrative Analysis of Shotgun Proteomic Data

Improves Peptide and Protein Identification Rates and Error Estimates. *Molecular & Cellular Proteomics*, *10*(12), M111.007690. https://doi.org/10.1074/mcp.M111.007690

Sturm, N., Jortzik, E., Mailu, B. M., Koncarevic, S., Deponte, M., Forchhammer, K., Rahlfs, S., & Becker, K. (2009). Identification of Proteins Targeted by the Thioredoxin Superfamily in Plasmodium falciparum. *PLoS Pathogens*, *5*(4), e1000383. https://doi.org/10.1371/journal.ppat.1000383

Ushioda, R., Hoseki, J., Araki, K., Jansen, G., Thomas, D. Y., & Nagata, K. (2008). ERdj5 Is Required as a Disulfide Reductase for Degradation of Misfolded Proteins in the ER. *Science*, *321*(5888), 569–572. https://doi.org/10.1126/science.1159293

Vatolin, S., Phillips, J. G., Jha, B. K., Govindgari, S., Hu, J., Grabowski, D., Parker, Y., Lindner, D. J., Zhong, F., Distelhorst, C. W., Smith, M. R., Cotta, C., Xu, Y., Chilakala, S., Kuang, R. R., Tall, S., & Reu, F. J. (2016). Novel Protein Disulfide Isomerase Inhibitor with Anticancer Activity in Multiple Myeloma. *Cancer Research*, *76*(11), 3340–3350. https://doi.org/10.1158/0008-5472.CAN-15-3099

Vizcaıno, J. A., Csordas, A., Griss, J., Lavidas, I., Mayer, G., Perez-Riverol, Y., Reisinger, F., Ternent, T., Xu, Q.-W., Wang, R., & Hermjakob, H. (n.d.). *2016 update of the PRIDE database and its related tools*. 1.

West, J. D., Stamm, C. E., Brown, H. A., Justice, S. L., & Morano, K. A. (2011). Enhanced Toxicity of the Protein Cross-Linkers Divinyl Sulfone and Diethyl Acetylenedicarboxylate in Comparison to Related Monofunctional

Electrophiles. *Chemical Research in Toxicology*, *24*(9), 1457–1459. https://doi.org/10.1021/tx200302w

World Heath Organization, C. (2019). *World Malaria Report 2019*. 232.

Xu, S., Butkevich, A. N., Yamada, R., Zhou, Y., Debnath, B., Duncan, R., Zandi, E., Petasis, N. A., & Neamati, N. (2012). Discovery of an orally active small-molecule irreversible inhibitor of protein disulfide isomerase for ovarian cancer treatment. *Proceedings of the National Academy of Sciences*, *109*(40), 16348–16353. https://doi.org/10.1073/pnas.1205226109

Zhang, M., Wang, C., Otto, T. D., Oberstaller, J., Liao, X., Adapa, S. R., Udenze, K., Bronner, I. F., Casandra, D., Mayho, M., Brown, J., Li, S., Swanson, J., Rayner, J. C., Jiang, R. H. Y., & Adams, J. H. (2018). Uncovering the essential genes of the human malaria parasite *Plasmodium falciparum* by saturation mutagenesis. *Science*, *360*(6388), eaap7847. https://doi.org/10.1126/science.aap7847

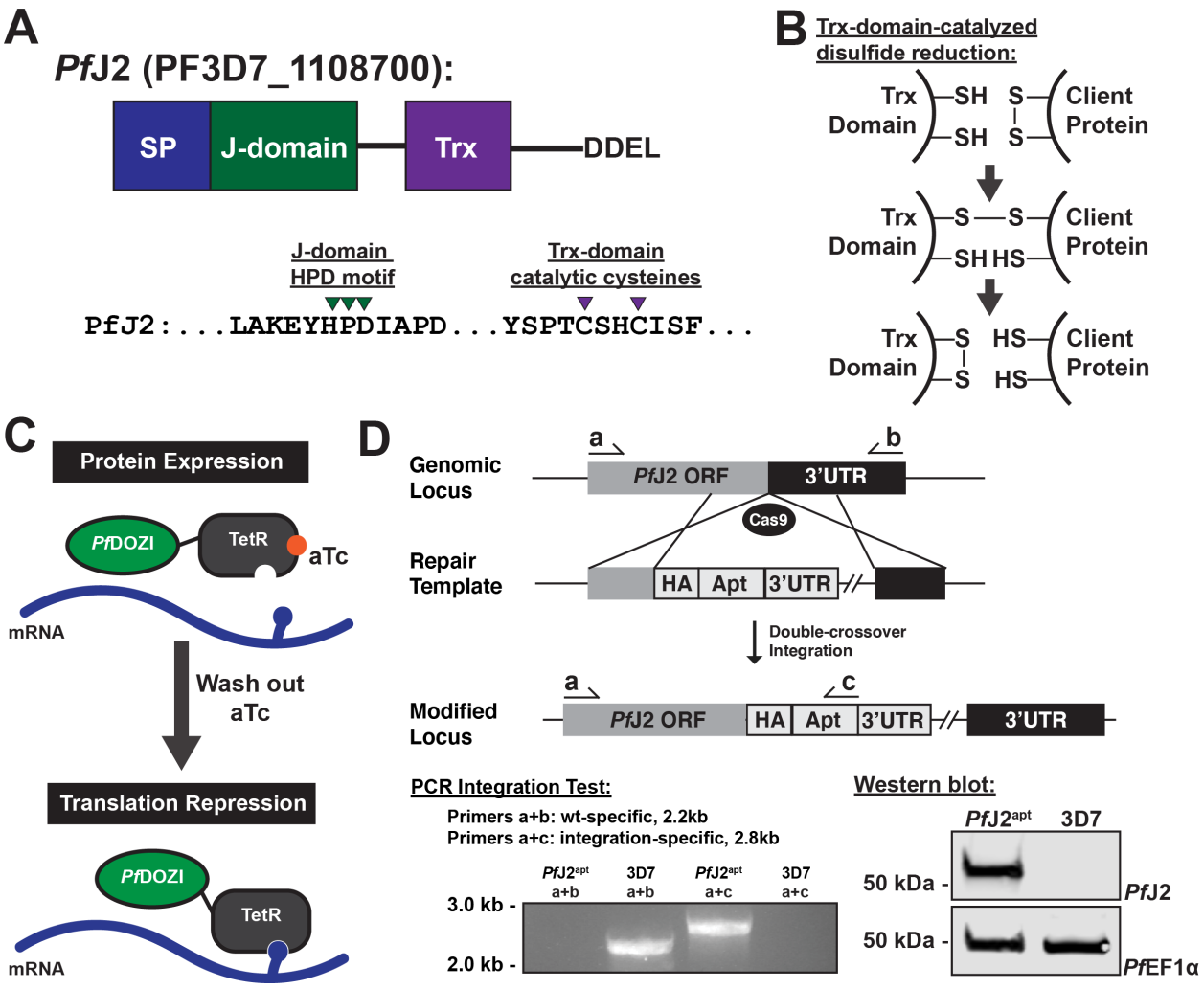

Figure 4.1. Generation of *Pf*J2 (PF3D7_1108700) conditional knockdown mutants using CRISPR/Cas9. A) Predicted domain structure of *Pf*J2 showing signal peptide (SP), Hsp40 J-domain, thioredoxin domain (Trx), and C-terminal ER retention signal. Essential, conserved residues are shown: the J-domain HPD motif is required for Hsp40 activity (i.e., stimulation of Hsp70 ATPase activity), and the Trx-domain CXXC motif is required for redox activity. **B)** Mechanism of disulfide bond reduction catalyzed by Trx-domain active site cysteines. **C)** Regulation of protein expression using the TetR-*Pf*DOZI knockdown system. TetR binds to aptamer sequences present in the mRNA, and *Pf*DOZI localizes

the complex to sites of mRNA sequestration, repressing translation. Anhydrotetracycline (aTc) blocks TetR-aptamer interaction. **D)** Schematic of CRISPR/Cas9-mediated introduction of the TetR-*Pf*DOZI knockdown system into the *pfj2* locus. A linearized repair template was transfected, along with a plasmid to express Cas9 and a gRNA, to introduce sequences for a 3xHA tag+*Pf*J2's DDEL ER retention signal, stop codon, and a 3'UTR. Included in the repair template but not shown was a cassette to express the TetR-*Pf*DOZI fusion protein and blasticidin deaminase for drug selection. Bottom left: two PCR integration tests were used to amplify either a sequence from only wild-type locus (primers a+b) or the modified locus (a+c). Bottom right: anti-HA western blot. Representative western blot of three biological replicates shown.

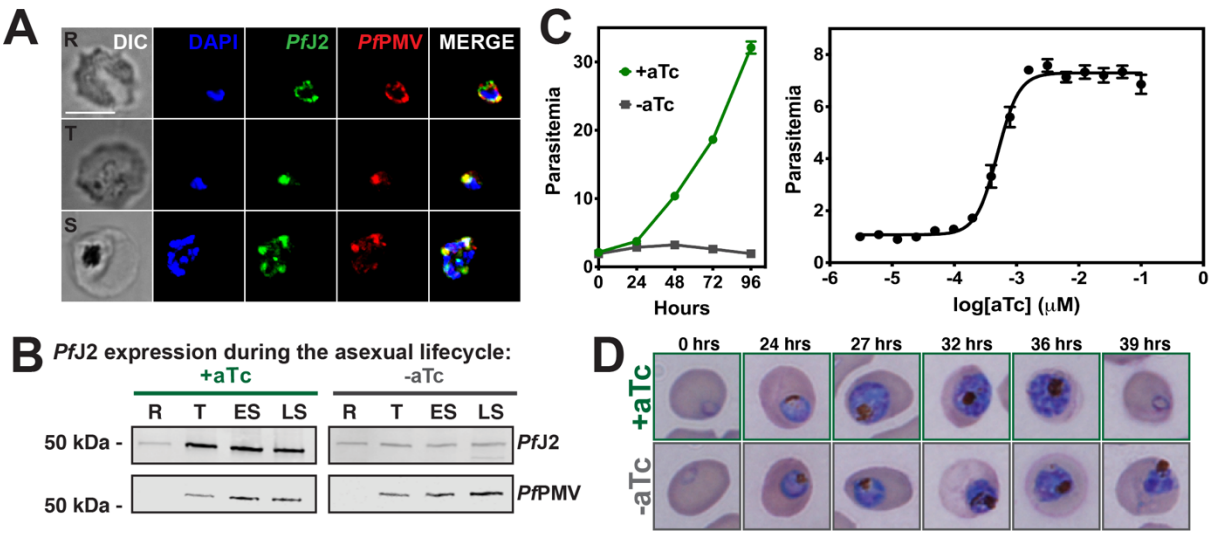

Figure 4.2. *Pf*J2 is an essential, ER-resident protein. A) *Pf*J2^{apt} parasites were fixed with paraformaldehyde and glutaraldehyde and stained with DAPI (blue) and with antibodies against HA (green) and the ER-marker *Pf*PMV (red). Ring (R), Trophozoite (T), and Schizont (S) stage parasites are shown. Z-stack

Images were deconvoluted and shown as a single, maximum intensity projection. Scale bar represents 5 μm. **B)** Parasites were tightly synchronized to the ring stage (0-3 hours) and split into two conditions: +aTc and –aTc. Samples were taken for western blot analysis at various time points in the life cycle (R = Ring, T = Trophozoite, ES = Early Schizont, LS = Late Schizont). Equal parasite equivalents were loaded into each lane, and membranes were stained with antibodies for HA and *Pf*PMV. Shown is a representative experiment of two biological replicates. **C)** Left: asynchronous parasites were grown in normal (+aTc) or *Pf*J2 knockdown (-aTc) conditions, and parasite growth was monitored daily for 96 hours via flow cytometry. Right: asynchronous parasites were grown in a range of aTc concentrations and growth measured at 72 hours via flow cytometry. The aTc EC_{50} was determined to be 0.5 nM. Representative of three biological replicates shown for each growth curve. Each data point represents the mean of three technical replicates; error bars represent standard deviation. **D)** Parasites were tightly synchronized to the ring stage (0-3 hours) and split into two conditions: normal (+aTc) and PfJ2 knockdown (-aTc). Samples from each condition were smeared and field-stained at time points throughout the lifecycle. A representative experiment from three biological replicates is shown.

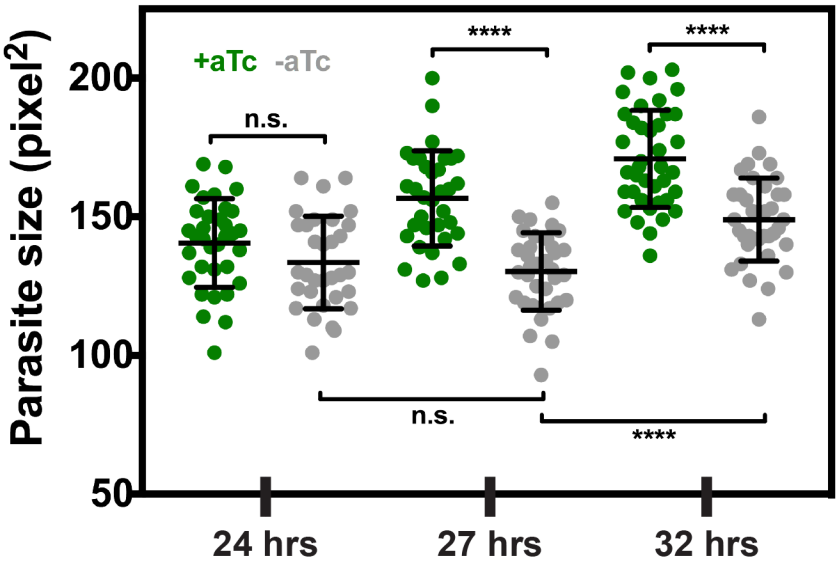

Figure 4.3. Parasite development is slowed during PfJ2 knockdown. *Pf*J2^{apt} parasites were tightly synchronized (0-3 hours) to the ring stage, then split into either +aTc (10 nM) or –aTc medium. Smears were made and field-stained at various time points throughout the asexual lifecycle. Stained slides were imaged and parasite size was measured. Unpaired t-test, **** indicates $p \leq 0.0001$. Representative experiment of 3 biological replicates shown.

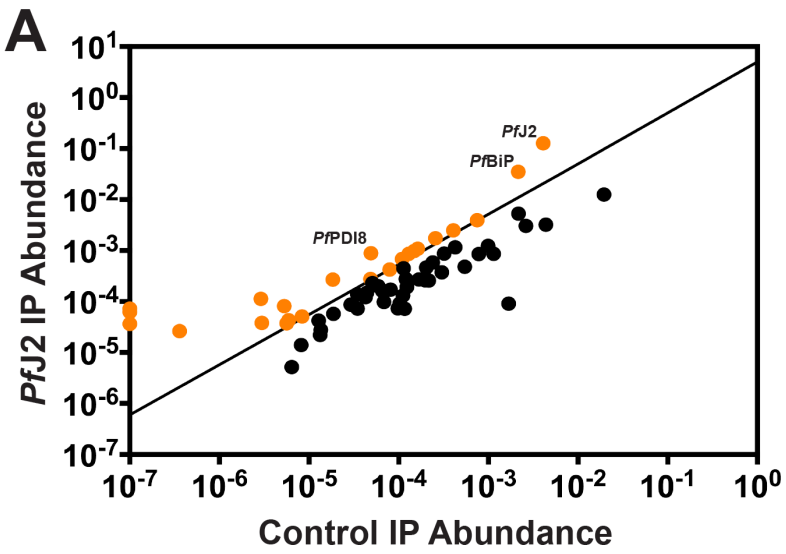

C

	Gene ID	Annotation	Fold-Enrichment	piggyBac Prediction
ER	PF3D7_1108700	PfJ2	31.2	Essential
	PF3D7_0827900	PDI8	18.1	Essential
	PF3D7_0917900	BiP	16.2	Essential
	PF3D7_1444300	1-acyl-sn-glycerol-3-phosphate acyltransferase, putative	6.7	Essential
	PF3D7_1222300	Endoplasmin, putative	6.7	Essential
	PF3D7_1246800	Signal Recognition Particle Receptor Subunit Beta, putative	623.0	Dispensable
	PF3D7_1346100	SEC61 subunit alpha	6.1	Dispensable
Rhoptry	PF3D7_0905400	RhopH3	6.8	Essential
	PF3D7_0501600	RAP2	6.6	Essential
	PF3D7_1410400	RAP1	5.3	Dispensable
PPM	PF3D7_0930300	MSP1	6.1	Essential
Unknown	PF3D7_0318900	Conserved Protein, Unknown Function	725.0	Essential
	PF3D7_1136800	DnaJ protein, putative	72.8	Essential
	PF3D7_1419200	ATrx1	15.4	Essential
	PF3D7_1459400	Conserved Protein, Unknown Function	14.6	Essential
	PF3D7_0710100	Conserved Protein, Unknown Function	7.3	Essential
	PF3D7_0823800	DnaJ protein, putative	6.6	Essential
	PF3D7_1324900	L-lactate dehydrogenase	6.3	Essential
	PF3D7_0821000	Conserved Plasmodium Protein, Unknown Function	5.3	Essential
	PF3D7_0912400	alkaline phosphatase, putative	363.0	Dispensable
	PF3D7_1143200	DnaJ protein, putative	38.8	Dispensable
	PF3D7_1409600	Conserved Plasmodium Protein, Unknown Function	12.8	Dispensable
	PF3D7_0612100	Eukaryotic Translation Initiation Factor 3 Subunit L, putative	5.7	Dispensable

Figure 4.4. *Pf*J2 interacts with other essential chaperones, proteins in the secretory pathway. A) *Pf*J2 was immunoprecipitated from *Pf*J2^{apt} parasites using anti-HA antibody, and co-immunoprecipitated proteins were identified by tandem mass spectrometry analysis. Control, parental parasites were also used for immunoprecipitation and analyzed in the same manner. Each coIP

experiment was performed in triplicate, and the abundance of each identified protein was calculated as previously described in Boucher et al. 2018 and Florentin et al. 2020. Candidate proteins of interest were further identified as those in the secretory pathway (predicted to contain a signal peptide and/or transmembrane domains) and those which were present in all three *Pf*J2^{apt} replicates and demonstrated a 5-fold enrichment compared to control experiments (shown in orange). **B)** The 23 proteins meeting our strict criteria were assessed against the piggyBac mutagenesis screen performed in Zhang, Wang *et al*. 2018, and 16 were predicted to have essential functions in the *P. falciparum* asexual stages. **C)** Identified proteins were categorized by subcellular localization (ER, Rhoptry, Parasite Plasma Membrane [PPM], or Unknown). Also shown are GeneIDs and annotations from PlasmoDB.org, calculated fold-enrichment compared to control experiments, and essentiality as predicted by the piggyBac mutagenesis screen performed by Zhang et al., 2018.

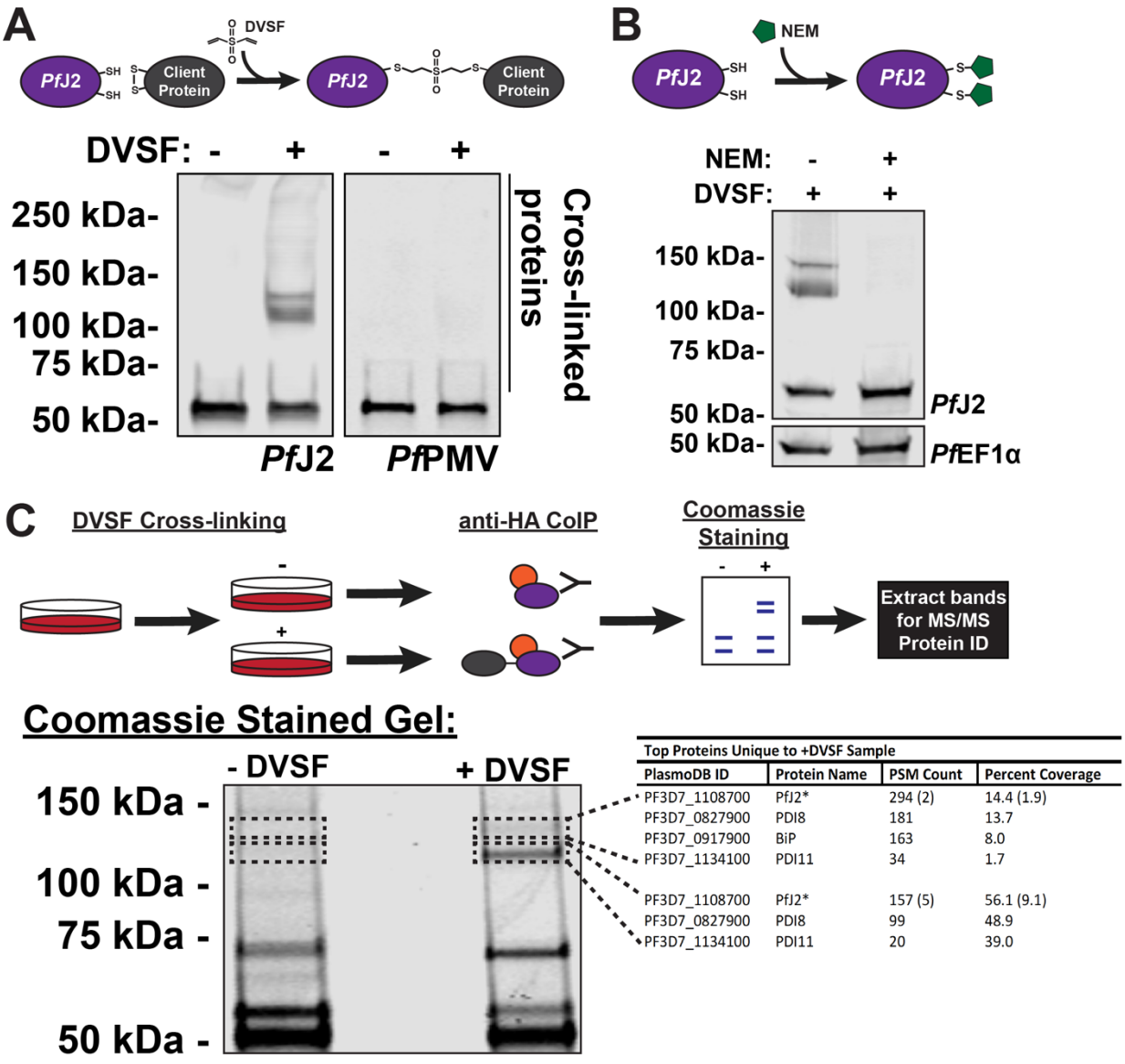

Top Proteins Unique to +DVSF Sample

PlasmoDB ID	Protein Name	PSM Count	Percent Coverage
PF3D7_1108700	PfJ2*	294 (2)	14.4 (1.9)
PF3D7_0827900	PDI8	181	13.7
PF3D7_0917900	BiP	163	8.0
PF3D7_1134100	PDI11	34	1.7
PF3D7_1108700	PfJ2*	157 (5)	56.1 (9.1)
PF3D7_0827900	PDI8	99	48.9
PF3D7_1134100	PDI11	20	39.0

Figure 4.5. *Pf*J2 redox partners identified as *Pf*PDI8 and *Pf*PDI11. A) *Pf*J2^{apt} parasites were incubated with 3 mM divinyl sulfone (DVSF) in 1x PBS for 30 minutes at 37°C, then samples were taken for western blot analysis. Membranes were incubated with antibodies against HA and *Pf*PMV. Representative western blot of three biological replicates is shown. **B)** *Pf*J2^{apt} parasite cultures were incubated with 1 mM N-ethylmaleimide (NEM) for 3 hours prior to removal of NEM and addition of 3 mM DVSF as described above. Samples were taken for

western blot analysis. Membranes were incubated with antibodies against HA and *Pf*EF1α. Representative western blot of two biological replicates is shown. **C)** *Pf*J2^{apt} parasite cultures were evenly split into two conditions: 3 mM DVSF or PBS only for 30 minutes at 37°C, after which parasite lysates were used for anti-HA immunoprecipitation. Immunoprecipitated proteins were separated via SDS-PAGE and visualized using Coomassie. Bands unique to the DVSF-treated sample were extracted, along with the corresponding section of gel in the untreated sample. Proteins were identified by tandem mass spectrometry, and proteins identified in both plus and minus DVSF samples eliminated for further study. The GeneID, protein name, PSM count, and percent coverage for all proteins with more than 1% coverage are shown in the table. A small amount of PfJ2 was identified in the -DVSF samples, and the PSM count and percent coverage is shown in parentheses. One of two biological replicates shown.

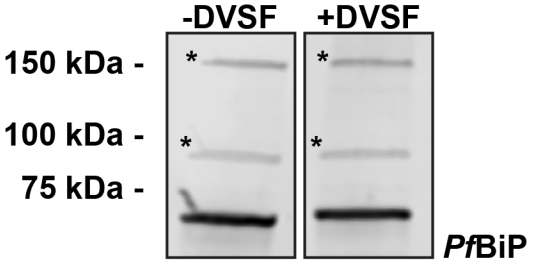

Figure 4.6. *Pf*BiP SDS-PAGE migration is unaffected by DVSF. *Pf*J2^{apt}-PDI8^{glms} parasites were treated with 3 mM DVSF in 1xPBS for 30 minutes at 37°C, or left untreated as a control, and parasite lysates were used for western blotting. Membranes were probed with antibodies against *Pf*BiP. Asterisks (*) denote nonspecific bands.

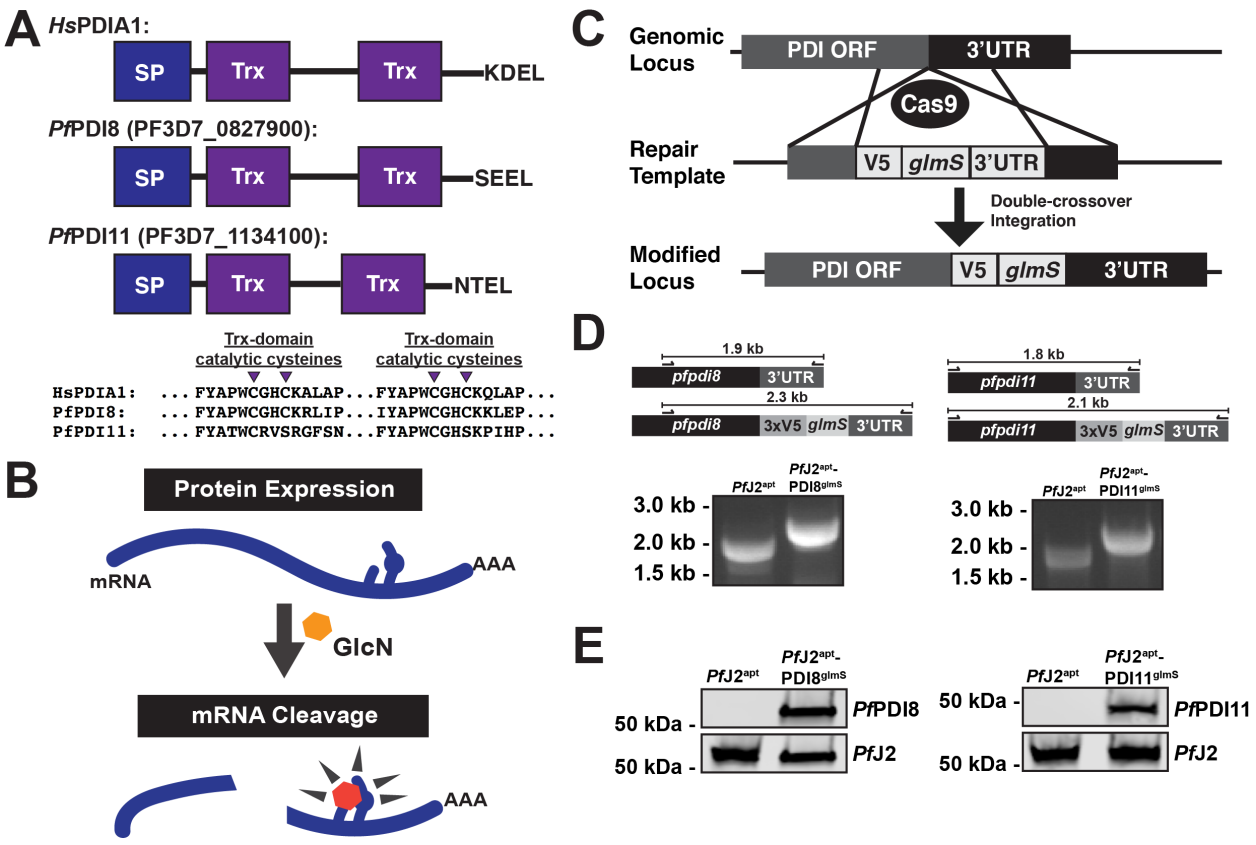

Figure 4.7. Generation of *Pf*PDI8 (PF3D7_0827900) and *Pf*PDI11 (PF3D7_1134100) conditional knockdown mutants using CRISPR/Cas9. A) Predicted domain structure of *Pf*PDI8, *Pf*PDI11, and human PDIA1, showing signal peptide (SP), thioredoxin domains (Trx), and C-terminal ER retention signals. Essential, conserved cysteine residues are shown for each of the proteins' Trx domains. **B)** Regulation of protein expression using the *glmS* ribozyme system. The mRNA of interest encodes the ribozyme in the 3'UTR. Upon addition of glucosamine (GlcN, orange hexagon), which is converted to glucosamine-6-phosphate (pink hexagon) by the parasite, the ribozyme is

activated to cleave the mRNA, leading to transcript instability and degradation (Prommana et al., 2013) **C)** Schematic of CRISPR/Cas9 mediated introduction of the *glmS* knockdown system into the genome. A repair template was transfected, along with a plasmid to express Cas9 and a gRNA, to introduce sequences for a 3xV5 tag, ER retention signals, stop codon, and *glmS* ribozyme. **D)** PCR integration test confirming correct modification of *pfpdi8* and *pfpdi11*. Correct integration results in increased amplicon size due to the V5 and *glmS* sequences. **E)** Western blots showing V5-tagged proteins in the *Pf*J2^{apt}-PDI8^{glmS} and *Pf*J2^{apt}-PDI11^{glmS} parasite lines at the predicted sizes for *Pf*PDI8 and -11. For each western blot, one of two biological replicates shown.

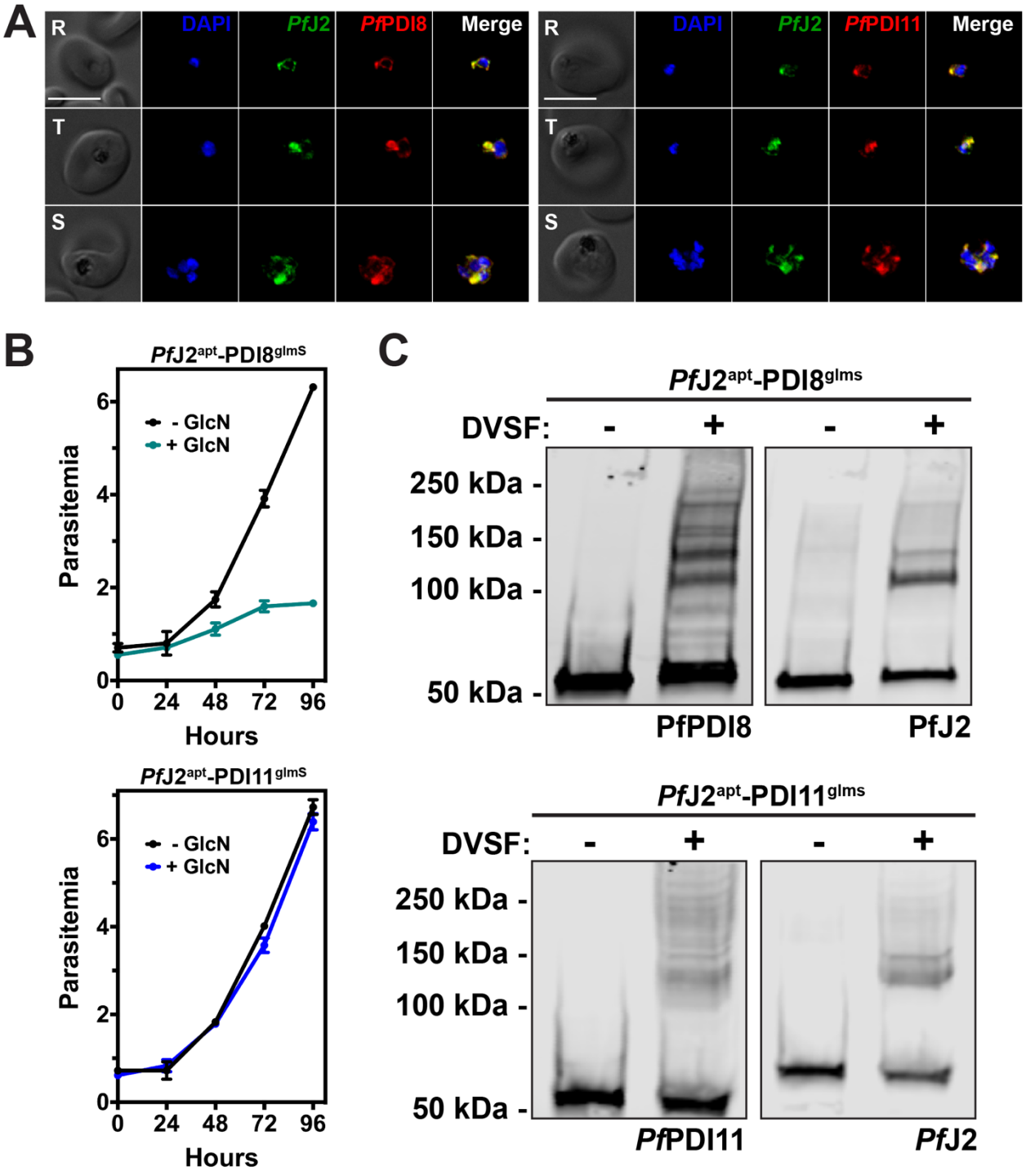

Figure 4.8. *Pf*PDI8 and *Pf*PDI11 are redox-active ER proteins. A) *Pf*J2^{apt}-PDI8^{glmS} and *Pf*J2^{apt}-PDI11^{glmS} parasites were fixed with paraformaldehyde and glutaraldehyde and stained with DAPI (blue) and with antibodies against HA

(green) and V5 (red). Ring (R), Trophozoite (T), and Schizont (S) stage parasites are shown. Z-stack Images were deconvoluted and shown as a single, maximum intensity projection. Scale bar represents 5 μm. **B)** Asynchronous *Pf*J2^{apt}-PDI8^{glmS} (top) and *Pf*J2^{apt}-PDI11^{glmS} (bottom) parasites were grown in normal (-GlcN) or knockdown (+ 5mM GlcN) conditions, and parasite growth was monitored daily for 96 hours via flow cytometry. Data points represent the mean of three technical replicates, with error bars representing standard deviation. For each growth curve, a representative experiment of two biological replicates is shown. **C)** *Pf*J2^{apt}-PDI8^{glmS} and *Pf*J2^{apt}-PDI11^{glmS} parasites were incubated with 3 mM DVSF in 1x PBS for 30 minutes at 37°C, then samples were taken for western blot analysis. Membranes were incubated with antibodies against HA (*Pf*J2) and V5 (*Pf*PDI8 or -11). For each western blow, one of two biological replicates is shown.

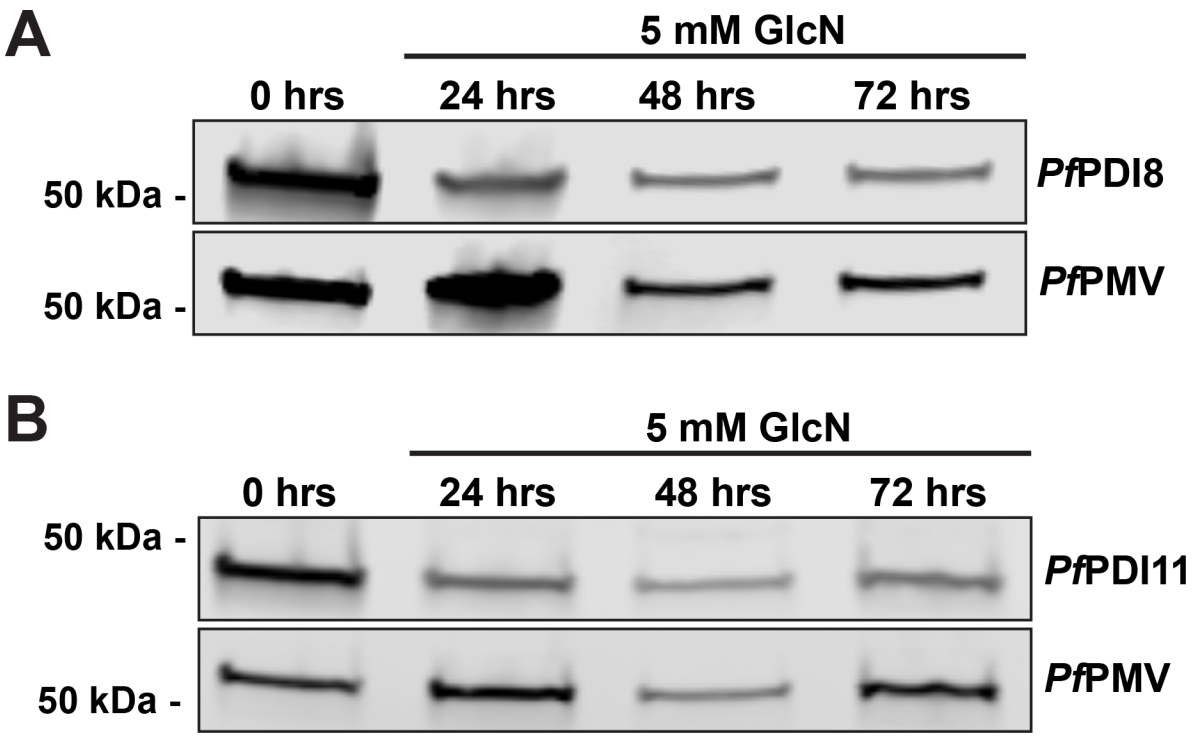

Figure 4.9. GlcN treatment leads to knockdown of *Pf*PDI8 and *Pf*PDI11. Asynchronous *Pf*J2^{apt}-PDI8^{glms} (top) and *Pf*J2^{apt}-PDI11^{glms} (bottom) parasites were treated with 5 mM GlcN and samples were taken for western blot analysis at 0 (before addition of GlcN), 24, 48, and 72 hours. Membranes were probed with antibodies for V5 and *Pf*PMV.

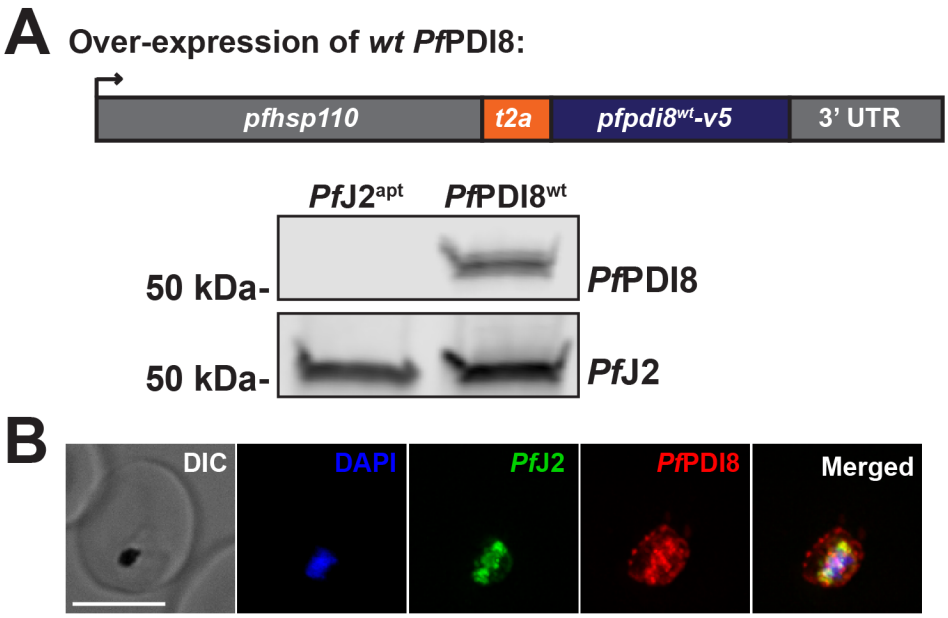

Figure 4.10. Overexpression of *Pf*PDI8 results in mislocalization. A) Top: schematic of exogenous V5-tagged, wild-type *Pf*PDI8 expression using the *pfhsp110* (PF3D7_ 0708800) locus and a T2A skip peptide in the *Pf*PDI8^{wt} parasite line, created in the background of *Pf*J2^{apt} parasites. Bottom: western blot of parental *Pf*J2^{apt} and *Pf*PDI8^{wt} parasite lysates, probed for antibodies against the V5 tag (*Pf*PDI8) and the HA tag (*Pf*J2). **B)** *Pf*PDI8^{wt} parasites were glutaraldehyde/paraformaldehyde fixed and used for IFA. Staining was carried out using DAPI (blue), antibodies against the HA tag (*Pf*J2, green), and the V5 tag (*Pf*PDI8, red). Scale bar represents 5 μm.

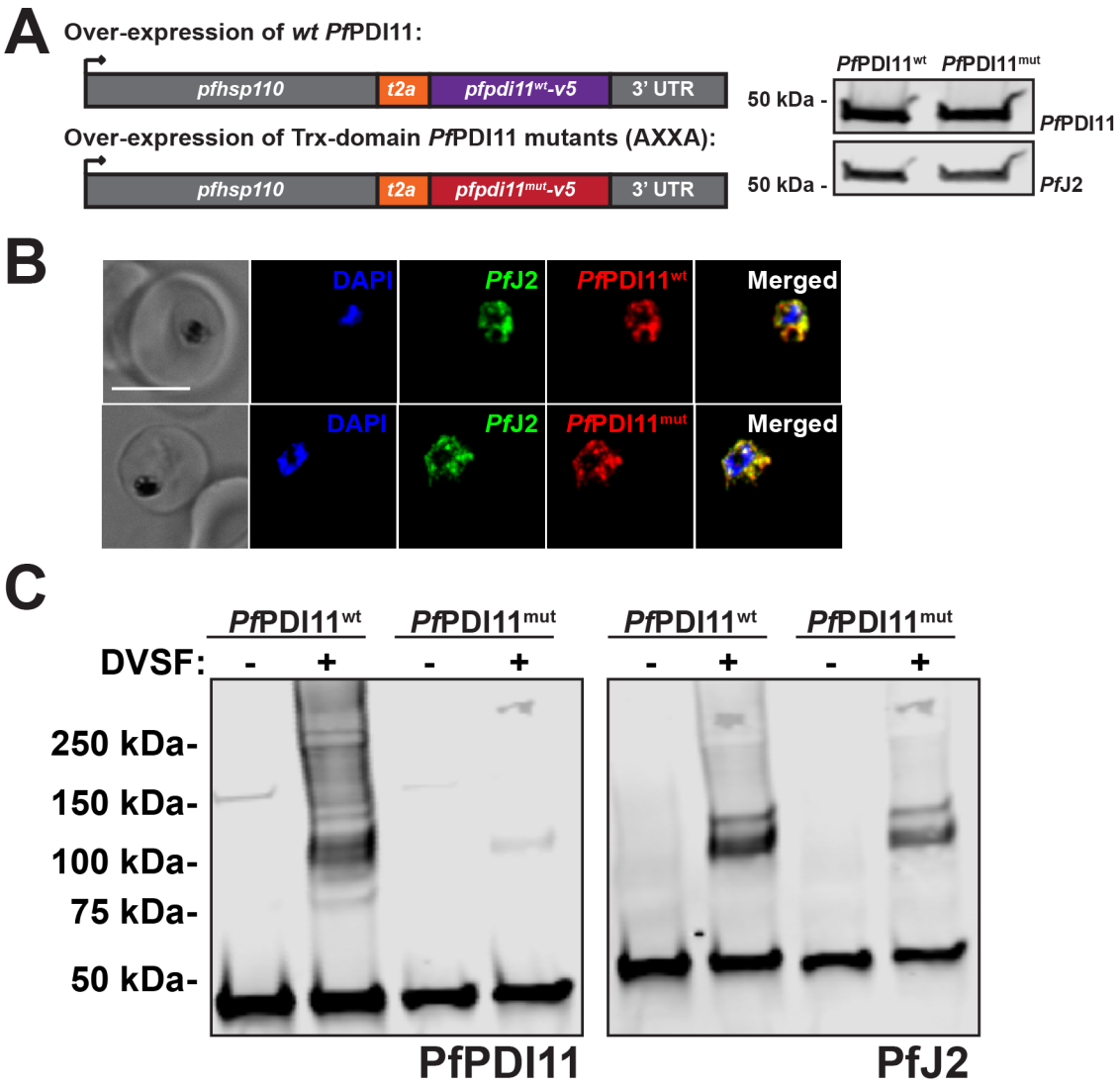

Figure 4.11. Characterization of PfPDI11 overexpression lines. A) Left: schematic of exogenous V5-tagged, *Pf*PDI11 expression using the *pfhsp110* (PF3D7_ 0708800) locus and a T2A skip peptide in the *Pf*PDI11^{wt} and *Pf*PDI11^{mut} parasite lines, created in the background of *Pf*J2^{apt} parasites. In *Pf*PDI11^{mut} parasites, both Trx-domain CXXS active sites were changed to AXXA. Right: western blot of *Pf*PDI11^{wt} and *Pf*PDI11^{mut} parasite lysates, probed for antibodies against the V5 tag (*Pf*PDI11) and the HA tag (*Pf*J2). **B)** *Pf*PDI11^{wt} and *Pf*PDI11^{mut} parasites were glutaraldehyde/paraformaldehyde fixed and used

for IFA. Staining was carried out using DAPI (blue), antibodies against the HA tag (*Pf*J2, green), and the V5 tag (*Pf*PDI8, red). Scale bar represents 5 µm**. C)** *Pf*PDI11^{wt} and *Pf*PDI11^{mut} parasites were treated with 3 mM DVSF in 1x PBS for 30 minutes at 37°C, then parasite lysates used for western blotting. Membranes were probed with antibodies against the V5 tag (*Pf*PDI11) and the HA tag (*Pf*J2).

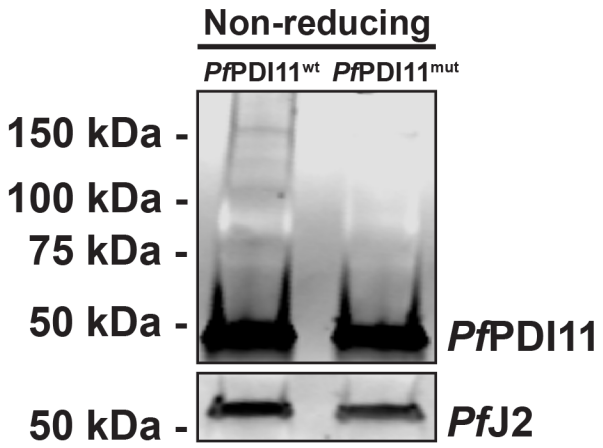

Figure 4.12. PfPDI11 non-reducing western blots. Saponin-isolated *Pf*PDI11^{wt} and *Pf*PDI11^{mut} parasites were dissolved in protein loading dye lacking a reducing agent and used for western blotting. Membranes were probed with antibodies against the V5 tag (*Pf*PDI11) and the HA tag (*Pf*J2).

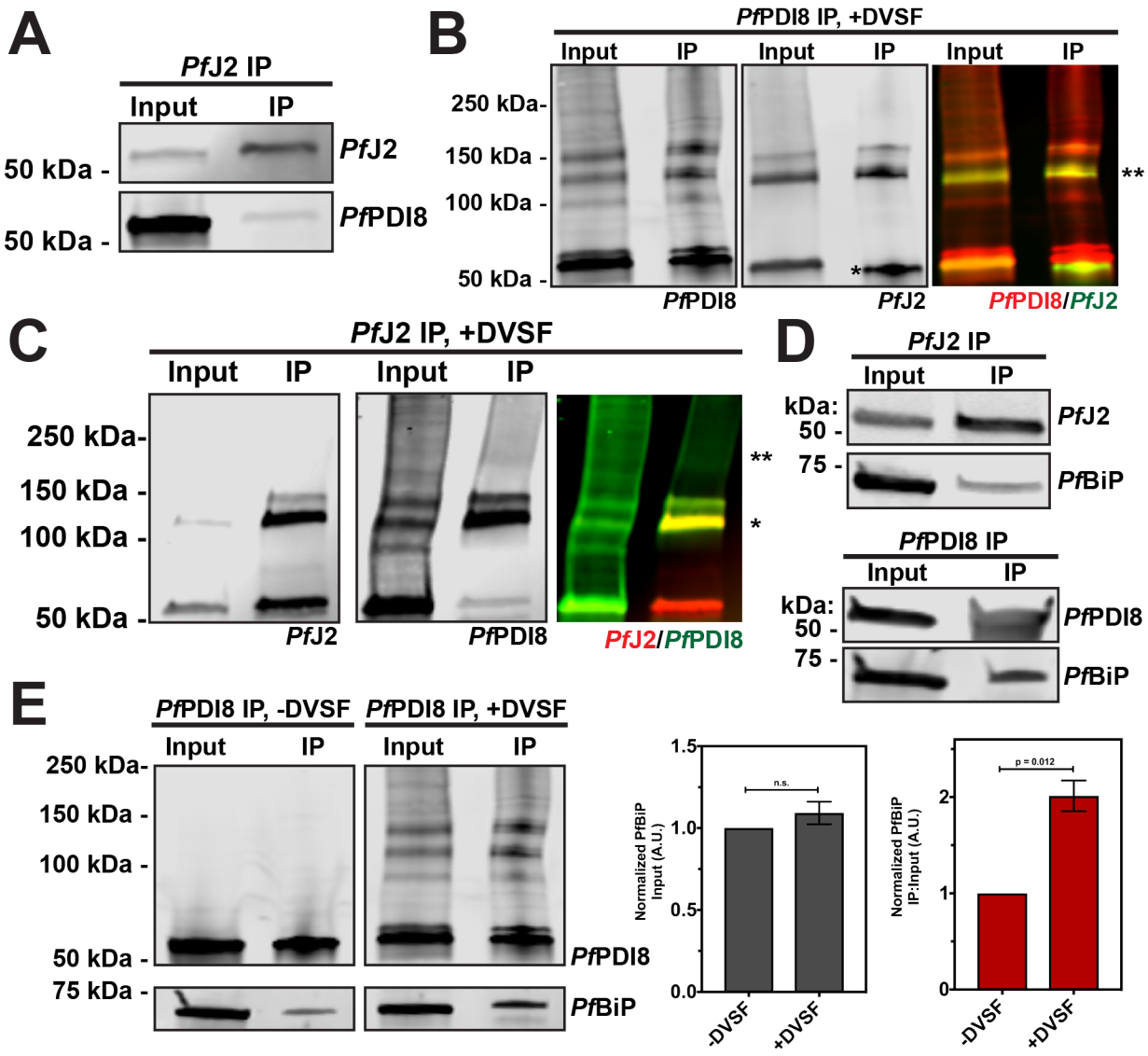

Figure 4.13. The *Pf*BiP-*Pf*J2-*Pf*PDI8 oxidative folding complex. A) *Pf*J2 and interacting proteins were immunoprecipitated from *Pf*J2^{apt}-PDI8^{glmS} parasite lysate using anti-HA antibodies. Input and eluted IP samples were used for western blot analysis. Membrane was probed with HA and V5 antibodies to detect *Pf*J2 and *Pf*PDI8, respectively. **B)** *Pf*J2^{apt}-PDI8^{glmS} parasites were incubated with 3 mM DVSF as described above, then V5 antibodies were used to immunoprecipitate *Pf*PDI8 and interacting proteins. Input and eluted IP samples were used for western blot analysis. Membrane was probed with V5 and HA

antibodies to detect *Pf*PDI8 and *Pf*J2, respectively. Antibody heavy chain is indicated by the single asterisk (*) in the *Pf*J2 panel. A merged image of the *Pf*PDI8 (red) and *Pf*J2 (green) signal is shown, with the yellow overlap in signal indicated by a double asterisk (**). **C)** *Pf*J2^{apt}-PDI8^{glmS} parasites were incubated with 3 mM DVSF as described above, then HA antibodies were used to immunoprecipitate *Pf*J2 and interacting proteins. Input and eluted IP samples were used for western blot analysis. Membrane was probed with HA and V5 antibodies to detect *Pf*J2 and *Pf*PDI8, respectively. A merged image of the *Pf*J2 (red) and *Pf*PDI8 (green) signal is shown, with a single asterisk (*) indicating the yellow overlap in signal and a double asterisk (**) indicating *Pf*PDI8+subtrates that co-immunoprecipitated with *Pf*J2. **D)** *Pf*J2 and *Pf*PDI8 were immunoprecipitated from *Pf*J2^{apt} and *Pf*J2^{apt}-PDI8^{glmS} parasite lysates, respectively. Input samples and eluted IP proteins were used for western blot analysis. Membrane was probed with HA and *Pf*BiP antibodies (top) or V5 and *Pf*BiP antibodies (bottom). Immunoprecipitations were performed in biological duplicate or triplicate, and representative results are shown in A-D. **E)** *Pf*J2^{apt}-PDI8^{glmS} parasite cultures were evenly split into two conditions: 3 mM DVSF or PBS only for 30 minutes at 37°C, after which parasite lysates were used for anti-V5 immunoprecipitation. Input and eluted IP proteins were analyzed by western blot using V5 and *Pf*BiP antibodies. The PfBiP signal was measured for each lane and the ratio of IP-to-Input signal was determined. N = 3 biological replicates. Error bars represent standard deviation.

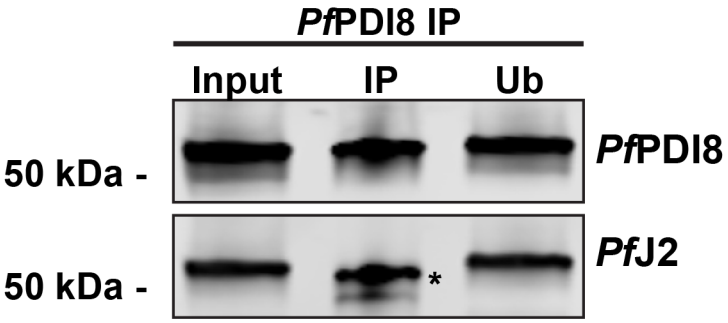

Figure 4.14. Immunoprecipitation of PfPDI8. *Pf*PDI8 and interacting proteins were immunoprecipitated from *Pf*J2^{apt}-PDI8^{glmS} parasite lysate using anti-V5 antibodies. The pre-IP input sample, the sample eluted from the antibodies (IP), and the sample removed from the beads containing the unbound proteins (Ub) were used for western blotting. Membranes were probed with antibodies against V5 and HA. The asterisk (*) denotes the heavy chain of the antibody used for immunoprecipitation.

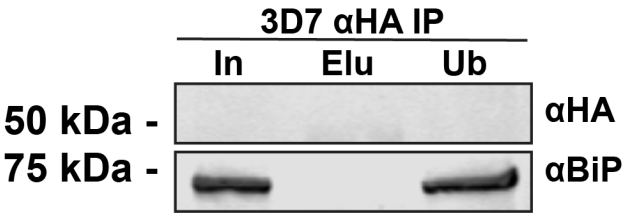

Figure 4.15. Anti-HA BiP IP. 3D7 parasite lysates were used for anti-HA immunoprecipitation (IP). The pre-IP input sample (In), the sample eluted from the antibodies (Elu), and the sample removed from the beads containing the unbound proteins (Ub) were used for western blotting. Membranes were probed with antibodies against HA and *Pf*BiP.

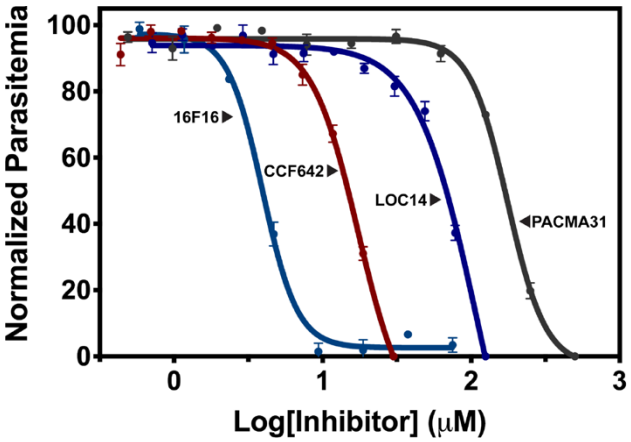

Specific Inhibitors of HsPDIA1		
Inhibitor	**Proposed Mode of Action**	***Pf*** **IC_{50} (μM) at 72 hrs**
16F16	Covalently binds Trx-domain cysteines (Kaplan, *et al.*)	3.94
CCF642	Covalently binds lysine in CGHCK motif (Vatolin, *et al.*)	17.3
LOC14	Binds adjacent to active site, forcing PDI to adopt oxidized confirmation (Kaplan, *et al.*)	110
PACMA31	Covalently binds Trx-domain cysteines (Xu, *et al.*)	176

Figure 4.16. PDI Inhibitor IC50s. Left: Asynchronous 3D7 parasites were incubated in various concentrations of human PDI inhibitors. Each data point represents the mean parasitemia at a given concentration, in technical triplicate, at 72 hours. Error bars, which are not shown for data points in which they are smaller than the circle symbol, represent standard deviation from the mean. Representative IC_{50} curves are shown for each drug. Experiments were performed in biological triplicate. Right: table describing each of the human PDI inhibitors used and their calculated *P. falciparum* IC_{50} values.

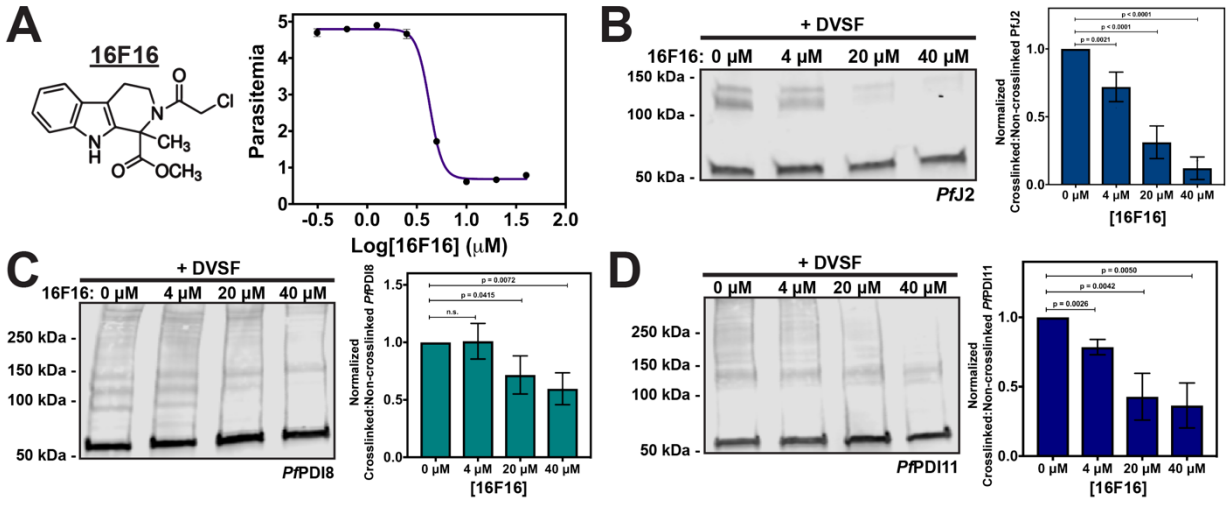

Figure 4.17. ER redox interactions are sensitive to interruption by a small molecule. A) Asynchronous *Pf*J2^{apt} parasites were incubated in various concentrations of the human PDI inhibitor 16F16. Parasite growth was determined via flow cytometry at 72 hours and the 16F16 IC_{50} was determined to be approximately 4 μM. Each data point in the curve represents the mean parasitemia at a given concentration, in technical triplicate. Error bars, which are not shown for data points in which they are smaller than the circle symbol, represent standard deviation from the mean. A representative IC_{50} curve is shown for one of three biological replicates. **B)** *Pf*J2^{apt}, **C)** *Pf*J2^{apt}-PDI8^{glmS}, and **D)** *Pf*J2^{apt}-PDI11^{glmS} parasites cultures were equally split and incubated with three concentrations of 16F16 for 3 hours prior to removal of 16F16, then incubation with 3 mM DVSF as described above. Samples were taken for western blot analysis, loading equal parasite equivalents into each gel. Membranes were incubated with antibodies against HA or V5. Signal for non-crosslinked (the band at approximately 50 kDa) and crosslinked proteins (>50 kDa) was measured. Inhibition was measured by determining the ratio of crosslinked to non-crosslinked signal. N = 3 biological replicates for each parasite line. Error bars represent standard deviation.

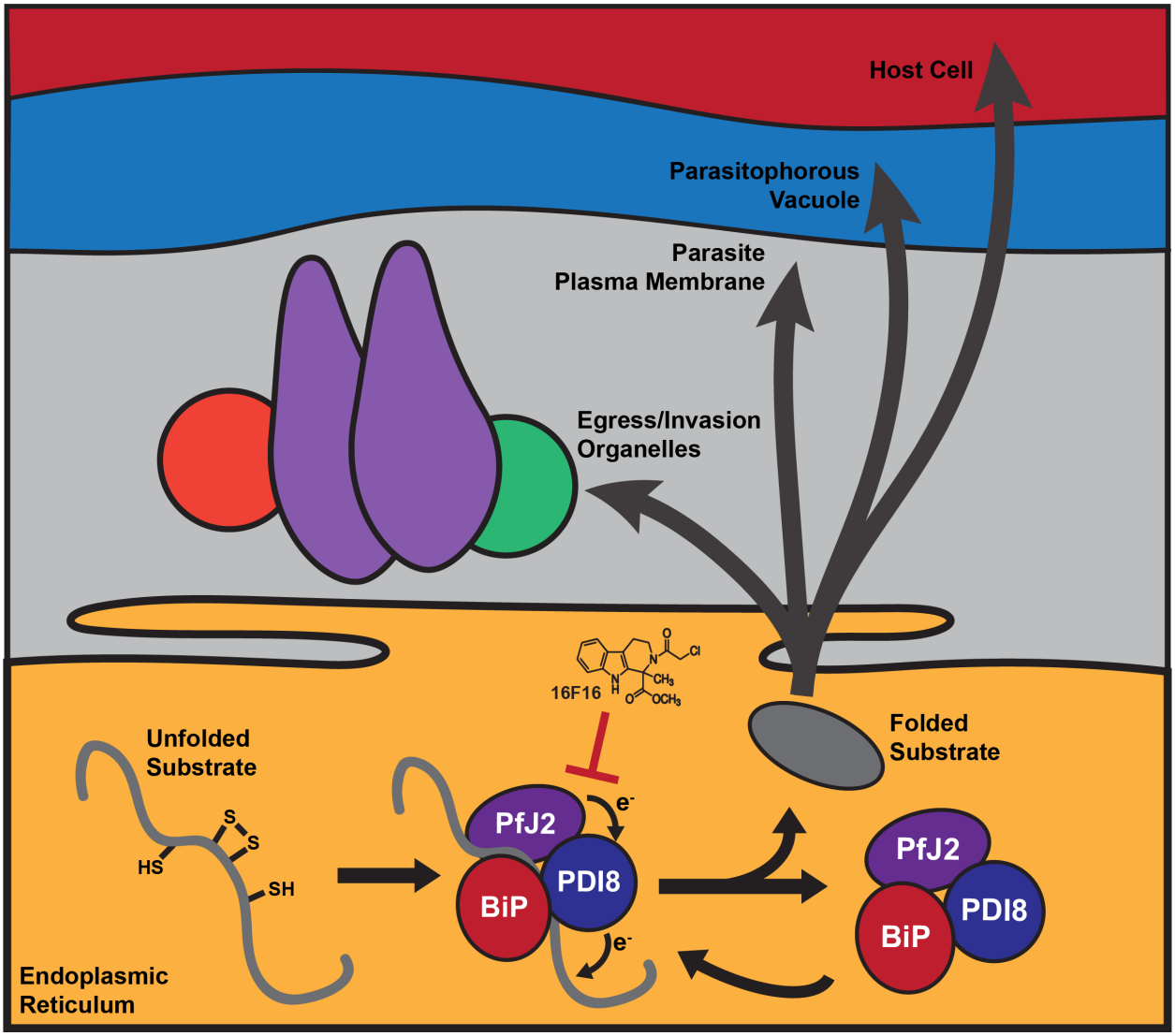

Figure 4.18. Oxidative folding in the *P. falciparum* ER. We propose that Trx-domain proteins like *Pf*J2 and *Pf*PDI8 work with *Pf*BiP to help nascent proteins, which perform essential functions within the ER and throughout the parasite secretory pathway, achieve their native states. The redox interactions between *Pf*J2, *Pf*PDI8, and their substrates are sensitive to inhibition by small molecules like 16F16, which could be expected to disrupt oxidative folding and impair the parasite's ability to perform functions essential for survival and replication.

CHAPTER 5

POTENTIAL ROLES FOR *PF*J2 AT THE ER MEMBRANE

5.1 Introduction

In addition to a protein trafficking hub, the ER is a site of Ca^{2+} storage and lipid synthesis in Eukaryotes. The *Plasmodium* ER is no different in this regard, but compared to many other organisms, the parasite genome and proteome are much reduced; therefore, fewer proteins exist to support these functions. Our work has shown that *Pf*J2 is an essential ER-resident chaperone with redox partnerships with other, essential ER proteins (Chapter 4). I anticipate roles for *Pf*J2 in ER biology beyond—or in conjunction with—its interactions outlined above. Supporting this idea, *Pf*J2 was identified in an analysis of the *P. falciparum* asexual stage palmitome, which suggests some or all of the protein may be associated with the ER membrane[1]. I therefore sought to experimentally confirm the membrane association of *Pf*J2 and investigate roles the chaperone might play at the ER membrane, specifically in regard to ER Ca^{2+} storage and the synthesis of lipids, as these are critical functions within the parasite which occur at the ER membrane.

5.2 A fraction of *Pf*J2 is membrane-associated

Protein palmitoylation is a reversible post-translational modification in which palmitic acid is attached—typically—to cysteine residues[2]. The hydrophobicity of

palmitic acid allows the palmitoylated protein to associate with cell membranes (**Figure 5.1A**). Protein palmitoylation in *P. falciparum* is required for completion of the asexual lifecycle, with impairment of palmitoylation interfering with schizont development and parasite invasion[1,2]. *Pf*J2 was identified in an analysis of the *P. falciparum* asexual-stage palmitome[1]. As a redox-active chaperone, reversible membrane-association of *Pf*J2 via palmitoylation could be a method by which the parasite regulates specific *Pf*J2-substrate interactions. In order to determine whether a fraction of *Pf*J2 is associated with membranes, sodium carbonate was used to fractionate *Pf*J2^{apt} parasites expressing soluble, ER-targeted GFP (*Pf*J2^{apt}-GFP) (**Figure 5.1B**). Sodium carbonate fractionation and ultracentrifugation results in a supernatant containing soluble proteins and a pellet containing membrane-associated proteins[3]. Western blot analysis of *Pf*J2^{apt}-GFP sodium carbonate fractions revealed *Pf*J2 in both the supernatant and the pellet, indicating that a portion of *Pf*J2 is found associated with the ER membrane (**Figure 5.1C**). Successful fractionation was confirmed by probing for the integral ER-resident protease *Pf*PMV—found in the pellet—and for soluble GFP expressed in the ER lumen—found in the supernatant (**Figure 5.1C**).

5.3 Regulatory redox cysteines are conserved in *Pf*SERCA

One critical function of the ER is storage of Ca^{2+}, which serves to keep cytoplasmic calcium concentrations low and allows for stored Ca^{2+} release in regulated signaling processes. In *P. falciparum*, calcium signaling is known to play a role in egress and invasion during the asexual lifecycle, although very little

is known about the proteins involved in regulation of calcium storage/release in the parasite ER[4]. However, the *P. falciparum* genome does encode a homolog for the sarco/endoplasmic reticulum Ca^{2+}-ATPase (*Pf*SERCA) (**Figure 5.2A)**. The SERCA pump is responsible for loading the ER with Ca^{2+} and counteracts the natural leakage of Ca^{2+} from the organelle[4,5]. In human cells, SERCA function is regulated by a disulfide formed between Cys875 and Cys887[5]. At high Ca^{2+} concentrations, the cysteines are oxidized and SERCA is inactive; when Ca^{2+} is depleted in the ER, the reductase ERdj5 reduces the disulfide to activate SERCA[5]. Alignment of PfSERCA with SERCA2b from humans revealed conservation of the regulatory cysteines (**Figure 5.2B**). Interestingly, the regulatory cysteines are predicted to be encoded within a short exon in the *pfserca* gene, leading to the possibility that alternative splicing could exclude them from the translated protein (**Figure 5.3A**). To determine whether alternative splicing of *pfserca* could be detected, total mRNA extracted from *wild-type P. falciparum* and *Pf*J2^{apt} parasites was used to generate *pfserca* cDNA, and the region between exons 1 and 2 was PCR amplified (**Figure 5.3B)**. The only product detected was a 600 bp amplicon, indicating the presence of exon 2, which encodes the regulatory cysteine residues (**Figure 5.3B)**. I next asked whether alternative splicing of *pfserca* could be detected following parasite redox stress. *P. falciparum* parasites were treated with either the oxidizing agent diamide or the reducing agent dithiothreitol for 2 hours, after which RNA was extracted and *pfserca* cDNA generated (**Figure 5.3C**). No alternative splicing was detected in response to 2 hour treatment with the chemicals (**Figure 5.3C**).

These data indicate that the conserved cysteines which regulate SERCA function in humans are present in *Pf*SERCA expressed by asexual *P. falciparum* parasites.

Because ERdj5 is an Hsp40/reductase with homology to *Pf*J2, and because *Pf*SERCA in the asexual stage contains the conserved regulatory cysteines, I hypothesize that the putative reductase function of *Pf*J2 regulates SERCA activity within the parasite. To investigate whether *Pf*J2 and PfSERCA are redox partners, *Pf*J2^{apt} parasites were treated with the redox-specific crosslinker divinyl sulfone (DVSF), then *Pf*J2 and its crosslinked interactors were immunoprecipitated from parasite lysates (See Chapter 4). Immunoprecipitated proteins were separated via SDS-PAGE and visualized using Coommassie, then two gel slices were extracted and proteins within those slices identified via tandem mass spectrometry (**Figure 5.4, Appendix D**). The “DVSF-1” portion of the gel contained proteins with a molecular weight higher than 75 kDa, and within this slice *Pf*SERCA was detected in low abundance (**Appendix D**). Because *Pf*SERCA is large, multi-pass transmembrane protein, its low abundance in this experiment was unsurprising, and a more targeted approach (such as epitope-tagging *Pf*SERCA and probing for interactions with *Pf*J2 via immunoprecipitation) is needed to confirm the interaction. However, these results are suggestive that *Pf*J2 and *Pf*SERCA are redox partners, and the reductase function of *Pf*J2 may regulate *Pf*SERCA and therefore the ability of the ER to store Ca^{2+}.

5.4 *Pf*J2 knockdown impairs lipid synthesis

The production of triacylglycerol (TAG) is another essential function which occurs at the ER membrane of nearly all Eukaryotes[6]. A series of transmembrane ER proteins produce TAG, which is packaged into cytosolic droplets known as lipid bodies, from which TAG can be utilized by the cell for production of phospholipids and other biological processes[6,7]. *P. falciparum* synthesizes TAG and lipid bodies, with TAG synthesis peaking in the late trophozoite stage[8,9]. Orlistat, an inhibitor of TAG hydrolysis, kills cultured asexual *P. falciparum* parasites with an IC_{50} of approximately 1 μM[10] (**Figure 5.5**). Treatment of *P. falciparum* with Orlistat prevents TAG hydrolysis to release free fatty acids, resulting in parasite death late in the lifecycle, with fully mature merozoites failing to form[10].

Because *Pf*J2 knockdown results in parasite death late in the life cycle, coincident with peak TAG synthesis and the timing of Orlistat-induced death, I hypothesized that *Pf*J2 may play a role in TAG synthesis in the ER. *Pf*J2 was immunoprecipitated from *Pf*J2^{apt} parasites, and co-immunoprecipitating proteins were identified by tandem mass spectrometry (See Chapter 4). Among the identified proteins were two enzymes associated with triacylglycerol synthesis. Specifically, Glycerol-3-phosphate Acyl Transferase (GPAT, PF3D7_1212500) was identified in one of three replicates, and 1-Acylglycerol-3-phosphate-O-acyltransferase (AGPAT, PF3D7_1444300) was identified in three of three replicates (**Figure 5.6A**). GPAT produces lysophosphatidic acid (LPA) through

the acylation of glycerol-3-phosphate; AGPAT produces phosphatidic acid (PA) through the acylation of LPA[6] (**Figure 5.6B**).

Because two enzymes required for TAG synthesis were identified in the *Pf*J2 coIP mass spectrometry data, I reasoned that knockdown of *Pf*J2 may result in impaired lipid body formation, which can be imaged used BODIPY 493/503[9,10] (**Figure 5.7A**). *Pf*J2[apt] parasites were tightly synchronized to the ring stage, and PfJ2 knockdown initiated by removal of aTc from culture medium. Then, samples of live parasites were taken throughout the last half of the asexual lifecycle, stained with BODIPY 493/503, and imaged. Quantification of the number of lipid bodies present at each time point revealed that during *Pf*J2 knockdown, parasites were slower to produce lipid bodies (**Figure 5.7B**). For example, by 27 hours in Replicate 1, nearly all control parasites had produced at least one lipid body, but less than half of *Pf*J2 knockdown parasites had done so. By 30 hours in the same experiment, 2+ lipid bodies were observed in nearly half of the control parasites, whereas most *Pf*J2 knockdown parasites had only produced one lipid body. In the second replicate, the differences at the earlier timepoints appear less dramatic, but by the final timepoint at 34 hours, the control parasites were clearly able to produce more lipid bodies. These results demonstrate that *Pf*J2 knockdown does impair the ability of parasites to produce lipid bodies, perhaps through impaired ability of GPAT and/or AGPAT to produce TAG.

5.5 Methods

Sodium Carbonate Fractionation and Western Blotting. Four 12 mL cultures of *Pf*J2^{apt}-GFP parasites (each at approximately 10% parasitemia) were treated with ice cold saponin to isolate parasites (see Chapter 4 Methods). Parasites were washed with cold 1x PBS, resuspended in 1 mL 1x PBS and 100 µL saved as the "Input" sample. Parasites were pelleted, then resuspended in cold 0.1 M Na_2CO_3 at pH 11 and left on ice for 20 minutes. Samples were spun at 100,000 x g for 1 hour at 4°C. The supernatant containing soluble proteins was saved, and the pellet containing membrane-associated proteins was gently rinsed (without resuspending) with 1 mL cold, deionized water. The pellet was dissolved in Laemmli Buffer + Beta-mercaptoethanol. Western blotting was perfomed as described in Chapter 4.

mRNA Extraction and* pfserca *cDNA Generation. To purify RNA, *P. falciparum* cultures were pelleted and treated with ice-cold 0.1% saponin in 1x PBS to isolate parasites from host cells. The parasites were then resuspended in 0.5 mL Trizol + Ribolock RNAse inhibitor and incubated at room temperature for 5 min. 100µl $CHCl_3$ was added and the samples were incubated at room temperature for 2 min, then centrifuged at 12,000 x g at 4°C for 15 min. The supernatant (the top phase out of 3) was transferred to a new tube and 250 µL Isopropanol was added. Samples were incubate at room temperature for 10 min, then centrifuged at 12000 x g, 4°C for 10 min. The RNA pellets were then washed with 250 µL 70% EtOH (without resuspending) and centrifuged at 12,000 x g at 4°C for 5 min. The supernatant was removed and pellets were allowed to

dry for 10 minutes then were resuspended in 25 uL sterile, deionized water and stored at -80°C. *pfserca*-specific cDNA was generated using Superscript III Reverse Transcriptase according to manufacturer instructions (Invitrogen, Catalog Number 18080093) and the primer 5'-ttcgtcaagtataataactgggaaggac. To detect Exon 2 by PCR, the primers 5'-tgggtaaatttggttactgacggattaccag and 5'-ttcgtcaagtataataactgggaaggac were used, using the *pfserca* cDNA as the template.

Identification of PfJ2-interacting Proteins. *Pf*J2 co-immunoprecipitation and protein identification was carried out as described in Chapter 4. For identification of redox-specific partnerships: DVSF treatment, *Pf*J2 immunoprecipitation, and mass spectroscopy was also carried out as described in Chapter 4.

Parasite Growth Assay using Flow Cytometry. Aliquots of parasite cultures were incubated in 8 μM Hoescht 33342 (Thermofisher Scientific) for 20 minutes at room temperature, then fluorescence was measured using a CytoFlex S (Beckman Coulter, Hialeah, Florida). Flow cytometry data were analyzed using FlowJo software(Treestar, Inc., Ashland, Oregon). For IC_{50} determination, data were analyzed using the 4-parameter dose-response-curve function of Prism (GraphPad Software, Inc.).

BODIPY 493/503 Staining. Stock BODIPY 493/503 was prepared at a concentration of 1250 μg/mL in DMSO and stored at -20°C. To stain parasites, 100 μL culture was spun down, washed 1x with 100 μL incomplete RPMI (culture medium prepared without Albumax I), then resuspended in 100 μL of 2 μg/mL

BODIPY 493/503 and 8 μM Hoescht 33342 prepared in incomplete RPMI. Parasites were incubated at 37°C for 10 min, washed 1x with 1 mL incomplete RPMI, then resuspended in 100 uL incomplete RPMI. 8 uL were added to a glass slide, over which a glass coverslip was placed and sealed with clear nail polish. Parasites were imaged using a DeltaVision II microscope system with an Olympus IX-71 inverted microscope.

5.6 References

1. Jones, M. L., Collins, M. O., Goulding, D., Choudhary, J. S. & Rayner, J. C. Analysis of Protein Palmitoylation Reveals a Pervasive Role in Plasmodium Development and Pathogenesis. *Cell Host Microbe* **12**, 246–258 (2012).
2. Siddiqui, M. A., Singh, S., Malhotra, P. & Chitnis, C. E. Protein S-Palmitoylation Is Responsive to External Signals and Plays a Regulatory Role in Microneme Secretion in *Plasmodium falciparum* Merozoites. *ACS Infect. Dis.* **6**, 379–392 (2020).
3. Dvorin, J. D. *et al.* A Plant-Like Kinase in Plasmodium falciparum Regulates Parasite Egress from Erythrocytes. *Science* **328**, 910–912 (2010).
4. Brochet, M. & Billker, O. Calcium signalling in malaria parasites: Calcium in malaria parasites. *Mol. Microbiol.* **100**, 397–408 (2016).
5. Ushioda, R. *et al.* Redox-assisted regulation of Ca^{2+} homeostasis in the endoplasmic reticulum by disulfide reductase ERdj5. *Proc. Natl. Acad. Sci.* **113**, E6055–E6063 (2016).

6. Coleman, R. Enzymes of triacylglycerol synthesis and their regulation. *Prog. Lipid Res.* **43**, 134–176 (2004).

7. Walther, T. C., Chung, J. & Farese, R. V. Lipid Droplet Biogenesis. *Annu. Rev. Cell Dev. Biol.* **33**, 491–510 (2017).

8. Vielemeyer, O., McIntosh, M. T., Joiner, K. A. & Coppens, I. Neutral lipid synthesis and storage in the intraerythrocytic stages of Plasmodium falciparum. *Mol. Biochem. Parasitol.* **135**, 197–209 (2004).

9. Palacpac, N. M. Q. Developmental-stage-specific triacylglycerol biosynthesis, degradation and trafficking as lipid bodies in Plasmodium falciparum-infected erythrocytes. *J. Cell Sci.* **117**, 1469–1480 (2004).

10. Gulati, S. *et al.* Profiling the Essential Nature of Lipid Metabolism in Asexual Blood and Gametocyte Stages of Plasmodium falciparum. *Cell Host Microbe* **18**, 371–381 (2015).

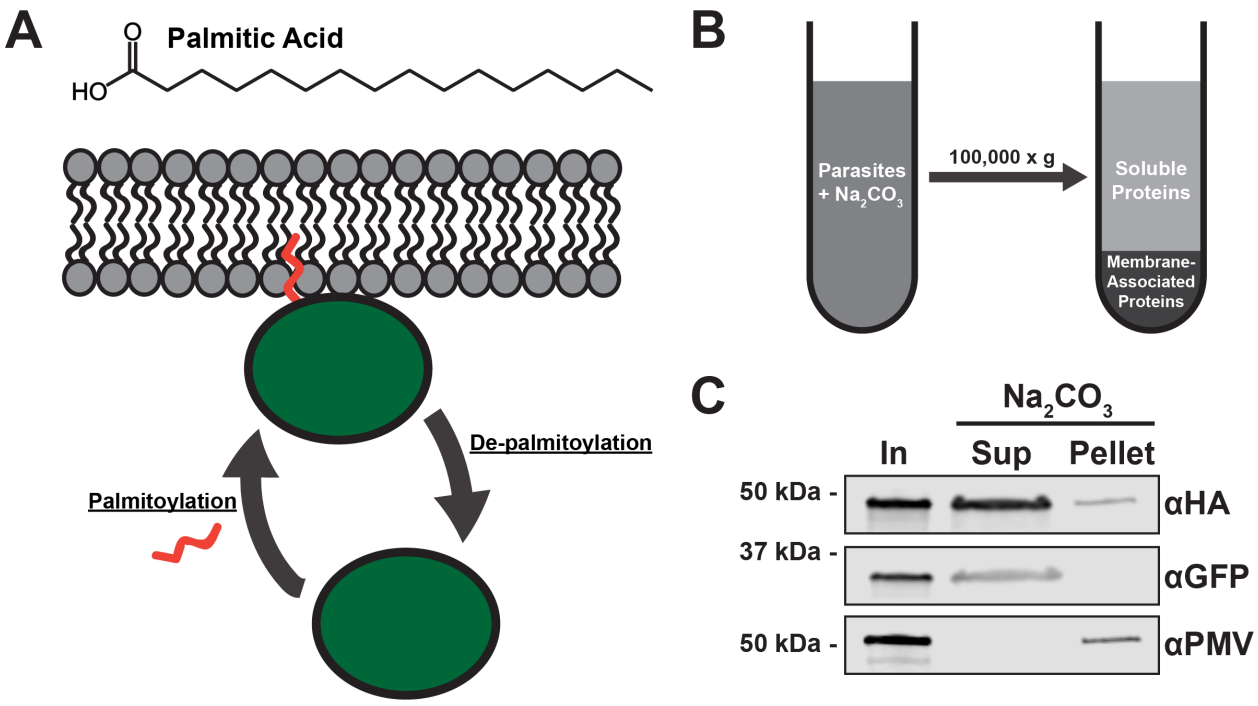

Figure. 5.1. PfJ2 is found associated with membranes. A) *Pf*J2 was identified as a potentially palmitoylated protein in the *P. falciparum* asexual stage[1]. Palmitoylation is a post-translational modification in which palmitic acid is attached to a protein, allowing it to associate with lipid bilayers. **B)** Schematic representing membrane fractionation using sodium carbonate and ultracentrifugation. **C)** *Pf*J2^{apt}-GFP parasites were subjected to membrane fractionation as shown in B and proteins were detected in each fraction by western blotting. *Pf*J2 was detected using antibodies against its 3xHA tag.

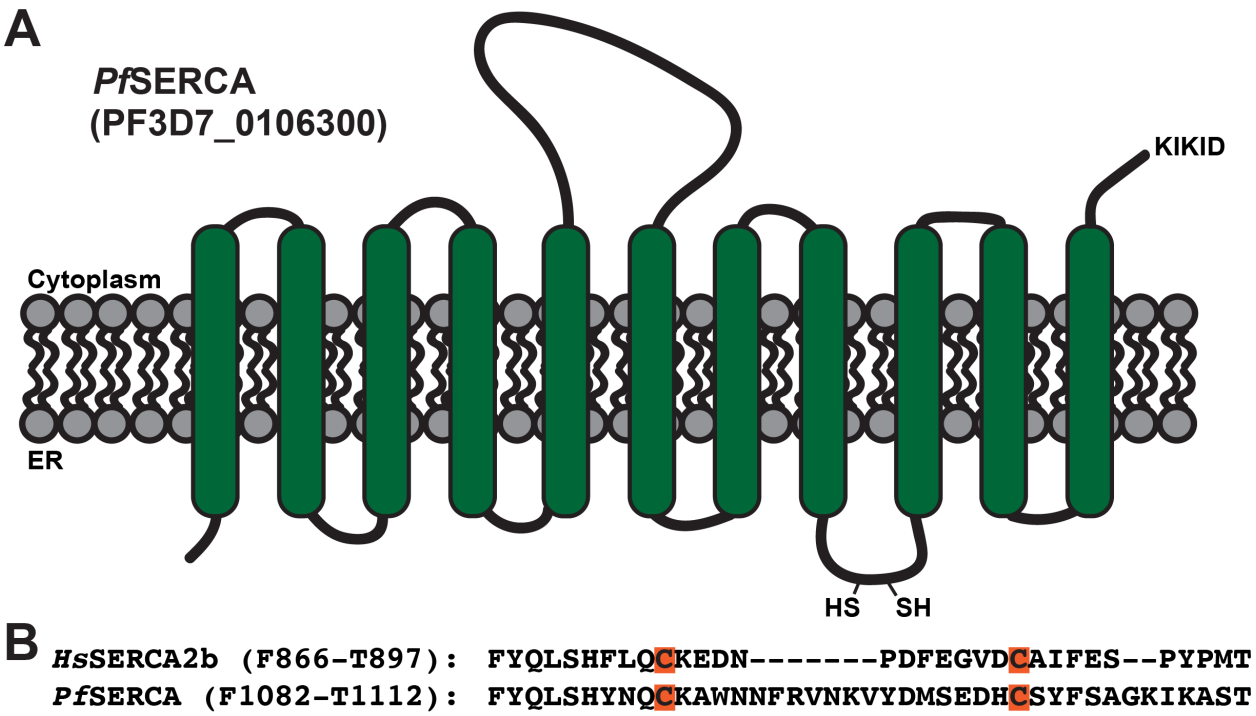

Figure 5.2. *Pf*SERCA is a multi-pass transmembrane protein with conserved redox regulatory cysteine residues. A) Predicted topology of *Pf*SERCA (PF3D7_0106300) with transmembrane domains predicted using TMpred (https://embnet.vital-it.ch/software/TMPRED_form.html). Shown are the sulfhydryl groups of the predicted redox regulatory cysteines in the ER lumen and the KIKID ER-retention signal. **B)** The primary sequences of human SERCA2b and *Pf*SERCA were aligned using MegAlign (DNASTAR, Inc.), revealing conservation of the redox regulatory cysteines in *P. falciparum*, highlighted in orange.

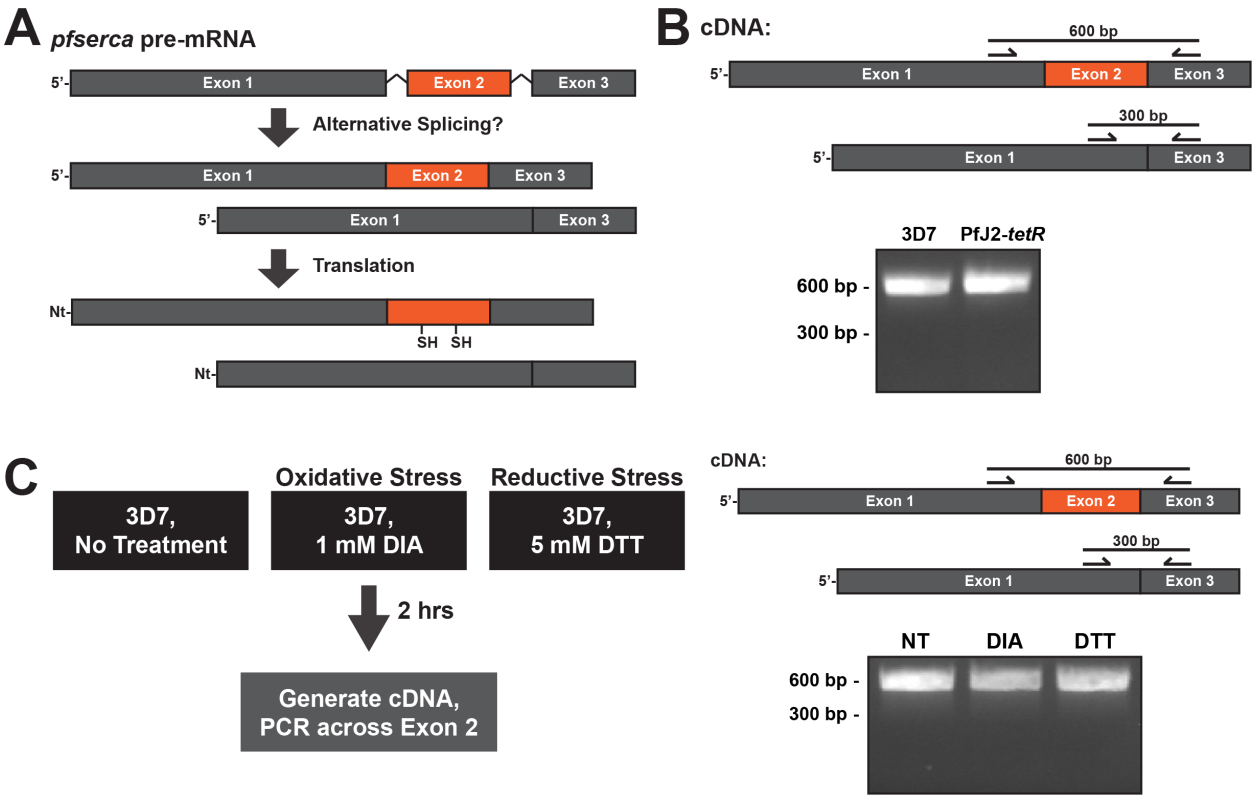

Figure 5.3. PfSERCA conserved redox regulatory cysteine residues are encoded within a short, predicted exon. A) *pfserca* is predicted to encode 3 exons, one of which contains the codons for the regulatory cysteine residues. **B)** PCR strategy to detect Exon 2. **C)** 3D7 parasites were treated with oxidative and reductive stressors, then cDNA was generated and PCR used to probe for the presence or absence of Exon 2.

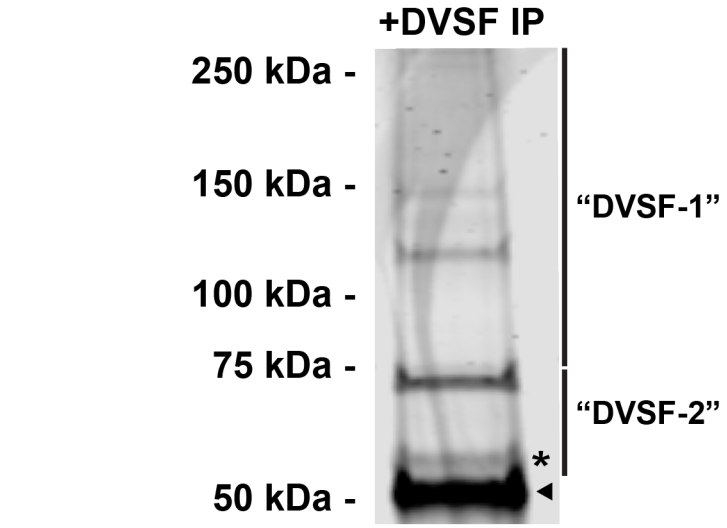

Figure 5.4. Separation of redox-crosslinked PfJ2 and partners with SDS-PAGE. *Pf*J2^{apt} parasite cultures were treated with 3 mM DVSF for 30 minutes at 37°C, after which parasite lysates were used for anti-HA immunoprecipitation. Immunoprecipitated proteins were separated via SDS-PAGE and visualized using Coomassie. Two sections of the gel were extracted and the proteins within were identified by tandem mass spectrometry. The band corresponding to the predicted size of *Pf*J2 is indicated with an asterisk, and the heavy chain of the anti-HA antibody used for immunoprecipitation is indicated with an arrowhead.

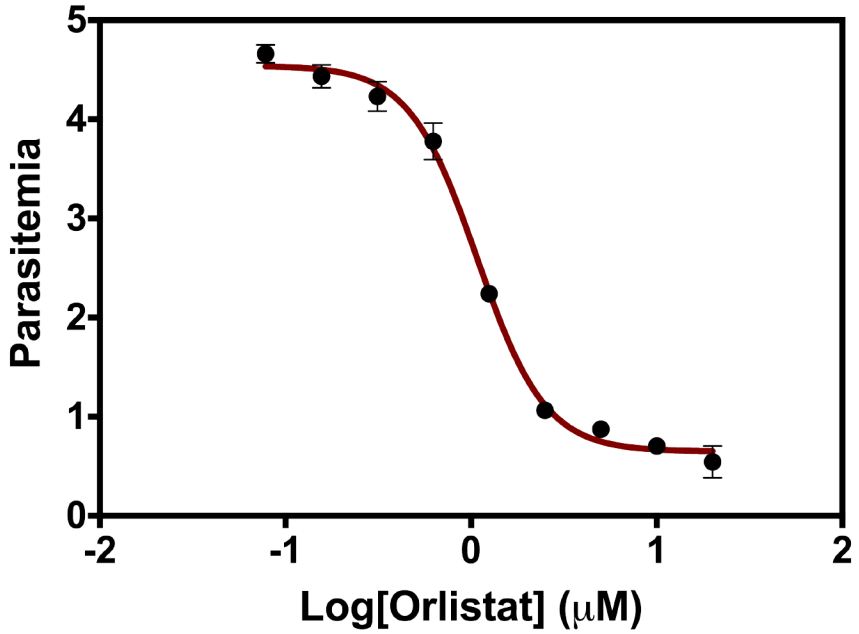

Figure 5.5. Anti-*P. falciparum* activity of Orlistat. Asynchronous *P. falciparum* parasites were incubated in various concentrations of the inhibitor Orlistat. Parasite growth was determined via flow cytometry at 72 hours and the Orlistat IC_{50} was determined to be approximately 1 μM. Each data point in the curve represents the mean parasitemia at a given concentration, in technical triplicate. Error bars, which are not shown for data points in which they are smaller than the circle symbol, represent standard deviation from the mean

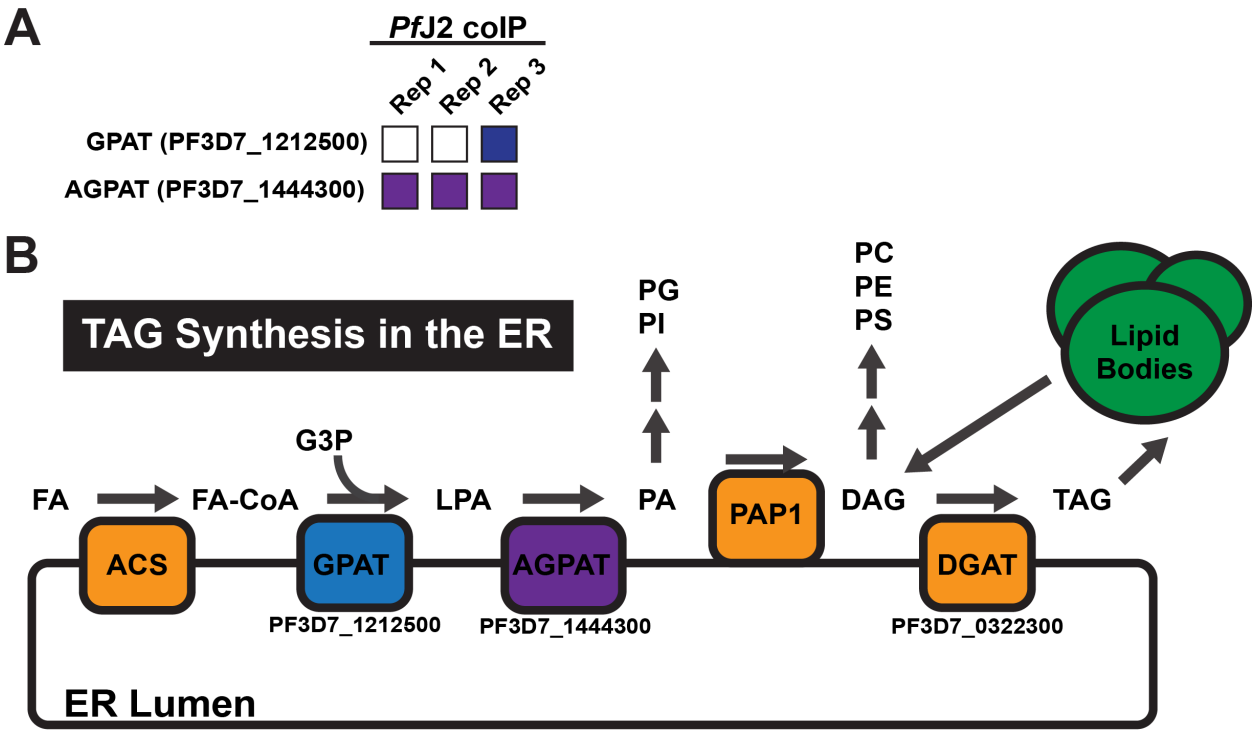

Figure 5.6. GPAT and AGPAT co-immunoprecipitate with *Pf*J2. A) *Pf*J2 was immunoprecipitated from *Pf*J2^{apt} parasites and coimmunoprecipitating proteins were identified by tandem mass spectrometry, in biological triplicate. Glycerol-3-phosphate Acyl Transferse (GPAT, PF3D7_1212500) was identified in one of three replicates, and 1-Acylglycerol-3-phosphate-O-acyltransferase (AGPAT, PF3D7_1444300) was identified in three of three replicates. **B)** Schematic of triacylglycerol (TAG) synthesis at the ER membrane, adapted from RA Coleman and DP Lee, 2004(CITE). PlasmoDB geneIDs of predicted *P. falciparum* homologs are shown. ACS, acyl-CoA synthetase; PAP1, phosphatidic acid phosphohydrolase; DGAT, diacylglycerol acyltransferase. FA, fatty acid; G3P, glycerol-3-phosphate; LPA, lysophosphatidic acid; PA, phosphatidic acid; PI,

phosphatidylinositol; PG, phosphatidylglycerol; DAG, diacylglycerol; PS, phosphatidylserine; PE, phosphatidylethanolamine; PC, phosphatidylcholine.

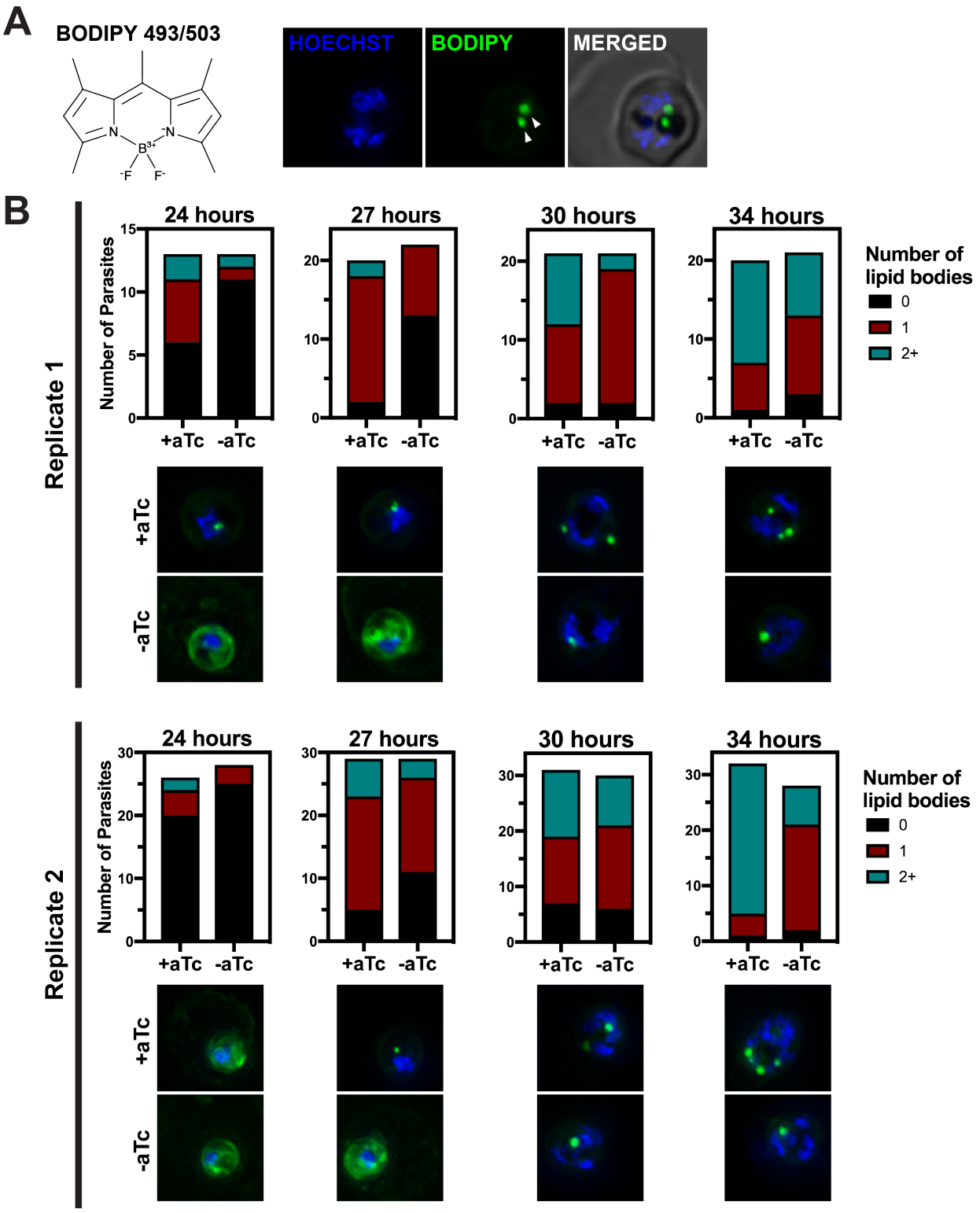

Figure 5.7. *Pf*J2 knockdown impairs lipid body production. A) BODIPY 493/503 stains Lipid Bodies. The DNA stain Hoechst 33342 is shown in blue, and

BODIPY 493/503 shown in green. Lipid bodies indicated with white arrowheads. **B)** *Pf*J2^{apt} parasites were tightly synchronized to the ring stage and aTc was removed from culture medium to initiate *Pf*J2 knockdown. The number of lipid bodies detected in each parasite at 24, 27, 30, and 34 hours after knockdown was counted. Prior to the production of lipid bodies, BODIPY 493/503 staining is diffuse throughout the parasite.

CHAPTER 6

CONCLUSIONS AND DISCUSSION

In this dissertation, I present three manuscripts concerning the use of cutting-edge genetic tools to study conserved chaperones and their roles in the *Plasmodium falciparum* asexual lifecycle, and an additional chapter describing new preliminary data for one of those chaperones. The first manuscript provides a detailed protocol for the use of CRISPR/Cas9 genome editing in the parasite and the application of a conditional knockdown system to explore protein function. The second and third manuscripts demonstrate the use of these and other genetic and chemical tools to reveal insights into the roles that two chaperone proteins—*Pf*Hsp70x and the Hsp40 *Pf*J2—have in *P. falciparum* cellular biology. Finally, another chapter provides new data concerning possible roles for *Pf*J2 regulating functions within the endoplasmic reticulum (ER) that are critical for the parasite's survival.

Asexual replication of *P. falciparum* within human red blood cells results in the clinical manifestations of malaria; this step within the parasite's lifecycle is therefore an attractive target for anti-malarial therapeutics and research. However, the parasite's cellular biology has been difficult to probe due to inefficient means of editing the *P. falciparum* genome. The haploid nature of the parasite during asexual replication further complicates studying essential processes. The introduction of CRISPR/Cas9 genome editing into *P. falciparum*

research has provided the tool needed to efficiently modify the parasite genome in a targeted manner, and the development of conditional knockdown approaches has opened up essential proteins for study[1–4].

In Chapter 2, I describe our approach to the use of CRISPR/Cas9 for editing the parasite genome, specifically to introduce epitope tags and the *glmS* ribozyme sequence into the parasite's DNA. This manuscript provides a detailed walkthrough of each step needed to use CRISPR/Cas9 within the parasite—from selecting a gRNA sequence that targets a gene-of-interest; to producing plasmids that express the gRNA, Cas9, and a repair template that introduces the epitope tag and *glmS* sequence; to verifying successful modification and methods for detecting the protein knockdown. The core components of CRISPR/Cas9 editing in *P. falciparum* are the Cas9 endonuclease, the gRNA guiding Cas9 to a specific place in the genome, and the repair template the parasite uses to repair its genome. We demonstrate a successful three-plasmid approach, in which each of these components are transfected on separate plasmids. We and others have since shown that a simplified two-plasmid approach combining Cas9 and gRNA expression into one plasmid is another option[5,6]. We also show that we were unable to recover parasites after attempting to modify the genome with short homology arms (50, 75, and 100 base pairs in length), although slight modifications to the approach could increase chances of successful modification (i.e. the use of positive selection with a drug cassette). Altogether, the manuscript presented in Chapter 2 is an important guide for the

field of *P. falciparum* research, assisting others in the use of CRISPR/Cas9 and conditional protein knockdown.

In Chapter 3, I present a manuscript that uses the techniques described in Chapter 2 to investigate *Pf*Hsp70x, the only Hsp70 known to be exported by the parasite into the host red blood cell (RBC). Two independent conditional knockdown approaches were used to determine whether *Pf*Hsp70x is essential for the asexual lifecycle, and we found that knockdown of the chaperone did not result in an observable growth defect in culture. We therefore next used CRISPR/Cas9 to knock out *pfhsp70x* from the parasite genome, and we successfully recovered *Pf*Hsp70x-null parasites. The prevailing theory within our lab and the *Plasmodium* field was that PfHsp70x may assist in the trafficking of other virulence factors that are made within the parasite and exported out into the host RBC. We were unable to detect trafficking defects for select virulence factors during *Pf*Hsp70x knockdown or in the knockout parasites, including for *Pf*EMP1[7]. Another study using independently-generated *Pf*Hsp70x knockout parasites detected a brief and minor defect in *Pf*EMP1 trafficking[8]. Because *PfHsp70x* is the only detected parasite Hsp70 within the host RBC, despite numerous exported Hsp40 co-chaperones, *Pf*Hsp70x was thought by many to be important for parasite survival and pathogenesis; our results provided refutation of that widely-held hypothesis, showing that *Pf*Hsp70x is in fact dispensable for cultured parasites.

Chapter 4 consists of a manuscript detailing the investigation of an ER-resident Hsp40 known as *Pf*J2. CRISPR/Cas9 was used to generate transgenic

parasites in which *Pf*J2 was epitope tagged, and its expression conditionally controlled by the presence of anhydrotetracycline (aTc). Knockdown of *Pf*J2 revealed its essentiality for the asexual lifecycle, and leveraging of the epitope tag for co-immunoprecipitation experiments identified several potential interactions with other proteins that pass through the ER and into the parasite's secretory pathway. *Pf*J2 also contains a thioredoxin (Trx) domain, consisting of a "CXXC" active site motif. I used divinyl sulfone (DVSF)—a redox-specific chemical crosslinker that reacts with nucleophilic cysteines such as those in the CXXC active site—to trap PfJ2 with its redox partners. These partners were then identified as *Pf*PDI8 and *Pf*PDI11, two conserved Protein Disulfide Isomerases which also contain Trx domains and likely contribute to disulfide bond formation in proteins folding within the ER[9,10].

With a combination of conditional knockdown mutants for both PDIs and overexpression mutants of *Pf*PDI11, I concluded that *Pf*PDI8 is an essential protein for asexual replication and that *Pf*PDI11 forms mixed disulfides with other proteins despite its unusual "CXXS" active sites, potentially acting as a "holdase" in the ER. Given the essentiality of both *Pf*J2 and *Pf*PDI8, I investigated their interaction more deeply, and found that they both interact with the critical ER Hsp70 known as *Pf*BiP. I propose a model in which *Pf*J2, as a redox-active Hsp40 co-chaperone, bridges the two essential components of protein folding in the ER: chaperone-mediated folding assisted by *Pf*BiP and disulfide bond formation mediated by *Pf*PDI8. Finally, I demonstrated the disruption of interactions between *Pf*J2, *Pf*PDI8, and *Pf*PDI11 and their redox substrates using

a small molecule that targets Trx-domain active sites, concluding that these proteins within the ER may be anti-malarial drug targets[11–13].

An examination of the essentiality of *Pf*J2, its interactions with specific partners, and a proposed cooperative role in protein folding with *Pf*BiP and *Pf*PDI8 is presented in Chapter 4. Hypotheses of other roles for *Pf*J2 in the ER—either independently or in conjunction with its known partners in Chapter 4—along with supporting data are presented in Chapter 5. Such a pervasive role in multiple processes is not without precedent for an ER chaperone; for example, BiP is known to regulate several aspects of ER function in other organisms[14]. The hypotheses presented in Chapter 5 state that *Pf*J2 has a role in regulating ER Ca^{2+} storage through reduction of a regulatory disulfide bond within the calcium-pumping ATPase *Pf*SERCA, and that *Pf*J2 contributes to the lipid synthesis that occurs at the ER membrane through interactions with two of the enzymes required for triacylglycerol production. Both of these scenarios would presumably require *Pf*J2 in close proximity to the ER membrane, and an analysis of *P. falciparum* palmitoylated proteins—which are recruited to membranes—identified *Pf*J2[15]. I present a fractionation experiment that confirmed *Pf*J2 is found both soluble and in association with membranes. Using sequence alignment, I showed that cysteines that regulate human SERCA are conserved in *Pf*SERCA. In human cells, those cysteines are reduced by ERdj5, which like *Pf*J2 is an Hsp40 chaperone with Trx domains[16]. Using the redox-specific crosslinker DVSF and immunoprecipitation to capture *Pf*J2 trapped to its redox partners, I was able to detect a potential interaction between *Pf*J2 and *Pf*SERCA. These data

together suggest that *Pf*J2 may indeed regulate *Pf*SERCA function, which would implicate *Pf*J2 in Ca^{2+} storage in the parasite ER.

In an analysis of proteins that co-immunoprecipitated with *Pf*J2 (in this case, in the absence of DVSF) the enzyme Glycerol-3-phosphate Acyl Transferse (GPAT) was identified in one of three replicates, and 1-Acylglycerol-3-phosphate-O-acyltransferase (AGPAT) was identified in three of three replicates. In other organisms, these enzymes are found in the ER membrane and function in the production of triacylglycerol (TAG), which is packaged into lipid bodies for downstream production of phospholipids[18–20]. Neither enzyme is well-studied in *Plasmodium*, but *Pf*GPAT has been localized to the *P. falciparum* ER, and the *Pf*AGPAT homolog in *P. yoelii* has been localized to the parasite ER[21,22]. To functionally link *Pf*J2 to TAG synthesis, I showed that knockdown of *Pf*J2 delays production of lipid bodies. This defect is perhaps due to impairment in the abilities of *Pf*GPAT and/or *Pf*AGPAT to function during *Pf*J2 knockdown. Future work is needed to elucidate the exact nature of the interaction between the chaperone and these enzymes, and to determine why *Pf*J2 knockdown results in slower lipid body production. TAG hydrolysis is essential for completion of parasite maturation at the end of the asexual lifecycle, and confirmation of a direct role for *Pf*J2 in TAG production would link the chaperone to this essential process[23].

Together, this dissertation is a body of work demonstrating the use of cutting-edge tools in the malaria field to study the cellular biology of the deadly human parasite *P. falciparum*. Not only does it serve as a guide to others who

will use these same tools in the future, the proteins studied here underscore the value in investigating evolutionarily conserved proteins within the context of parasite biology. The core function may be conserved, but several millennia separate *P. falciparum* from the model organisms that inform what that conserved biology is. Based on the classical roles that Hsp70 chaperones have in protein trafficking, and because *Pf*Hsp70x is unique in its status as the only Hsp70 exported into an environment that requires extensive protein trafficking, many assumed an importance for the chaperone that our data suggests is outsized. The Hsp40 *Pf*J2 bears some conservation with the human protein ERdj5, which I leveraged to investigate the redox activity of *Pf*J2 and learned that while ERdj5 is most known for reducing client proteins during ER-Associated Degradation, the major redox partners of *Pf*J2 that we detected were Protein Disulfide Isomerases (PDIs), a class of enzymes in the ER with roles in disulfide bond formation[24]. We propose that *Pf*J2 and *Pf*PDI8, both essential for parasite survival in the RBC, work together to ensure other proteins within the ER fold/function properly, and identification of what those proteins are will likely show that they are factors unique to the parasitic existence of *P. falciparum*. Our data also suggest that small molecules specifically targeting oxidative folding in the parasite ER, which is mediated by proteins like *Pf*J2 and *Pf*PDI8, could have therapeutic potential. All of these observations were born from the choice to investigate conserved proteins with an open mind for what functions they may be performing to allow a single-cell, Eukaryotic parasite to survive within its human host.

References

1. Ghorbal, M. *et al.* Genome editing in the human malaria parasite Plasmodium falciparum using the CRISPR-Cas9 system. *Nat. Biotechnol.* **32**, 819–821 (2014).

2. Wagner, J. C., Platt, R. J., Goldfless, S. J., Zhang, F. & Niles, J. C. Efficient CRISPR-Cas9–mediated genome editing in Plasmodium falciparum. *Nat. Methods* **11**, 915–918 (2014).

3. Prommana, P. *et al.* Inducible Knockdown of Plasmodium Gene Expression Using the glmS Ribozyme. *PLoS ONE* **8**, e73783 (2013).

4. Ganesan, S. M., Falla, A., Goldfless, S. J., Nasamu, A. S. & Niles, J. C. Synthetic RNA–protein modules integrated with native translation mechanisms to control gene expression in malaria parasites. *Nat. Commun.* **7**, 10727 (2016).

5. Florentin, A., Stephens, D. R., Brooks, C. F., Baptista, R. P. & Muralidharan, V. Plastid biogenesis in malaria parasites requires the interactions and catalytic activity of the Clp proteolytic system. *Proc. Natl. Acad. Sci.* **117**, 13719 (2020).

6. Fierro, M. A. *et al.* An Endoplasmic Reticulum CREC Family Protein Regulates the Egress Proteolytic Cascade in Malaria Parasites. *mBio* **11**, e03078-19, /mbio/11/1/mBio.03078-19.atom (2020).

7. Lee, W.-C., Russell, B. & Rénia, L. Sticking for a Cause: The Falciparum

Malaria Parasites Cytoadherence Paradigm. *Front. Immunol.* **10**, 1444 (2019).

8. Charnaud, S. C. *et al.* The exported chaperone Hsp70-x supports virulence functions for Plasmodium falciparum blood stage parasites. *PLOS ONE* **12**, e0181656 (2017).

9. Mahajan, B. *et al.* Protein disulfide isomerase assisted protein folding in malaria parasites. *Int. J. Parasitol.* **36**, 1037–1048 (2006).

10. Mouray, E. *et al.* Biochemical properties and cellular localization of Plasmodium falciparum protein disulfide isomerase. *Biochimie* **89**, 337–346 (2007).

11. Hoffstrom, B. G. *et al.* Inhibitors of protein disulfide isomerase suppress apoptosis induced by misfolded proteins. *Nat. Chem. Biol.* **6**, 900–906 (2010).

12. Kaplan, A. *et al.* Small molecule-induced oxidation of protein disulfide isomerase is neuroprotective. *Proc. Natl. Acad. Sci.* **112**, E2245–E2252 (2015).

13. Harbut, M. B. *et al.* Targeting the ERAD pathway via inhibition of signal peptide peptidase for antiparasitic therapeutic design. *Proc. Natl. Acad. Sci.* **109**, 21486–21491 (2012).

14. Wang, J., Lee, J., Liem, D. & Ping, P. HSPA5 Gene encoding Hsp70 chaperone BiP in the endoplasmic reticulum. *Gene* **618**, 14–23 (2017).

15. Jones, M. L., Collins, M. O., Goulding, D., Choudhary, J. S. & Rayner, J. C. Analysis of Protein Palmitoylation Reveals a Pervasive Role in

Plasmodium Development and Pathogenesis. *Cell Host Microbe* **12**, 246–258 (2012).

16. Ushioda, R. *et al.* Redox-assisted regulation of Ca^{2+} homeostasis in the endoplasmic reticulum by disulfide reductase ERdj5. *Proc. Natl. Acad. Sci.* **113**, E6055–E6063 (2016).
17. Brochet, M. & Billker, O. Calcium signalling in malaria parasites: Calcium in malaria parasites. *Mol. Microbiol.* **100**, 397–408 (2016).
18. Coleman, R. Enzymes of triacylglycerol synthesis and their regulation. *Prog. Lipid Res.* **43**, 134–176 (2004).
19. Palacpac, N. M. Q. Developmental-stage-specific triacylglycerol biosynthesis, degradation and trafficking as lipid bodies in Plasmodium falciparum-infected erythrocytes. *J. Cell Sci.* **117**, 1469–1480 (2004).
20. Vielemeyer, O., McIntosh, M. T., Joiner, K. A. & Coppens, I. Neutral lipid synthesis and storage in the intraerythrocytic stages of Plasmodium falciparum. *Mol. Biochem. Parasitol.* **135**, 197–209 (2004).
21. Santiago, T. C., Zufferey, R., Mehra, R. S., Coleman, R. A. & Mamoun, C. B. The *Plasmodium falciparum* PfGatp is an Endoplasmic Reticulum Membrane Protein Important for the Initial Step of Malarial Glycerolipid Synthesis. *J. Biol. Chem.* **279**, 9222–9232 (2004).
22. Lindner, S. E. *et al.* Enzymes involved in plastid-targeted phosphatidic acid synthesis are essential for *P lasmodium yoelii* liver-stage development: *Plasmodium* phosphatidic acid biosynthesis. *Mol. Microbiol.* **91**, 679–693 (2014).

23. Gulati, S. *et al.* Profiling the Essential Nature of Lipid Metabolism in Asexual Blood and Gametocyte Stages of Plasmodium falciparum. *Cell Host Microbe* **18**, 371–381 (2015).

24. Ushioda, R. *et al.* ERdj5 Is Required as a Disulfide Reductase for Degradation of Misfolded Proteins in the ER. *Science* **321**, 569–572 (2008).

APPENDIX A

PROTEINS IDENTIFIED AS POTENTIAL *PF*J2 INTERACTING PARTNERS IN CHAPTER 4

Gene ID	Control Abundance	*Pf*J2^{apt} Abundance	Fold Change	Annotation
PF3D7_0318900	0.0000001	0.0000725	725	conserved protein, unknown function
PF3D7_1246800	0.0000001	0.0000623	623	signal recognition particle receptor subunit beta
PF3D7_0912400	0.0000001	0.0000363	363	alkaline phosphatase
PF3D7_1136800	0.00000036	0.0000262	72.7777778	DnaJ protein
PF3D7_1143200	0.0000029	0.00011263	38.8369241	DnaJ protein
PF3D7_1108700	0.00407876	0.12710782	31.1633212	PfJ2
PF3D7_0827900	0.0000489	0.00088386	18.0747587	PDI8
PF3D7_0917900	0.00214935	0.03487952	16.2279412	heat shock protein 70
PF3D7_1419200	0.00000528	0.0000812	15.3787879	thioredoxin-like protein
PF3D7_1459400	0.0000184	0.00026939	14.6409455	conserved protein, unknown function
PF3D7_1409600	0.00000297	0.000038	12.7946128	conserved Plasmodium protein, unknown function
PF3D7_0710100	0.00000591	0.0000429	7.25888325	conserved protein, unknown function
PF3D7_0905400	0.00025631	0.00173807	6.78107436	high molecular weight rhoptry protein 3
PF3D7_1444300	0.00000563	0.0000375	6.660746	1-acyl-sn-glycerol-3-

				phosphate acyltransferase
PF3D7_1222300	0.00012948	0.00086128	6.65166726	endoplasmin
PF3D7_0823800	0.00016253	0.00107965	6.64268338	DnaJ protein
PF3D7_0501600	0.00014884	0.00097904	6.57767003	RAP2
PF3D7_1324900	0.00010898	0.00068114	6.2503332	L-lactate dehydrogenase
PF3D7_0930300	0.00040573	0.00248967	6.13629621	merozoite surface protein 1
PF3D7_1346100	0.00000835	0.0000508	6.08383234	protein transport protein SEC61 subunit alpha
PF3D7_0612100	0.0000485	0.00027648	5.70070216	eukaryotic translation initiation factor 3 subunit L
PF3D7_0821000	0.0000791	0.00042284	5.34562647	conserved Plasmodium protein, unknown function
PF3D7_1410400	0.00074836	0.00393872	5.26310926	RAP1
PF3D7_0628300	0.0000508	0.00022962	4.51998713	CEPT
PF3D7_0922100	0.0000346	0.00013823	3.99496894	ubiquitin-like protein
PF3D7_1108600	0.00011323	0.00044701	3.94776303	ERC
PF3D7_1104400	0.0000591	0.0001997	3.37900244	Trx-mero
PF3D7_1105600	0.000044	0.00014819	3.36797527	PTEX88
PF3D7_1010300	0.0000128	0.0000421	3.2890625	SDH4
PF3D7_0702400	0.0000187	0.0000573	3.06417112	SEMP1
PF3D7_1239700	0.0000291	0.0000868	2.98281787	FTSH1
PF3D7_1471100	0.0000427	0.00012202	2.85770927	EXP2
PF3D7_1033200	0.00032043	0.00087178	2.72064775	ETRAMP10.2
PF3D7_1252100	0.00042654	0.0011555	2.70897094	RON3
PF3D7_1306200	0.0000656	0.00016152	2.46217862	Conserved proteins, unknown function
PF3D7_0929400	0.00216077	0.00528078	2.44392993	RhopH2
PF3D7_1116800	0.00023955	0.00058466	2.44072375	Hsp101
PF3D7_1037300	0.00012023	0.00027674	2.3017318	ADT
PF3D7_1121600	0.00020253	0.00046461	2.29409174	EXP1
PF3D7_1352500	0.000081	0.0001706	2.10613405	Thioredoxin-related protein

PF3D7_0702500	0.0000347	0.0000723	2.08357349	Plasmodium exported protein, unknown function
PF3D7_1358700	0.0000135	0.0000277	2.05185185	YOP1L
PF3D7_0622200	0.00000817	0.000014	1.71358629	Radical SAM
PF3D7_1462300	0.0000133	0.000022	1.65413534	GTP-binding protein
PF3D7_1420700	0.00016807	0.00026955	1.60381331	P113
PF3D7_0807300	0.00012315	0.00019208	1.5597363	RAB18
PF3D7_1134100	0.0000684	0.0000978	1.42982456	PDI11
PF3D7_0532400	0.00019724	0.00025966	1.31645876	LyMP
PF3D7_1133800	0.00099043	0.00123401	1.24593843	RNA (Uracil-5) methyltransferase
PF3D7_1407800	0.00030199	0.00037234	1.23294007	PMIV
PF3D7_0801800	0.00021575	0.00025711	1.19171613	Mannose-6-phosphate isomerase
PF3D7_0731300	0.0001113	0.00013095	1.17653812	PfG174
PF3D7_0629200	0.00262314	0.00303211	1.15591001	DnaJ protein
PF3D7_0831400	0.00078118	0.00085094	1.08929374	Plasmodium exported protein, unknown function
PF3D7_1364100	0.00010251	0.0000912	0.8896378	P92
PF3D7_1476300	0.00054448	0.00047972	0.88106073	PHISTb
PF3D7_0503000	0.0000064	0.00000517	0.8078125	Apicoplast 50S ribosomal protein
PF3D7_1010700	0.00114435	0.00086269	0.75387421	dolichyl-phosphate-mannose protein mannosyl-transferase
PF3D7_0707300	0.0000977	0.0000734	0.75127943	RAMA
PF3D7_1331800	0.0043733	0.00321598	0.73536655	60S protein
PF3D7_0312800	0.01941787	0.01251521	0.64452032	60S protein
PF3D7_0501200	0.00011639	0.0000721	0.61944717	PIESP2
PF3D7_0707200	0.0016814	0.0000905	0.05382434	Conserved plasmodium protein, unknown function

APPENDIX B

MASS SPECTROMETRY DATA USED TO IDENTIFY *PF*J2 REDOX PARTNERS IN CHAPTER 4

DVSF-treated sample, "Top Gel Slice"

Protein	PSM_Count	PercentCoverage	Annotation
PF3D7_1108700.1	294	14.36	PfJ2
PF3D7_0827900.1	181	8.92	PDI8
PF3D7_0929400.1	175	8.71	RhopH2
PF3D7_0917900.1	163	7.97	BiP
PF3D7_1134100.1	34	1.68	PDI11
PF3D7_0302500.1	19	0.88	CLAG3.1
PF3D7_1222300.1	15	0.76	Endoplasmin
PF3D7_0831700.1	13	0.8	Hsp70x
PF3D7_0811600.1	11	0.52	Conserved Plasmodium protein, unknown function
PF3D7_1352500.1	10	0.5	Trx-rellated protein
PF3D7_0935800.1	8	0.38	CLAG9
PF3D7_1344200.1	5	0.24	HSP110
PF3D7_0709100.1	5	0.2	Cg1
PF3D7_0930300.1	4	0.18	MSP1
PF3D7_0831400.1	3	0.15	Plasmodium exported protein
PF3D7_1108600.1	3	0.15	ERC
PF3D7_1311800.1	3	0.16	M1AAP
PF3D7_1451800.1	3	0.15	Sortilin
PF3D7_0310400.1	3	0.16	PIESP1
PF3D7_1123500.1	3	0.15	GP2
PF3D7_1252100.1	3	0.11	RON3
PF3D7_1104400.1	2	0.1	Trx-mero
PF3D7_1149500.1	2	0.1	RESA2
PF3D7_0801800.1	2	0.08	Mannose-6-phosphate isomerase

PF3D7_0105600.1	2	0.07	Conserved Plasmodium protein, unknown function
PF3D7_1456800.1	2	0.1	VP1
PF3D7_0711000.1	2	0.1	CDC48
PF3D7_1324900.1	1	0.05	LDH
PF3D7_1322000.1	1	0.05	Nucleoside diphosphatase
PF3D7_1016300.1	1	0.05	GBP130
PF3D7_1129100.1	1	0.05	PV1

DVSF-treated sample, "Bottom Gel Slice"

Protein	PSM_Count	PercentCoverage	Annotation
PF3D7_1108700.1	157	56.1	PfJ2
PF3D7_0827900.1	99	48.9	PDI8
PF3D7_1134100.1	20	39	PDI11
PF3D7_0917900.1	12	20.4	BiP
PF3D7_1311800.1	3	4.4	M1AAP
PF3D7_1352500.1	2	8.7	Trx-related protein
PF3D7_0831700.1	2	6.5	Hsp70x
PF3D7_0902600.1	2	1.5	FIKK9.7
PF3D7_1222300.1	2	4.5	Endoplasmin
PF3D7_1464500.1	1	0.8	Conserved Plasmodium protein, unknown function

Untreated sample, "Top Gel Slice"

Protein	PSM_Count	PercentCoverage	Annotation
PF3D7_0929400.1	8	4.3	RhopH2
PF3D7_0208800.1	2	5.1	Conserved Plasmodium protein, unknown function
PF3D7_1108700.1	2	1.9	PfJ2
PF3D7_1320100.1	1	10.9	ClpS

Untreated Sample, "Bottom Gel Slice"

Protein	PSM_Count	PercentCoverage	Annotation
PF3D7_0905400.1	32	15.1	RhopH3
PF3D7_1311800.1	28	11.6	M1AAP

PF3D7_0831700.1	10	8	Hsp70x
PF3D7_1241900.1	8	9.2	Tetratricopeptide repeat protein
PF3D7_1222300.1	8	7.6	Endoplasmin
PF3D7_0929400.1	7	5.4	RhopH2
PF3D7_0711000.1	7	6	CDC48
PF3D7_0917900.1	6	6	BiP
PF3D7_1108700.1	5	9.1	PfJ2
PF3D7_1409600.1	5	5.9	Conserved Plasmodium protein, unknown function
PF3D7_0935800.1	5	2.5	CLAG9
PF3D7_1228600.1	4	2.8	MSP9
PF3D7_1014100.1	3	2.3	MSA180
PF3D7_1452000.1	3	1.7	RON2
PF3D7_1239700.1	2	3.1	FTSH1
PF3D7_1351000.1	2	0.9	phophatidylinositol transfer protein
PF3D7_1016300.1	1	15.8	GBP130

APPENDIX C

PRIMERS USED IN CHAPTER 4

Primer Name	Sequence (5' - 3')
P1	cacatgtaaaacgatatcCGATTTTAATATTTTGTCATTAAAATTAAGTCACATTGTTGC
P2	ACGTCATAAGGATAGACGTCTCACAATTCATCATCAGCGTAATCTGG
P3	ctttccgggcgcgccttaaggatgctacatatataacaaaaaggcggatgagatataata
P4	ATATTAAAATCGgatatcgttttacatgtgtgatggtacaatatacacac
P5	CCCTTTCCGCGGAGCGCTaggattagctttccaatcaaatgaag
P6	GGGTTTGGTATCGGTTTACCcggccgtgtgccgtcCtcGaaCtcaggtaccccgtc
P7	ttataactcctcggaTGTCGAATCGAGGCCTAAAAG
P8	CGACAtccgaggagttataaATGTCCAGACCTGCAGTAATTATAG
P9	CCTTGAGCTCGCTAGCAAGCTTGCCGGCAAGATCATGTGATTTCTC
P10	ATGATCTTGCCGGCAAGCTTtccgaggagttataaaacatg
P11	TTGAATTTAGCGGCCGCcatattaaagaatgatttatatgacaaaatg
P12	CCCTTTCCGCGGAGCGCTcaaataaatcattatccatcttttagattatttc
P13	GGGTTTGGTATCGGTTTACCcggccgtatatcattagaagcgttaaaagaaaac
P14	ttacaattcggtattTGTCGAATCGAGGCCTAAAAG
P15	CGACAaataccgaattgtaaATGTCCAGACCTGCAGTAATTATAG
P16	CCTTGAGCTCGCTAGCAAGCTTGCCGGCAAGATCATGTGATTTCTC
P17	ATGATCTTGCCGGCAAGCTTtatatgacaaattatatgtttagaaaGaCgagatatatag
P18	TTGAATTTAGCGGCCGCgttatatatatgaattaatatataatggttc
P19	aaaatccaggtccacaattgATGAACAGAAAGTATTTTTCTTC
P20	GGTATCGGTTTACCcggccgTGTGCCGTCTTCAAATTCAGGTACCCCGTC
P21	ttattattttactagTTATAACTCCTCGGATGTCGAATCGAGGCCTAAAAG
P22	aaaatccaggtccacaattgATGAAAGTGTATAATTTTTCATTCATATG
P23	TGGTATCGGTTTACCcggccgTATATCATTAGAAGCGTTAAAAG

P24	ttattattttactagTTACAATTCGGTATTTGTCGAATCGAGGCCTAAAAG
P25	aaaatccaggtccacaattgATGAAAGTGTATAATTTTTCATTCATATG
P26	GAAAAACCTCGTGcAACCCTAgcCCATGTGGCATAAAACTGAAC
P27	TGCCACATGGgcTAGGGTTgCACGAGGTTTTTCTAACGACTTC
P28	GTATAGGTTTAgcATGACCAgcCCATGGAGCATAGAAAAAGACAAAC
P29	CTATGCTCCATGGgcTGGTCATgcTAAACCTATACATCCAATGTTTG
P30	TGGTATCGGTTTACCcggccgTATATCATTAGAAGCGTTAAAAG
P31	taagtatataatattGTTGATAATGTGGTTAGTGGgttttagagctagaa
P32	ttctagctctaaaacCCACTAACCACATTATCAACaatattatatactta
P33	taagtatataatattGGGGTACCTGAATTTGAAGAgttttagagctagaa
P34	ttctagctctaaaacTCTTCAAATTCAGGTACCCCaatattatatactta
P35	taagtatataatattCAAATTATATGTTTAGAAACgttttagagctagaa
P36	ttctagctctaaaacGTTTCTAAACATATAATTTGaatattatatactta
P37	taagtatataatattGACAAACTTGGATGCAAATGgttttagagctagaa
P38	ttctagctctaaaacCATTTGCATCCAAGTTTGTCaatattatatactta
P39	TCTCTTTATATTTTGATTTATTGGTATACCCCCGCTCACAACGTTATCAAC
P40	GTTGATAACGTTGTGAGCGGGGGTATACCAATAAATCAAAATATAAAGAGA

APPENDIX D

MASS SPECTROSCOPY DATA GENERATED FROM DVSF-TREATED SAMPLES, REFERENCED IN CHAPTER 5

"DVSF 1" Sample

Protein	PSM_Count	PercentCoverage	Annotation
PF3D7_1108700.1	104	45.7	PfJ2
PF3D7_0917900.1	107	50.5	BiP
PF3D7_0827900.1	86	35.8	PDI-8
PF3D7_0929400.1	154	41.4	RhopH2
PF3D7_1134100.1	38	40.9	PDI-11
PF3D7_0905400.1	59	32.6	RhopH3
PF3D7_1222300.1	35	24	Endoplasmin
PF3D7_0402000.1	9	11.4	PHISTa
PF3D7_0302500.1	33.25	19.6	CLAG3.1
PF3D7_0831400.1	9	9.3	Exported, unknown
PF3D7_1014100.1	23	14.2	MSA180
PF3D7_1108600.1	4	21.9	ERC
PF3D7_0831700.1	9	11.5	Hsp70x
PF3D7_1232100.1	10	12.3	CPN60
PF3D7_1410400.1	7	13.8	RAP1
PF3D7_0730900.1	19	22.5	PTP4
PF3D7_0501100.1	5	2.6	Hsp40, type II
PF3D7_1016300.1	5	47	GBP130
PF3D7_1352500.1	2	13.5	Trx-related protein
PF3D7_0935800.1	12	13.7	CLAG9
PF3D7_1228600.1	4	5.5	MSP9
PF3D7_1033200.1	1	10.7	ETRAMP10.2
PF3D7_1476300.1	4	8.6	PHISTb
PF3D7_1149500.1	3	1.8	RESA2
PF3D7_1252100.1	14	8.6	RON3
PF3D7_0207400.1	4	4.7	SERA7
PF3D7_1237700.1	1	5.7	Conserved, unknown
PF3D7_1116800.1	5	6.7	Hsp101
PF3D7_0532400.1	2	3.6	LyMP

PF3D7_0831600.1	4.75	6.8	CLAG8
PF3D7_0930300.1	4	3.6	MSP1
PF3D7_0310400.1	5	3.3	PIESP1
PF3D7_0409500.1	1	3.3	NAD(P)-binding protein
PF3D7_0207600.1	2	1.8	SERA5
PF3D7_0926400.1	1	2.5	Monocarboxylate transporter
PF3D7_1328300.1	1	2.7	Conserved, unknown
PF3D7_0801800.1	2	0.8	Mannose-6-phosphate Isomerase
PF3D7_0919400.1	1	2.3	PDI-9
PF3D7_1464600.1	3	2.4	UIS2
PF3D7_0412000.1	1	2.2	LITAF-like zinc finger protein
PF3D7_0106300.1	1	1.6	SERCA
PF3D7_0932100.1	1	0.7	MAM3
PF3D7_1024800.1	1	1.8	EXP3
PF3D7_1462300.1	1	1.8	GTP-Binding Protein
PF3D7_0107500.1	1	1	NPC1-related protein
PF3D7_0216300.1	1	1.2	Conserved, Unknown

“DVSF 2” Sample

Protein	PSM_Count	PercentCoverage	Annotation
PF3D7_0917900.1	69	45.9	BiP
PF3D7_1033200.1	20	48.5	ETRAMP10.2
PF3D7_1108700.1	24	27	PfJ2
PF3D7_0629200.1	13	35	DnaJ
PF3D7_1471100.1	7	16.4	EXP2
PF3D7_0827900.1	9	19.7	PDI-8
PF3D7_0702500.1	2	16.6	Exported protein
PF3D7_0731300.1	4	13.9	PHISTb
PF3D7_0831400.1	3	9.3	Exported protein
PF3D7_0501600.1	2	8.5	RAP2
PF3D7_0912400.1	3	8.7	Alkaline phosphatase
PF3D7_1232100.1	4	7.7	CPN60
PF3D7_0823900.1	2	6.6	Dicarboxylate/tricarboxylate carrier
PF3D7_1459400.1	3	7.9	Conserved, unknown
PF3D7_1134100.1	3	11.6	PDI-11
PF3D7_0823800.1	3	5.5	DnaJ

PF3D7_0936800.1	2	9.4	PHISTc
PF3D7_0918000.1	2	5.1	GAP50
PF3D7_0402000.1	3	5.6	PHISTa
PF3D7_0904700.1	1	4.8	Bacterial Histone-like protein
PF3D7_0501500.1	2	6.8	RAP3
PF3D7_0507500.1	2	5.2	SUB1
PF3D7_1013300.1	3	6.1	Conserved, unknown
PF3D7_1239700.1	4	4.5	FTSH1
PF3D7_0919100.1	1	3.5	DnaJ
PF3D7_1333000.1	1	4.7	CPN20
PF3D7_1237700.1	1	5.7	Conserved, unknown
PF3D7_1206000.1	1	3.3	SHLP2
PF3D7_1127000.1	1	3.1	Protein phosphatase
PF3D7_0318900.1	1	3.2	Conserved, unknown
PF3D7_0929400.1	4	4.5	RhopH2
PF3D7_1332600.1	2	3	APN1
PF3D7_1306200.1	1	5.9	Conserved, unknown
PF3D7_1108600.1	1	7	ERC
PF3D7_0905400.1	2	7.8	RhopH3
PF3D7_1401600.1	1	2.7	PHISTb
PF3D7_0528200.1	1	2.1	EIF3E
PF3D7_1344800.1	1	2.1	ATCase
PF3D7_0305000.1	1	2.3	EF-Ts
PF3D7_1129100.1	1	1.5	PV1
PF3D7_1014100.1	2	1.2	MSA180
PF3D7_1430200.1	1	2.4	Plasmpesin IX
PF3D7_1413400.1	1	1.4	30S ribosomal protein S9
PF3D7_1222300.1	1	3.2	Endoplasmin
PF3D7_1016300.1	1	15.3	GBP130
PF3D7_1464600.1	1	1.2	UIS2
PF3D7_1410400.1	1	0.9	RAP1
PF3D7_0831700.1	1	4	Hsp70x